TRACER FLUID FLOW THROUGH POROUS MEDIA: THEORY APPLIED TO ACID STIMULATION TREATMENTS IN CARBONATE ROCKS

A Dissertation

by

AHMED SALAHELDIN ZAKARIA MOHAMED REDA

Submitted to the Office of Graduate and Professional Studies of
Texas A&M University
in partial fulfillment of the requirements for the degree of

DOCTOR OF PHILOSOPHY

Chair of Committee,	Hisham A. Nasr-El-Din
Committee Members,	A. Daniel Hill
	Stephen A. Holditch
	Mahmoud El-Halwagi
Head of Department,	A. Daniel Hill

August 2014

Major Subject: Petroleum Engineering

ABSTRACT

Most carbonate rocks are heterogeneous at multiple length scales. These heterogeneities strongly influence the outcome of the acid stimulation treatments which are routinely performed to improve well productivity. At the pore scale, carbonate rocks are very complex and exhibit a wide variety of pore classes. However, most of the previous studies reported in the literature have focused on the injection rate, temperature, and fluid properties. This study focused primarily on the effect of carbonate pore structure on the acid stimulation treatments.

The objective of this study were to: 1) understand the effect of carbonate pore structure on the acid fluid flow through porous media by the use of thin section analysis, electrical measurements, nuclear magnetic resonance (NMR) and mercury injection capillary pressure (MICP) measurements, and tracer tests; 2) correlate the parameters that govern the tracer fluid flow through porous media to the acid fluid flow through the porous media of the carbonate rocks; 3) quantify the heterogeneity of the carbonate rocks at the pore scale so that the response of the carbonate rock to acid treatments in terms of acid volume needed to propagate the wormhole beyond the damaged zone, the wormhole fractal dimension, and the skin factor evolution during the treatment, can be correlated to the magnitude of pore scale heterogeneity; 4) find correlations between the flowing fraction obtained from tracer tests and the petrophysical parameters obtained from MICP and NMR measurements so that the response of the carbonate rocks to acid treatments can be connected to the basic petrophysical parameters; and 5) build a new

methodology to predict the performance of acid stimulation treatments in carbonate rocks using non-destructive tracer tests.

In order to achieve the objectives of the study, a carbonate characterization study was conducted first on different carbonate rock types using thin section analysis, electrical measurements, NMR, and MICP measurements. Then, tracer tests were conducted on these carbonates using two different tracer fluids. Following the tracer tests, coreflood experiments using two different acid systems (15 wt% HCl, and emulsified acid formulated at 1 vol% emulsifier and 0.7 acid volume fraction) were conducted at field conditions.

The results reveal that the pore scale heterogeneity has a significant effect on the acid stimulation treatments. It was also found that the response of carbonate rocks to acid treatments is correlated to the basic petrophysical parameters and the tracer fluid flow through porous media. A tracer fluid can be injected into a core, or on a field scale, between two wells, or injected into a single well configuration and then flow it back. The analysis of the tracer flowback samples can be then used to predict the acid stimulation treatments in carbonate rocks. This approach helps to optimize the acidizing job to get the ultimate benefit of the treatment.

DEDICATION

This dissertation is dedicated to my mom, my dad, and my brother.

ACKNOWLEDGEMENTS

I would like to take this opportunity to express my deepest gratitude and sincere appreciation to my advisor and committee chair, Dr. Hisham A. Nasr-El-Din, for his continuous encouragement, and his academic guidance. It was a real enriching experience to be one of his graduate students.

Appreciation is extended to the members of my committee, Dr. A. Daniel Hill, Dr. Stephen A. Holditch, and Dr. Mahmoud El-Halwagi, for their guidance towards the completion of this dissertation. It was a great honor to have them in my committee.

I also would like thank my colleagues, and my teammates for helping me to startup this work and during my graduate study.

Finally, I would like to acknowledge the financial support of Schlumberger Sugar Land Technology Center. The facilities and resources provided by the Harold Vance Department of Petroleum Engineering of Texas A&M University are gratefully acknowledged.

NOMENCLATURE

C	Tracer concentration in the core effluent samples, mg/l
C^*	Tracer concentration in the stagnant region, mg/l
C_0	Tracer concentration at the core inlet, mg/l
D	Dispersion coefficient, cm^2/s
E	Residence time distribution function, min^{-1}
F	Formation factor
f	Flowing fraction, dimensionless
h	Formation thickness, ft
K	Permeability, md
K_S	Permeability of the damaged zone, md
K_{wh}	Permeability of the stimulated zone, md
M	Mass transfer coefficient, cm/s
PV_{bt}	Pore volume to breakthrough, dimensionless
P_c	Capillary pressure, psi
R_{brine}	Brine resistivity, Ω.m
r	Pore throat radius, ft
r_w	Wellbore radius, ft
r_s	Damaged region radius, ft
r_{wh}	Wormhole penetration radius, ft
S	Skin factor, dimensionless

t	Time, min
V_{acid}	Cumulative acid injected volume, ft^3
σ	surface tension of mercury, dyne/cm
v	Interstitial velocity, cm/s
	Shear rate, 1/s
τ	Tortuosity
ϕ	Porosity, volume fraction
ϕ_{int}	Intergranular porosity, volume fraction

TABLE OF CONTENTS

Page

LIST OF FIGURES

LIST OF TABLES

CHAPTER I

INTRODUCTION

1.1 BACKGROUND

Matrix acidizing of carbonate reservoirs is a process designed to improve well productivity by increasing rock permeability in the region surrounding the wellbore (Hoefner and Fogler 1988). Acid stimulation of production and injection wells is routinely used to remove pore plugging deposits from damaged wells. These types of plugging are detrimental when they occur in the immediate vicinity of the wellbore where they form a low-permeability skin. This near wellbore permeability reduction can be effectively removed by proper acid treatments. Matrix acidizing can also enhance production in wells that exhibit low natural formation permeability. In this case permeability increase is achieved by partial dissolution of the original rock matrix instead of by removal of particulates. Natural flow channels are enlarged allowing increased production.

The acid used in a matrix acidizing process is usually HCl in concentration of 528 wt%. The low cost, availability, and the ease of inhibition make the HCl acid the most commonly used acid system in oil and gas industry.

In carbonate reservoirs, the reaction rate of hydrochloric acid with calcite is very fast (Nierode and Williams 1971). In conventional stimulations where 15 wt% HCl is used at low flow rates, the acid reacts with the carbonate rock and causes surface wash-out only (Hoefner and Fogler 1987). This means that the acid will not penetrate the damaged zone and, as a result, the efficiency of the stimulation treatment will be low. To

propagate deeper wormholes in the formation for better productivity enhancement, retarded acids should be used. Emulsified acids are one of the most widely used retarded acid systems. HCl acid is commonly used as the internal phase of the emulsion. For the external phase, oil and diesel are the most commonly used hydrocarbons. The external hydrocarbon phase acts as a diffusion barrier to reduce the diffusion of the acid droplets to the surface of the rock which helps in the creation of deep wormholes. Several studies (deRozieres et al. 1994; Navarrete at al. 1998; and Al-Mutairi et al. 2008) examined the reaction of emulsified acid with carbonate. Navarrette et al. (1998) indicated that the reaction rate of 28 wt% HCl emulsified acid with limestone is 8.5 times less than that of 28 wt% HCl with limestone.

The reaction of acid with carbonates results in the formation of large flow channels called wormholes. Wormholes are created because of the high dissolution rates that are encountered in carbonate formations. Wormholes originate at the wellbore and extend radially in random directions into the formation. Wormholes form because of the heterogeneity of natural porous media and the non-uniform flow or channeling that always results. Some areas of the rock receive more flow than others. Acid penetrates farther into those regions and so dissolution is accelerated there. Local permeability is increased through enlargement of pores and pore throats, and flow increases even more. A dominant channel quickly forms which then grows in length and propagates through the medium. Once wormholes form they carry essentially most of the fluid and regions near the wellbore, but not near the wormhole experience virtually no flow because of the negligible resistance to flow in the wormhole itself (Hoefner and Fogler 1988).

The shape and structure of these wormholes depend on the injection rate. Hoeffner and Fogler (1988) conducted a set of linear core experiments to study the effect of the injection rate on the wormhole pattern and the results are very similar to those obtained by Daccord and Lenormand (1987). Wang et al. (1993) also studied the effect of injection rate on wormhole propagation with a large number of coreflood acidizing experiments and theoretical modeling. The wormhole pattern formation is governed by a competition of axial convection, transverse diffusion, and reaction mechanisms. At low injection rates, the movement of the reaction front is suppressed by the transverse dispersion and face dissolution occurs (Panga et al. 2005). As the injection rate increases, the dissolution pattern changes from face dissolution to wormhole. Uniform dissolution pattern occurs at high injection rates. Hoefner and Fogler (1989) showed that the transition from one pattern to another depended on the Damköhler number: the ratio of acid reaction rate to acid transport by convection.

Bazin and Abdulahad (1999) conducted a large number of coreflood experiments with different emulsified acid systems on limestone cores. They studied the wormhole dissolution patterns using computed tomography scanning. It was found that increasing the acid concentration provides higher wormhole penetration rates.

Al-Anazi et al. (1998) studied the application of the emulsified acid in tight carbonate rocks using coreflood experiments and the results showed that the emulsified acid can form deep wormholes in tight carbonate cores. Buijse and Van Domelen (2000) studied the effect of the injection rate, viscosity, and acid volume fraction on the emulsified acid pore volume to breakthrough in carbonate rocks. It was found that these

parameters affect the acid pore volumes to breakthrough and the corresponding wormhole dissolution pattern. Sayed et al. (2012) studied the performance of the emulsified acid in low and high permeability carbonate formations using coreflood experiments. It was found that the high permeability carbonate cores consumed more acid volume to breakthrough than the low permeability ones. Also, an optimum injection rate was observed for the high permeability cores while the acid pore volumes to breakthrough decrease with an increase in the injection rate for low permeability formations.

It is clear that understanding the effect of the aforementioned parameters on matrix acidizing of carbonates is crucial for a better acidizing design in field acidizing operations. However, most of the previous studies focused on the effect on injection rate, temperature, injection concentration, and geometry of the domain on carbonate acidizing. On the other hand, there are few studies focused on the effect of heterogeneity in matrix acidizing.

Dong et al. (1999) examined the influence of the natural fractures on the acid etching pattern. They conducted a series of acidizing experiments on core samples with artificial fractures. Their experimental results show that the acid etching pattern of naturally fractured formations depends strongly on the width of the natural fracture. For typical natural fracture widths, the pattern tends to be wormholing, rather than etching of the fracture surfaces. It was found that one broad channel was created at the area near the inlet of the samples, and as acid flowed down the fracture, the channel narrowed quickly and finally became a deep narrow wormhole.

Dong et al. (2000) developed a mathematical model of acidizing naturally-fractured carbonates. The model includes bulk solution transport, acid transport and reaction, and the change of fracture width by acid dissolution. The model predicts the acid etching patterns and the relationships between acid etching patterns and the fracture width, surface roughness, and leakoff rate noticed in the flow of acid in naturally fractured formations.

Izgec et al. (2010) conducted experimental and theoretical studies to investigate the flow of regular 15 wt% HCl acid in vuggy carbonates. They studied the acidization of vuggy carbonates with high resolution computerized tomography imaging, image processing, geostatistical characterization, acid coreflood experiments with 4 in. by 20 in. cores, and numerical simulation. Their experiments showed that the vuggy pores are distributed in a manner that makes the acid propagate more rapidly in vuggy carbonates compared to homogenous ones. Consequently, less acid volume to breakthrough for vuggy carbonates is required than for the homogenous rocks.

There have been several attempts to understand the flow behavior in vuggy rocks, including the more pronounced works of Hidajat et al. (2004), Moctezuma Berthier et al. (2000), Xu et al. (1998), Zhang et al. (2004 and 2005), and Arbogast et al. (2004). Zhang et al. (2005) conducted number of experiments using vugular rocks to understand the flow characteristics of vuggy rocks. These studies have addressed flow through such media, but not reactive flow as occurs in acidizing.

Li et al. (2005) conducted a modeling study to understand the effect of small scale heterogeneities in matrix acidizing of sandstones. They concluded that the presence

of small-scale heterogeneities in a sandstone has a dramatic impact on the acidizing process. It has been shown that flow field heterogeneities cause acid to penetrate much farther into the formation than would occur if the rock were homogeneous. The correlation strength of petrophysical properties in flow direction increases the penetration time as much as 17 times. It is expected that in carbonate acidizing case this effect will be more pronounced.

Carbonate formations are very complex in their pore structure and exhibit a wide variety of pore classes, such as interparticle porosity, moldic porosity, vuggy porosity, and microporosity. Geologists have defined carbonate pore classes based on sedimentology, thin sections and porosity-permeability relationships, but the question remains as how these pore classes govern the acid fluid flow through porous media. Only one study (Ziauddin and Bize 2007) in the literature has been reported the effect of carbonate pore structure on the acid fluid flow through porous media.

Ziauddin and Bize (2007) recently studied the effects of pore-scale heterogeneities. In their study core samples from eight different carbonate rocks were studied. They characterized samples for mineralogy, texture, fabric, porosity and density distribution using Nuclear Magnetic Resonance (NMR), Computerized Tomography (CT), scanning electron microscopy (SEM), mercury injection, as well as resistivity measurements and chemical testing. They classified each sample into a Reservoir Rock Type (RRT). They found that the response of the carbonate rock to acid depends on the RRT it belongs to.

1.2 OBJECTIVES

The objectives of this research are to: 1) understand the physics of the acid fluid flow through the porous media of carbonate rocks at the pore scale by the use of thin section, electrical measurements, tracer tests, nuclear magnetic resonance, and mercury injection capillary pressures measurements; 2) correlate the parameters that govern the tracer fluid flow through porous media (dispersion, flowing fraction, and mass transfer) to the response of the carbonate rock to the acid treatment in terms of acid volume needed to propagate the wormhole beyond the damaged zone, the wormhole fractal dimension, and the skin factor evolution during the treatment; 3) find correlations between the flowing fraction obtained from tracer tests and the petrophyscial parameters obtained from mercury injection capillary pressure and nuclear magnetic resonance measurements so that the response of the carbonate rocks to acid treatments can be connected to the basic petrophyscial parameters; and 4) build a new methodology to predict the performance of acid stimulation treatments in carbonate reservoirs using non-destructive tracer tests.

To achieve these objectives, first a characterization study for the different carbonate rock types was performed. This study included thin section analysis, nuclear magnetic resonance, and mercury injection capillary pressure measurements. The objective of this study was to characterize the pore-scale heterogeneity for the different carbonate rock types in terms of pores size, distribution, shape and connectivity.

X-ray fluorescence and x-ray diffraction were also conducted for chemical and mineralogical composition examination.

Following the carbonate rock type characterization study, tracer tests were performed to understand the effect of carbonate pore-scale heterogeneity on the fluid flow in the porous media. By the aid of the Coats and Smith model, three parameters (dispersion coefficient, flowing fraction, and mass transfer coefficient) that govern the tracer fluid flow through the different carbonate rock types are determined. Two sets of tracer tests were performed. The first set was conducted using 8 wt% potassium chloride and the second set is conducted using polymer based tracer fluid.

Next, two sets of coreflood experiments were performed. The first set was conducted using regular treatment fluid (15 wt% HCl) and the other set was conducted using shear thinning treatment fluid (emulsified acid). Acid diversion experiments were also conducted to investigate the effect of the presence of different carbonate rock types of different pore structures in the reservoir on the acid fluid flow distribution.

Post-acid injection study was then preformed. This study included pressure drop analysis, wormhole pattern visualization and chemical analysis for the effluent samples to understand the effect of carbonate pore structure on the acid stimulation treatments.

Finally, a new methodology to predict the performance of acid stimulation treatments using non-destructive tracer tests was presented.

Chapter II gives an overview for the tracer fluid flow through the porous media and the use of the tracer tests in oil and gas industry. Discussed in this chapter are the different tracer fluid types and the different developed models in the literature to simulate the tracer fluid flow through porous media. An introductory study of the use of the tracer tests to characterize the carbonate pore structure is also presented.

Chapter III gives an overview for the different pore systems for carbonate rocks and the different schemes for carbonate rock type classification. Discussed in this chapter also are the use of different methods to characterize the carbonate pore structure. These methods include thin section analysis, electrical measurements, nuclear magnetic resonance, and mercury injection capillary pressure measurements.

Chapter IV summarizes the results of the characterization study on the different carbonate rock types that have been used in this study. This study includes the results of thin section, nuclear magnetic resonance, and mercury injection capillary pressure measurements. Following that, the results for the tracer and 15 wt% HCl acid coreflood experiments are presented and a new methodology to predict the performance of acid stimulation treatments in carbonate rocks using tracer tests is also discussed.

Chapter V shows the results for the tracer and emulsified acid coreflood experiments. Following that, a new formulation for the tracer fluid is presented and the use of this fluid type to predict the performance of emulsified acid stimulation treatments in carbonate rocks is discussed. Newly developed correlations are presented between the flowing fraction of carbonate rock obtained from tracer tests and the petrophysical parameters (relaxation time, and median pore throat diameter) obtained from nuclear magnetic resonance and mercury injection capillary pressure measurements.

Chapter VI investigates the effect of the presence of different carbonate rock types of different pore structures within the formation on the acid fluid flow distribution.

Chapter VII summarizes the conclusions of this study.

Chapter VIII summarizes the author's recommendations for a future work.

CHAPTER II

METHODS FOR CARBONATE PORE STRUCTURE CHARACTERIZATION

Carbonate formations are very complex in their pore structure and exhibit a wide variety of pore classes **(Fig. 2.1)**. Several methods are commonly used to describe the spatial distribution of pore sizes, pore types and shapes, and pores connectivity. These methods include thin section analysis, nuclear magnetic resonance, and mercury injection capillary pressure measurements.

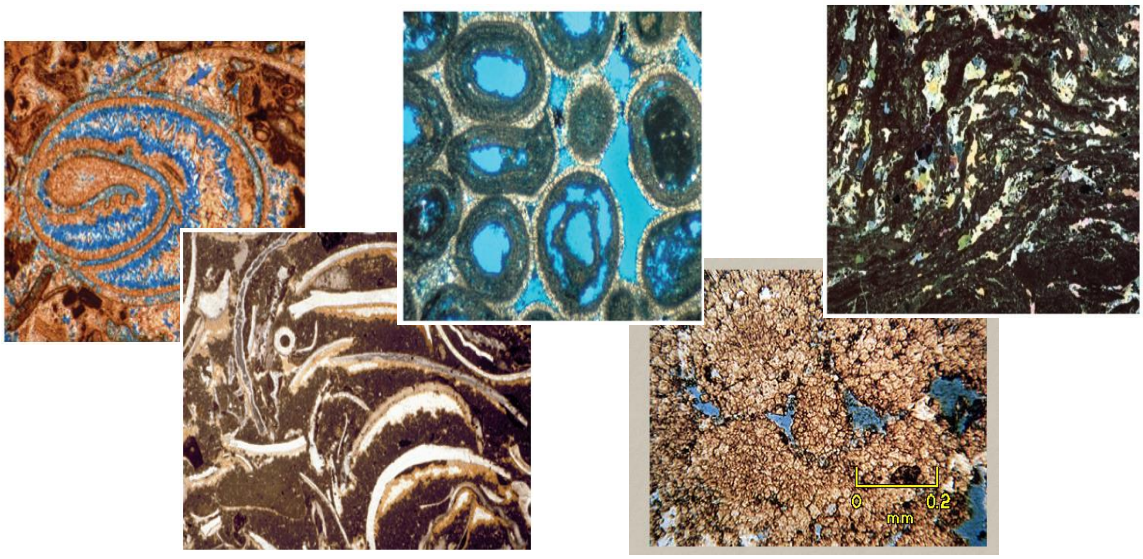

Fig. 2.1—Different types of carbonate pore structure.

Archie (1952) made the first attempt for pore space classification for carbonate rocks. Archie (1952) recognized that not all the pore space can be observed using a 10 power microscope and that the surface texture of the broken rock reflected the amount of

matrix porosity. Therefore, pore space is divided into matrix and visible porosity **(Fig. 2.2)**. Visible pore space is described according to pore size; A for no visible pore space and B, C, and D for increasing pore sizes from pinpoint to larger than cutting size.

Lucia (1983) showed that the most useful division of pore types was between pore space located between grains or crystals, called interparticle porosity, and all other pore space, called vuggy porosity **(Fig. 2.2)**. Vuggy pore space is further subdivided by Lucia (1983) into two groups based on how the vugs are interconnected: (1) vugs that are interconnected only through the interparticle pore network are termed separate vugs and (2) vugs that form an interconnected pore system are termed touching vugs.

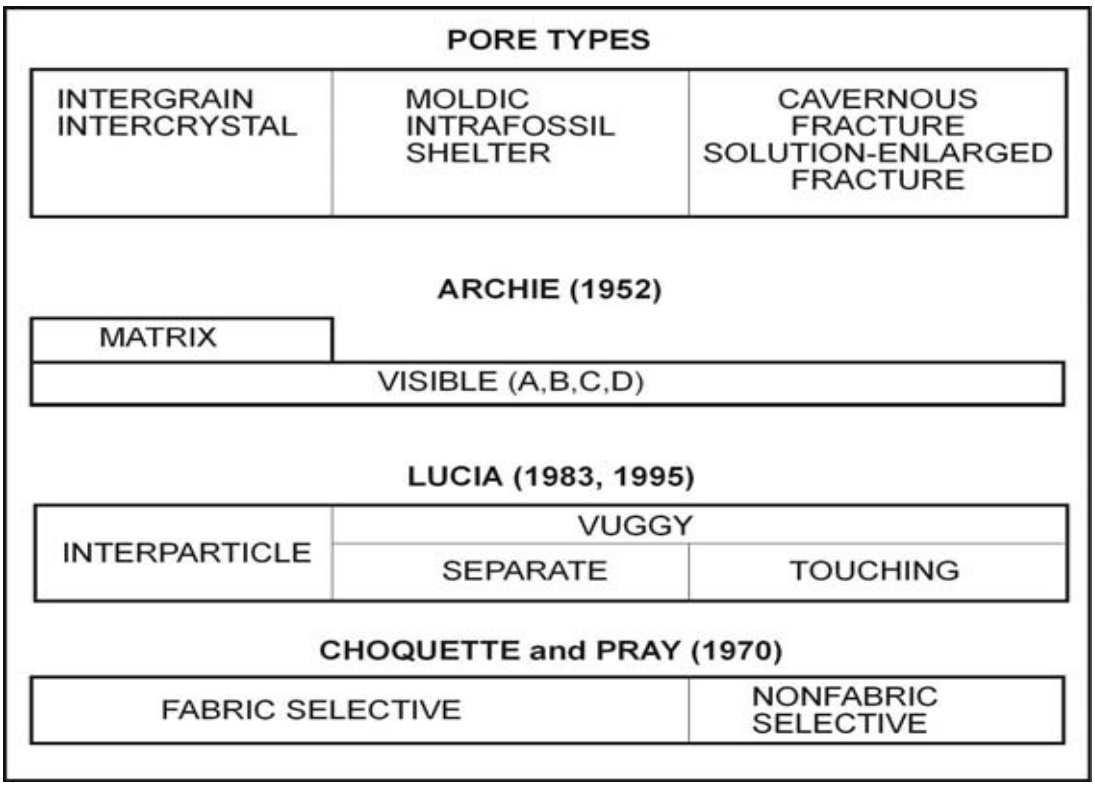

Fig. 2.2—Classification of carbonate pore types.

When the pore space is located between grains, the interparticle porosity is called intergrain porosity. When the pore space is located between crystals, the interparticle porosity is called intercrystal porosity.

The addition of vuggy pore space to interparticle pore space alters the petrophysical characteristics by altering the manner in which the pore space is connected, all pore space being connected in some fashion. Separate vugs are defined as pore space that is interconnected only through interparticle pore space. Touching vugs are defined as pore space that forms an interconnected pore system independent of interparticle pore space **(Fig. 2.3)**.

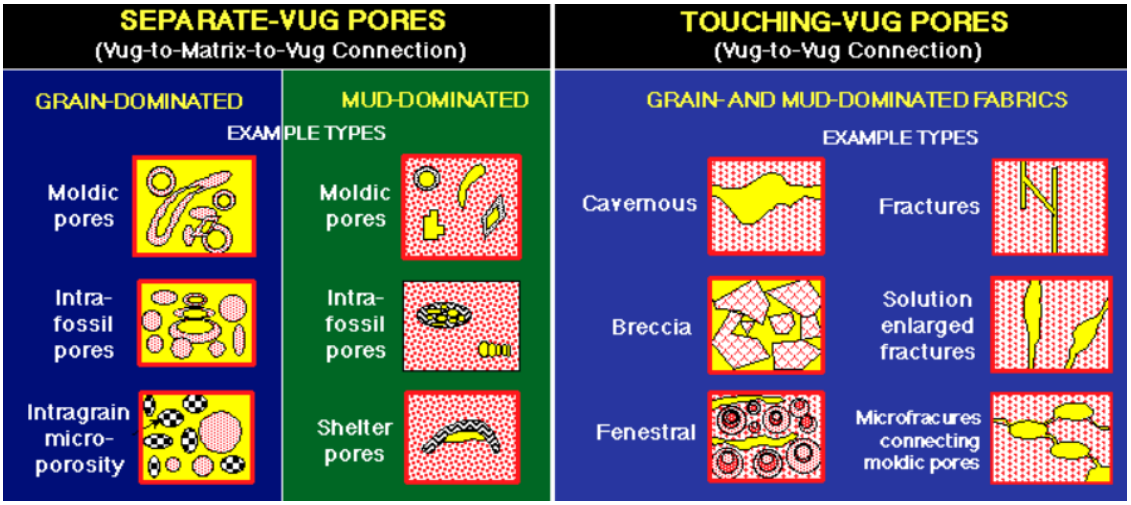

Fig. 2.3—Classification of vuggy pore space.

Separate-vug pore space is defined as pore space that is 1) either within particles or is significantly larger than the particle size (generally >2x particle size) and 2) interconnected only through interparticle pore space **(Fig. 2.3)**. Separate vugs are typically fabric-selective in their origin. Moldic pore space, descriptive of pores formed by the selective removal of a former individual constituent of the sediment or rock. Micro pore space, size term proposed by Choquette and Pray (1970) for microscopic pores or pores small enough to hold water against the pull of gravity and to inhibit the flow of water. These pores have an average diameter of 1/16 mm. Shelter pore space, a type of primary interparticle porosity created by the sheltering effect of relatively large sedimentary particles which prevent the infilling of pore space beneath them by finer clastic particles.

Touching-vug pore systems are defined as pore space that (1) is significantly larger than the particle size and (2) forms an interconnected pore system of significant extent **(Fig. 2.3)**. Touching vugs are typically nonfabric selective in origin. Breccia pore space, type of interparticle porosity in a breccia. Breccia is a rock structure marked by an accumulation of angular fragments, or of an ore texture showing mineral fragments without notable rounding. Fenestral pore space, fenestrae occur as somewhat rounded features of spherical, lenticular, or more irregular shapes. Fenestrae are commonly somewhat flattened parallel with the laminae or stratigraphic planes of the rock. Cavernous, collapse breccia, fractures, and solution-enlarged fracture pore types commonly form an interconnected pore system on a reservoir scale and are typical touching-vug pore types.

Choquette and Pray (1970) discussed the geologic concepts surrounding carbonate pore space and presented a classification that is widely used. They emphasize the importance of pore space genesis, and the divisions in their classification are genetic and not petrophysical. They divide all carbonate pore space into two classes: fabric selective and nonfabric selective **(Fig. 2.2)**. Moldic and intraparticle pore types are classified as fabric selective porosity by Choquette and Pray (1970) and grouped with interparticle and intercrystalline pores.

2.1 USE OF THIN SECTION WITH DIFFERENT CARBONATE ROCK TYPES

In this study, different carbonate rock types are used to cover a wide range of pore structures. Six calcite carbonate rock types are studied. These include Indiana Limestone, Austin Chalk, Edwards Yellow, Pink Desert, Winterset, and Edwards White **(Fig. 2.4)**. On the other hand, two dolomite carbonate rock types are studies. These include Homogenous Dolomite, and Vuggy Dolomite (Fig. 2.5).

Blue epoxy impregnated thin sections were prepared for each carbonate rock type to obtain a detailed description of the types of porosity, the connectivity of pores, fabric, and texture to assess the pore-scale heterogeneity. The thin section was viewed under an optical microscope. Images for each carbonate rock sample were captured at 2.5 and 10X magnifications using a digital camera and a personal computer.

Fig. 2.4—Different calcite carbonate rock types.

Fig. 2.5—Different dolomite carbonate rock types.

2.2 NUCLEAR MAGNETIC RESONANCE MEASUREMENTS

Nuclear magnetic resonance in the laboratory and field applications has gained recognition for being one of the most valuable rock characterization tools. Among various applications for NMR, measurement of rock porosity, which is independent of mineralogy, becomes one of the standard uses. The measured total amplitude of H^1-NMR signal is directly proportional to the total amount of hydrogen nuclei in the rock sample. Thus, when all pores inside the rock sample is filled with fluid contains proton nuclei, the total amplitude of NMR signal represents the total porosity.

Another well-received NMR application is the determination of pore size distribution by NMR relaxation measurements. The two NMR relaxation times, T1 (spin-lattice relaxation) and T2 (spin-spin relaxation) are directly correlated with pore size distribution (Kenyon 1992; Straley et al. 1997; Kleinberg et al. 1994; Sørland et al. 2007). Since T1 measurement is more time consuming, T2 measurement is widely used in the modern NMR laboratory application. The principles of NMR T2 relaxation in porous media can be described as (Korringa et al. 1962):

$$\frac{1}{T_2} = \rho_2 \frac{S}{v} + \frac{1}{T_2{}^{Bulk}} + \frac{1}{T_2{}^{diff}} \quad \text{(2.1)}$$

Under fast diffusion regime or surface limited regime with low-field NMR, the above equation of T2 relaxation rate can be approximated by (Kleinberg et al. 1994):

$$\frac{1}{T_2} = \rho_2 \frac{S}{v} \quad \text{(2.2)}$$

The direct relationship between NMR relaxation time and pore size distribution mentioned above breaks down in pore system with complicated connectivity between different pore types, such as micro- and macropores in carbonates. Due to the diffusion of magnetization, called diffusion coupling, between various pore types, the determination of pore sizes from NMR relaxation times from the multi-modal porosity system is non-trivial (Freeman et al. 1999; Toumelin et al. 2002; Grunewald and Knight 2011; Toumelin et al. 2003; Ramakrishnan et al. 1998). **Fig. 2.6** shows two bi-modal pore systems with different connectivity. When two types of pores are completely isolated, the T2 time is directly related to the pore body size. When they are, however, connected to each other, T2 distributions are getting close to each other.

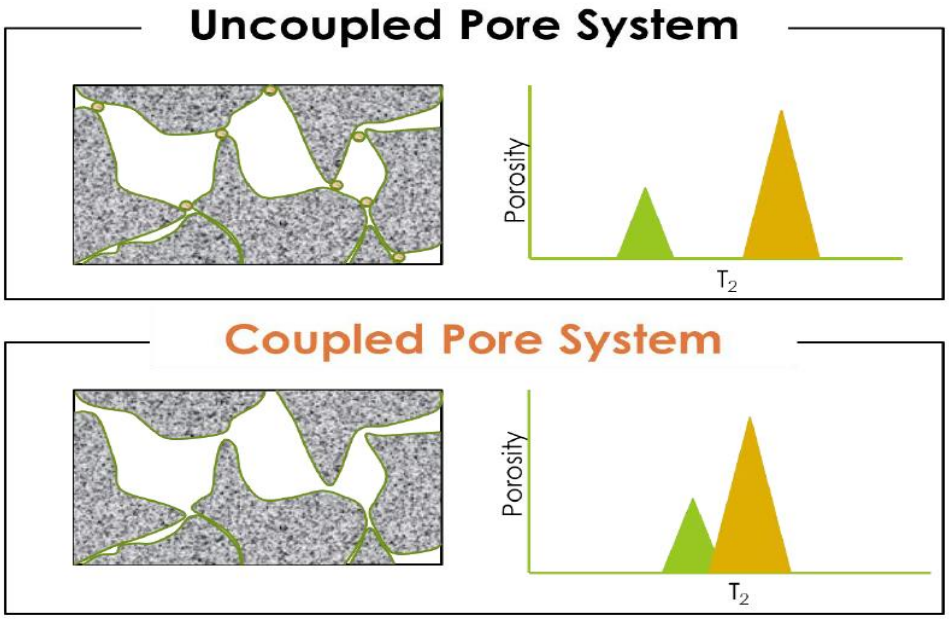

Fig. 2.6—Bimodal pore system with different connectivity.

Neeraj and Hirasaki (2011) studied the NMR T2 response for different carbonate rock types. For example, **Fig. 2.7** shows that the porosity in this carbonate rock type resides in large vugs and the contribution of small-sized pores is very small. The T2 response in **Fig. 2.8** shows that the porosity that resides in this carbonate has contributions from small-sized micropores, vugs, and some intermediate-sized pores.

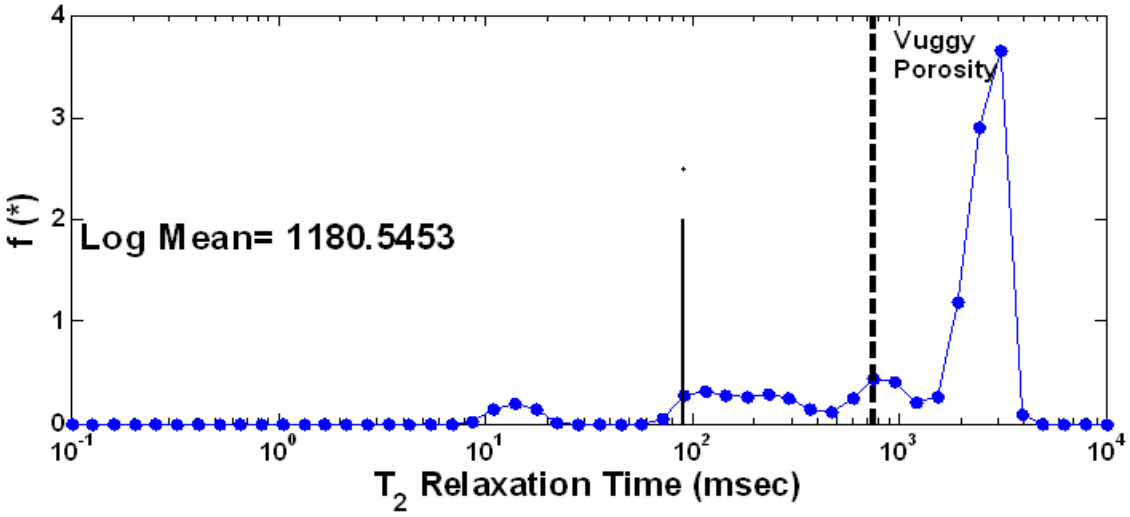

Fig. 2.7—T2 relaxation time spectrum for 100% brine saturated vuggy carbonate sample.

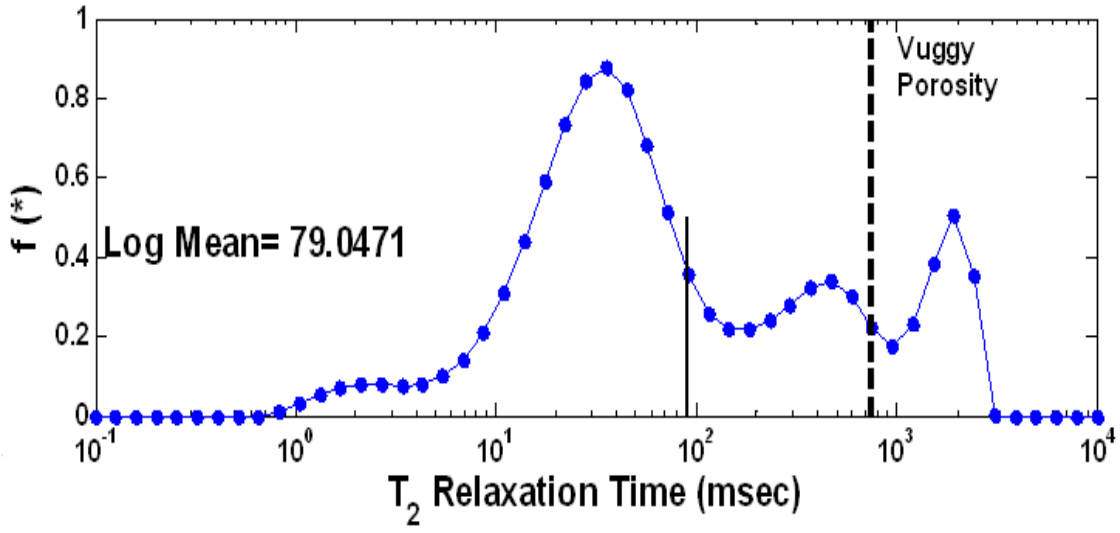

Fig. 2.8—T2 relaxation time spectrum for 100% brine saturated carbonate sample.

In this study, nuclear magnetic resonance (NMR) experiments were performed using a MARAN low field (2 MHz) hydrogen magnetic resonance instrument. The T2 distributions were computed by evaluating the Carr-Purcell-Meiboom-Gill (CPMG) measurements. The inter-echo spacing used in these experiments was 600 μsec and the delay time was 10 seconds. The NMR of the fully brine saturated samples for each carbonate rock type was measured and the pore size distribution was presented.

2.3 MERCURY INJECTION CAPILLARY PRESSURE MEASUREMENTS

In this study, mercury-air capillary pressure was measured using a Micromeritics AutoPore IV 9520 mercury porosimeter. Endtrims were put in the penetrometers. They were then evacuated under vacuum. Mercury was injected at multiple pressures up to 60,000 psi. The volume of mercury injected at each pressure increment is automatically recorded until the maximum pressure is achieved.

The apparent mercury injection volume was corrected for conformance determined for each sample. The conformance is the volume of mercury pressed into surface roughness and around sample edges after the penetrometer chamber is initially filled with mercury, due to mercury being an extremely non-wetting phase. Swanson permeability was calculated from the mercury injection results using the method described by Swanson (1981).

Mercury injection capillary pressure measurement provides information on the pore size distribution of the rock. Loucks et al. (2012) divided pores into megapore, macropore, mesopore, micropore, nanopore, and picopore **(Fig. 2.9)**.

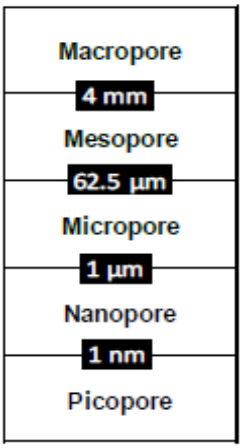

Fig. 2.9—Pores types

Mercury porosimetry is based on the capillary law governing liquid penetration into small pores. Assuming cylindrical pores, pore throat size can be calculated from the Washburn equation:

$$r = \frac{2\,\sigma\,cos\theta}{P_c} \quad \text{(2.3)}$$

The surface tension of mercury is 485 dyne/cm. The contact angle of the mercury in air on rock varies with rock composition, however, 140° is generally accepted by industry. The median pore throat diameter size is defined in this study as the pore throat diameter at 50% of mercury intrusion during the experiment.

CHAPTER III

TRACER FLUID FLOW THROUGH POROUS MEDIA

3.1 INTRODUCTION

In fluid flow applications, tracer is a defined as a substance that is added to the fluid to track the fluid flow through the porous media. Tracers can be divided into two general groups: (1) chemical tracers, and (2) radioactive tracers. Chemical tracers are those which can be identified and measured quantitatively by general analytical methods such as conductivity, refractive index and elemental spectrometry. Radioactive tracers are detected by their emitted radiation, usually beta or gamma.

Tracer tests have been used along the past years for characterization of rock heterogeneity. Strum and Johnson (1950) studied the results of several tracer tests using brine, fluorescein dye, and a surface active compound. Their results verified the existence of directional permeabilities which had already been measured on core samples. Their findings are generally considered the first to illustrate the important use of tracers in verifying reservoir heterogeneity.

Bretz et al. (1988) found that the spatial correlation of pore sizes observable on the scale of thin section affects the tracer fluid flow through porous media and produces early breakthrough and tailing. Bretz et al. (1988) also found that the wide pore size distributions and preferential flow paths are characterized in the Coats and Smith (1964) model by high dispersion coefficient and low flowing fraction.

Dauba et al. (1999) conducted an experimental study to examine the effect of longitudinal heterogeneity on the tracer profile and it was found that long tail is an

indication for high permeability contrast. On the contrary, the profile is not sensitive to cross section heterogeneity.

Moctezuma-Berthier and Fleury (2000) used tracer experiments and streamline simulations to map permeability in an artificial and uniformly vuggy core sample (5 cm in diameter by 20 cm in length). A vug to matrix permeability ratio of 360 was used to match numerical simulation results to the experiment. They characterized a preferential faster flow path of vugs connecting to vugs through the matrix (separate-vug pore type). They concluded that heterogeneity in the sample could be modeled by layered systems with large correlation lengths.

Shook (2003) used the tracer test results analysis to estimate the flow geometry and heterogeneity in fractured, geothermal reservoirs.

Hidajat et al. (2004) studied the flow of the tracer in vuggy carbonates. They found that the vugs are distributed in a way that causes a high permeability streak in tight matrix. This is reflected on the tracer profile which is characterized by very early breakthrough and long tail behavior.

Skauge et al. (2006) studied the flow of the tracer in different carbonate rock types that are representative of different carbonate pore classes. They found that each carbonate pore class has a characteristic response to the tracer flow, which affects the breakthrough curve. For example, **Fig. 3.1** shows the tracer profile for intercrystalline pore types. The profile is dominated by a high fraction of inaccessible pores and less capacitance effects. **Fig. 3.2** shows the tracer profile for chalky micro pore type and the profile is dominated by negligible amount of inaccessible pores and significant fraction

of dead-end pores. Their findings show that tracer tests are useful way to characterize the carbonate pore scale heterogeneity.

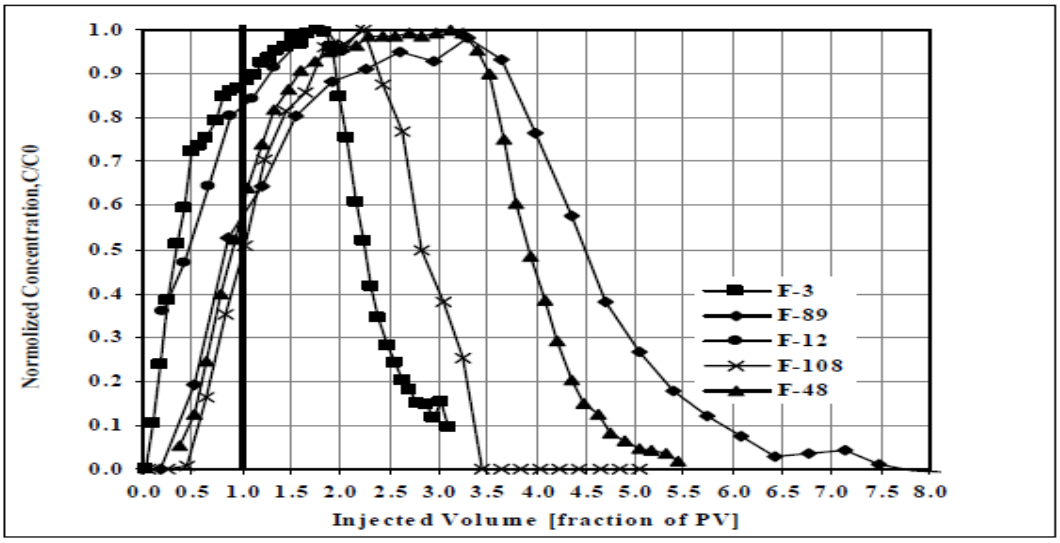

Fig. 3.1—Tracer profile for intercrystalline pore types (After Skauge 2006).

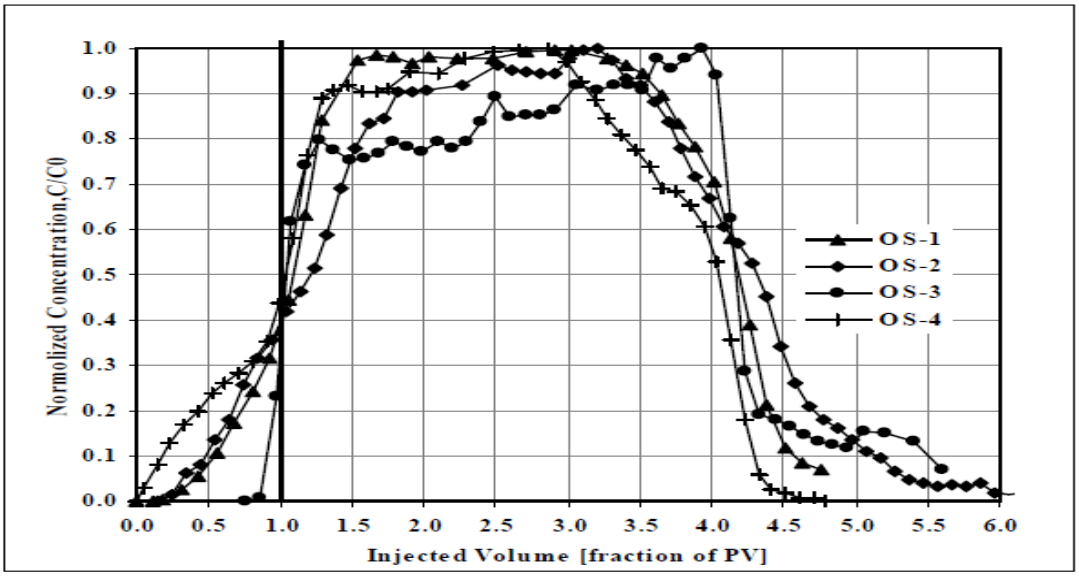

Fig. 3.2—Tracer profile for chalky-micro pore types (After Skauge 2006).

Izgec et al. (2010) developed a numerical simulator to understand the flow of the tracer in vuggy carbonates. It was observed that a single separate vug creates as high flow velocity channel acting as a high permeability streak. In their study, three important parameters (total amount, size, and spatial distribution of vugs) were analyzed. It was found that although the presence and amount of vugs does not change the effective permeability of the formation a lot, it could highly effect fluid direction through porous media.

3.2 COATS AND SMITH MODEL

The Coats and Smith (1964) dead-end pore model was used in this work to simulate the normalized tracer concentration profiles for the different carbonate rock types. The model equations in a differential form are given in equations 3.1 through 3.5:

$$D\frac{\partial^2 C}{\partial x^2} - v\frac{\partial C}{\partial x} = f\frac{\partial C}{\partial t} + (1-f)\frac{\partial C^*}{\partial t} \quad \text{(3.1)}$$

$$(1-f)\frac{\partial C^*}{\partial t} = M(C - C^*) \quad \text{(3.2)}$$

Initial and boundary conditions should be defined to solve the differential equations:

Initial condition

$$C(x,0) = 0 \quad \text{for } x \geq 0 \quad \text{(3.3)}$$

Boundary Conditions

$$x = 0,\ vC_0 = v\,C - D\,(\partial C/\partial x) \quad \text{(3.4)}$$

$$x \to \infty,\ C(\infty, t) = 0 \quad \text{(3.5)}$$

The model is characterized by three parameters: (1) the dispersion coefficient (D); (2) the flowing pore volume fraction (f); and (3) the mass transfer coefficient (M). The three parameters were obtained for each carbonate rock type.

3.3 RESIDENCE TIME DISTRIBUTION

It is expected that the time the tracer remains in each carbonate rock type is different. This time is called the residence time. To obtain the residence time distribution function, we differentiate the normalized tracer concentration as follows:

$$E(t) = \frac{d}{dt}\left[\frac{C(t)}{C_0}\right] \quad (3.6)$$

Residence time distribution (RTD) analysis was first used by Shook (2003) to describe the flow and storage geometry of flow paths. In this work, the flow and storage capacity for each carbonate rock type were computed as follows:

$$\varphi(t) = \int_0^t E(t)t\,dt \Big/ \int_0^\infty E(t)t\,dt \quad (3.7)$$

$$F(t) = \int_0^t E(t)dt \Big/ \int_0^\infty E(t)dt \quad (3.8)$$

3.4 TRACER EXPERIMENTS

3.4.1 Objectives

Large set of cores were drilled for each carbonate rock type. Tracer experiments were conducted on all of them and the results of the tracer experiments were used as a screening criteria to select cores for acid experiments. Cores from each carbonate rock

type that exhibit similar tracer concentration profile are selected for acid experiments so that each carbonate rock type is represented by one tracer concentration profile.

The other two objectives of tracer experiments are to: 1) understand the effect of carbonate pore structure on the fluid flow through porous media so the outcomes of this study can be used to explain the difference in the response of different carbonate rock types to the acid treatment; 2) develop a new method based on tracer experiments results for quantification of carbonate pore scale heterogeneity so that the response of different carbonate rock types to acid treatment can be correlated to the pore structure.

3.4.2 Core Preparation

Large set of cylindrical cores of 1.5-in. in diameter and 6-in. in length were drilled from each carbonate rock type. Six calcite carbonate rock types and two dolomite carbonate rock types were studied in this research. The calcite rocks include: Indiana Limestone, Austin Chalk, Edwards Yellow, Winterset, Pink Desert, and Edwards White. The dolomite rocks include: Homogenous and Vuggy dolomites. The large blocks were obtained from Bedford, Edwards Plateau and Kansas formations, respectively. The drilled cores were placed in an oven at 230°F for 24 hours and then weighed to get the dry weight. The cores were then saturated under vacuum for other 24 hours in deionized water and then weighed to get the wet weight. The pore volume and porosity were determined from the difference between the two weights.

Computed Tomography (CT) measurements were used to select cores for tracer experiments. In this technique, an X-ray beam from the CT scanner is attenuated when it is passed through the carbonate sample. The attenuation depends on the density of the

minerals and can be calibrated to the bulk density of rock. Volume units in the tomograph are called voxels. In this work, the voxel size in the x- and y-directions (in-slice) were 0.293 mm, (which was improved to 0.166 mm in some samples after reconstructing) and the slice distance in the z-direction varies from 0.5 mm to 1 mm.

CT measurement is a useful technique to identify core scale heterogeneities. If significant core scale heterogeneities were found in a core sample, it was not used for tracer tests. Features like laminations, faults and fractures can easily be identified from a CT scan and shows the usefulness of the techniques in identifying core scale heterogeneities.

3.4.3 Experimental Setup

Fig. 3.3 shows a schematic diagram of the coreflood setup used for the tracer experiments. The coreflood setup included a core holder, accumulators, a syringe pump, a hydraulic pump, and a differential pressure transducer to monitor the pressure drop across the core. The core holder made of Hastelloy C276, a corrosion resistant material. It is capable of withstanding a working pressure of 3000 psi and temperature of about 300°F. The core holder comes with the regular inlet and outlet tip with ports 1/8″ and the distribution pattern to contact the total face area of the core; inside the cylinder a special temperature resistant rubber, Viton sleeve has been adapted to confine the core once in use. During the coreflood experiment, the overburden pressure was kept at least 300 psi above the initial core inlet pressure so that the fluid did not bypass the core. The tracer fluid was stored in an accumulator and was injected at the desired rate using syringe

pump. A Teledyne ISCO D500 precision syringe pump, which has a maximum allowable working pressure equal to 2000 psi, was used to inject the tracer fluid inside the core. A back pressure of 500 psi was set during the tracer experiment. This backpressure was applied using pressure-regulated nitrogen tanks and backpressure regulators, which did not allow fluid to flow unless the core outlet pressure equals the applied backpressure. Pressure drops were monitored using differential pressure transducers with varying ranges. The data were recorded using a data acquisition system and commercial software (LabView)on a personal computer. The tracer effluent samples were collected at predetermined time intervals.

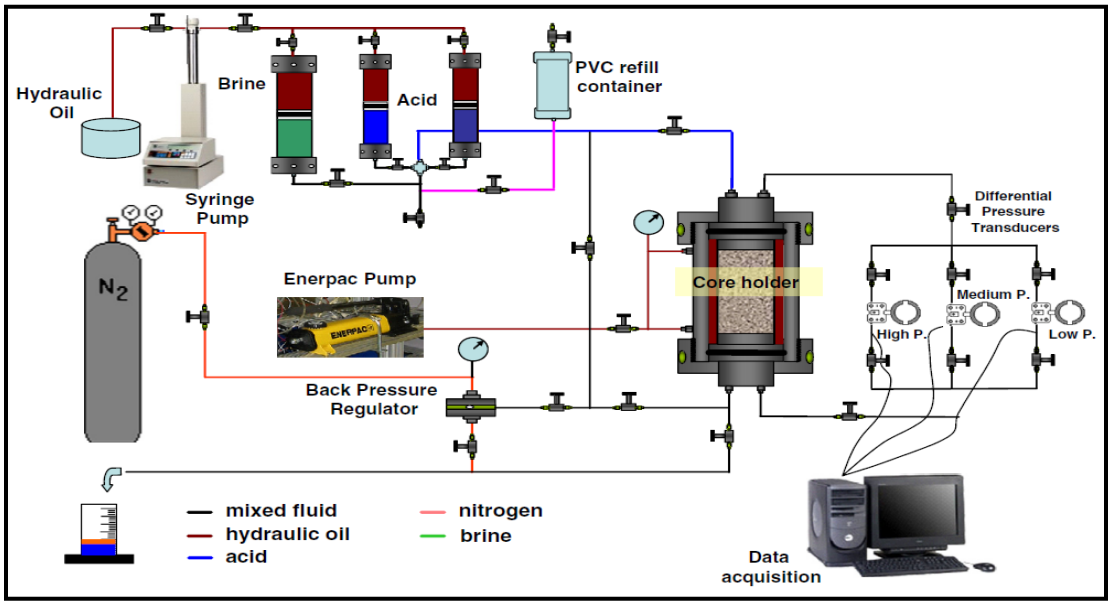

Fig. 3.3—Coreflood setup used for tracer experiments.

3.4.4 Tracer Test Design

3.4.4.1 Tracer Fluids

Tracer Fluid 1: A brine solution of 8 wt% potassium chloride (KCl) (ACS Reagent, >99 wt%). The concentration of potassium ions in the tracer solution was measured by Inductively Coupled Plasma Spectrometer and the measurement was repeated three times to give an average concentration of 36.70 ± 0.05 g/l.

Tracer Fluid 2. A mixture of polymer and 8 wt% potassium chloride (KCl) (ACS Reagent, >99 wt%) was used as a conservative tracer. The polymer type and concentration were selected based on rheological measurements as discussed in details in chapter V.

3.4.4.2 Experimental Procedure

Prior to commencing the tracer experiments, the cores for each carbonate rock type were saturated with deionized water under vacuum, and then preflushed with deionized water. The tracer fluid was then injected into the cores for six pore volumes. Core effluent samples were collected and analyzed by inductively coupled plasma (ICP-OES) for K^+ ion concentration.

3.4.4.3 Tracer Sampling

The core effluent samples were collected at a predetermined time intervals. The time interval was set based on the expected tracer concentration profile. It was found that as the carbonate pore structure is more heterogeneous based on thin section observation, the time interval becomes shorter. For Indiana limestone and homogenous

dolomites, the interval time was set to be each 0.25 pore volume injected. For other carbonate rock types, the time interval was set to be each 0.125 pore volume injected.

Optima 8300 ICP-OES Spectrometer, **Fig. 3.4**, to analyze core effluent samples for the total potassium ion concentrations was used. Knowing the total amount of potassium ions injected, the volume and the potassium ions concentration for each collected sample, the adsorption for potassium ions in the carbonate cores was determined. It was found that the adsorption of the ions on the carbonate rock surface was negligible and did not affect the tracer experiments results.

Fig. 3.4—Inductively Coupled Plasma Spectrometer.

3.4.4.4 Dead Volume Contributions

A simple steady-state flow test using tracer fluid was used to determine the amount of dead volume in the tubing and fittings in the experimental setup shown in **Fig. 3.3**. The tracer fluid used for dead volume calculations is 8 wt% potassium chloride. First, the core was removed from the setup leaving only the dead volume in the system. Then, the tracer fluid was injected throughout the setup at flow rate of 5 cm^3/min. The potassium ions concentration in the tracer effluent samples were measured using inductively coupled plasma spectrometer. The breakthrough time for the potassium ions concentration was determined. Thereby, the dead volume in the system was calculated at 20.5 cm^3. In addition, we needed to calculate the temporal variance of the mean residence times in the dead volume. The value of the variance of the mean residence times in the dead volume was calculated as 0.3 sec^2.

Typically, the values of temporal variance in the cores were higher than 200 sec^2. Hence, It was concluded that the tracer dispersion in the tubings and fittings was negligible compared to the core samples and could be ignored.

CHAPTER IV

PREDICTING THE PERFORMANCE OF THE ACID STIMULATION TREATMENTS IN CARBONATE RESERVOIRS USING NON-DESTRUCTIVE TRACER TESTS

Carbonate formations are very complex in their pore structure and exhibit a wide variety of pore classes, such as interparticle porosity, moldic porosity, vuggy porosity, and microporosity. Geologists have defined carbonate pore classes based on sedimentology, thin sections, and porosity-permeability relationships, but the question remains as how these pore classes govern the acid fluid flow through porous media.

Core samples from six different carbonates, mainly limestone, were selected for the study. The samples were first investigated using thin-section analysis, high pressure mercury injection tests, and nuclear magnetic resonance measurements for pore structure characterization, and X-ray diffraction for mineralogy examination. Next, tracer experiments were conducted and the tracer concentration profiles were analyzed to quantify the carbonate pore-scale heterogeneity. The heterogeneity is expressed using a parameter f—the available fraction of pore structure contributing to the flow. The data was used to study the flow of acid fluid through the porous media of carbonate rocks and correlate the carbonate pore classes to the acid response.

More than 30 acid coreflood experiments were conducted at 150°F and HCl concentration of 15 wt% on 1.5 in. x 6 in. core samples at different injection rates on each carbonate rock type. The objective of these sets of experiments was to determine

the acid pore volume to breakthrough for each carbonate pore class.

Findings in this study help to connect the results from different characterization methods to the acid fluid flow through the porous media of carbonate rocks. It was also found that the response of the acid depends on the carbonate pore classes. Applications to the design of matrix acid treatments in carbonate rocks are discussed.

4.1 INTRODUCTION

The goal of acid-stimulation treatments in carbonate reservoirs is to remove or bypass the formation damage by creating high-conductivity channels known as wormholes. The shape and structure of these wormholes depend on the injection rate. Hoeffner and Fogler (1988) conducted a set of linear core experiments to study the effect of the injection rate on the wormhole pattern and the results are very similar to those obtained by Daccord and Lenormand (1987). The wormhole pattern formation is governed by a competition of axial convection, transverse diffusion, and reaction mechanisms. At low injection rates, the movement of the reaction front is suppressed by the transverse dispersion and face dissolution occurs (Panga et al. 2005). As the injection rate increases, the dissolution pattern changes from face dissolution to wormhole. Uniform dissolution pattern occurs at high injection rates. Hoefner and Fogler (1989) showed that the transition from one pattern to another depended on the Damköhler number (the ratio of acid reaction rate to acid transport by convection).

The initiation of wormholes occurs when the live acid penetrates into pores present in carbonate rocks and then pore structure evolution occurs. The process is more

efficient when only the large pores in the matrix lead to wormholes (Huang et al. 2000). Carbonate formations are very complex in their pore structure and exhibit multiporosity such as intergranular, microporosity, vuggy, and moldic porosity.

Several attempts have been made to study the effect of carbonate pore structure on flow behavior including the work of Xu et al. (1998); Hidajat et al. (2004); and Bretz et al. (1988). However, all these studies focused on non-reactive flow. A few studies have been reported on the effect of pore structure on carbonate stimulation treatments. Huang et al. (2000) defined a critical pore size in carbonate rocks, at which the reaction mechanism changes from mass transfer to reaction rate controlled. They developed a model to predict the acid optimal flux in the field based on pore size distribution and other treatment variables.

Ziauddin and Bize (2007) studied core samples from eight different carbonate rocks and classified them into a Reservoir Rock Type (RRT) based on the results obtained from different characterization methods. They found that the response of the carbonate rock to acid depends on the RRT it belongs to.

Izgec et al. (2010) conducted experimental and theoretical studies to investigate the flow of regular 15 wt% HCl acid in vuggy carbonates. They studied the acidization of vuggy carbonates with high resolution computerized tomography imaging, image processing, geostatistical characterization, acid coreflood experiments with 4 in. by 20 in. cores, and numerical simulation. Their experiments showed that the vuggy pores are distributed in a manner that makes the acid propagate more rapidly in vuggy carbonates

compared to homogenous ones. Consequently, less acid volume to breakthrough for vuggy carbonates is required than the homogenous rocks.

In an attempt to predict the performance of acid stimulation treatments in carbonate rocks with respect to their pore structure, the objectives of the present study are to: 1) understand the physics of the acid fluid flow in carbonate rocks at pore scale; 2) quantify the carbonate rock heterogeneity at the pore scale so that the acid response can be correlated to the magnitude of pore scale heterogeneity; and 3) develop a new methodology to predict the acid PV_{bt} using non-destructive tracer test. The approach presented in this chapter is very useful to optimize the acid stimulation treatments by conducting a non-destructive tracer test in the field prior to the treatment execution.

4.2 CHARACTERIZATION OF CARBONATE ROCK TYPE

4.2.1 Cores Selection

Six cylindrical cores of 1.5-in. diameter and 6-in. length were drilled from each carbonate rock type. Six carbonate rock types were studied: Indiana Limestone, Austin Chalk, Edwards Yellow, Winterset, Pink Desert, and Edwards White. The large blocks were obtained from Bedford, Edwards Plateau and Kansas formations, respectively. The drilled cores were weighed dry and after saturation. Pore volume and porosity were determined from these measurements. **Table 4.1** lists the properties of the cores for each carbonate rock type.

Table 4.1–Range of Core Properties			
Rock Type	Pore Volume (cm^3)	Porosity (vol%)	Permeability, md
Indiana Limestone	23-25	13-15	60-65
Edwards Yellow	32-38	18-22	53-62
Austin Chalk	25-35	14-20	19-22
Winterset Limestone	35-45	20-26	3-4
Pink Desert	40-48	23-28	75-82
Edwards White	32-37	18-21	3-5

4.2.2 XRD and XRF Analyses

To solely study the effect of pore-scale heterogeneity on carbonate stimulation treatments, X-ray diffraction was conducted for mineralogy examination **(Table 4.2).** X-ray fluorescence analysis was also conducted to determine the elemental composition of the carbonate rock types used in this study **(Table 4.3)**. All studied carbonates are more than 98% calcite, almost the same composition and clean from clays, therefore the difference in their response to acid stimulation treatments is because of the difference in their pore structure.

Table 4.2—XRD Composition in Percent for the Carbonate Rock Types Used in this Study						
Mineral	Winterset	Indiana Limestone	Edwards Yellow	Pink Desert	Edwards White	Austin Chalk
Calcite	98.1	98.6	99.1	98.5	99.1	98.9
Dolomite	—	0.7	—	—	—	—
Quartz	1.9	0.7	0.9	1.5	0.9	1.1

Table 4.3—XRF Composition in Percent for the Carbonate Rock Types Used in this Study					
Element	Winterset	Indiana Limestone	Edwards Yellow	Pink Desert	Edwards White
Ca	68.1	69.1	69.8	70.7	70.1
O	29.4	28.8	28.7	28.6	28.7
Mg	0.345	0.854	0.599	—	—
Fe	0.76	0.0584	0.164	0.113	0.272
Si	0.48	0.225	0.105	0.129	0.287
K	0.253	0.285	0.217	0.095	0.193
Al	0.24	0.185	0.206	0.172	0.23
Mn	0.0553	0.012	—	0.0184	0.0125
Cl	0.156	0.275	0.146	0.0155	0.0327
Sr	0.154	0.0574	0.0606	0.0465	0.0663
Sn	0.0228	0.0224	0.026	0.0251	0.0237
Ti	0.0183	—	—	—	—
S	—	0.113	—	—	—

4.2.3 Thin Section

Blue epoxy impregnated thin sections were prepared to obtain a detailed description of the types of porosity, the connectivity of pores, fabric, and texture to assess the pore-scale heterogeneity. The thin section was viewed under an optical microscope. Images for each rock sample were captured at 2.5 and 10X magnifications using a digital camera and a personal computer.

4.2.4 High Pressure Mercury Injection

High pressure mercury injection tests were performed on all carbonate rock types using the Micrometrics AutoPore IV 9520 mercury porosimeter. Mercury was injected at multiple pressures up to 60,000 psi. The volume of the mercury injected at each pressure increment was automatically recorded until the maximum pressure was achieved. The median pore throat diameter size is defined as the pore throat diameter at 50% of mercury intrusion during the experiment. **Table 4.4** shows the median pore throat diameters for the carbonate rock types.

Table 4.4–Mercury Injection Capillary Pressure Results for Different Carbonate Rock Types		
Rock Type	Mercury Entry Pressure (psi)	Median Pore Throat Diameter (μm)
Indiana Limestone	4.45	16.04
Edwards Yellow	12.69	6.95
Austin Chalk	33.90	1.64
Winterset Limestone	57.17	1.52
Pink Desert	18.15	6.44
Edwards White	67.49	1.11

4.2.5 Nuclear Magnetic Resonance Measurements

Nuclear magnetic resonance (NMR) experiments were performed using a MARAN low field (2 MHz) hydrogen magnetic resonance instrument. The T2distributions were computed by evaluating the Carr-Purcell-Meiboom-Gill (CPMG) measurements. The inter-echo spacing used in these experiments was 600 μsec and the delay time was 10 seconds. The NMR of the fully brine saturated samples was measured in this study.

4.3 COREFLOOD EXPERIMENTS

4.3.1 Tracer Experiments

A brine solution of 8 wt% potassium chloride (KCl) (ACS Reagent, > 99 wt%) was used as a conservative tracer. The solution was injected for five pore volumes on each core before acidizing. Prior to commencing the tracer injection, the core was

saturated with deionized water under vacuum, and then preflushed with deionized water. Core effluent samples were collected and each sample was analyzed by Inductively Coupled Plasma (ICP-AES) for K^+ ions concentration measurements. The tracer concentration at each point was plotted versus the cumulative pore volume injected.

Tracer experiments were conducted on different cores for each carbonate rock type to select similar cores and represent each rock type with a single effluent concentration curve. The relationship between the observations from thin section and tracer experiments results is presented.

4.3.2 Pore Volume to Breakthrough Experiments

Fig. 4.1 shows the schematic of the coreflood setup used in this study. The coreflood setup includes a core holder, three accumulators, a syringe pump, a hydraulic pump and a differential pressure transducer to monitor the pressure drop across the core. A Teledyne ISCO D500 precision syringe pump, which has a maximum allowable working pressure equal to 2000 psi, was used to inject acid inside the core. A back pressure of 1100 psi was set to keep most of the carbon dioxide in the solution. Acid PV_{bt} experiments are destructive so the tracer experiments were conducted before acid injection on different cores for each carbonate rock type to select similar cores. Prior to commencing the acid injection, deionized water was injected at different flow rates at room temperature to measure the core permeability **(Table 4.1)**. During injection, an overburden pressure at least 300 psi higher than the inlet pressure was kept to prevent the fluid from bypassing the core. The water injection continues during heating the

system to 150ºF. The acid (15 wt% HCl and 1 vol% corrosion inhibitor) was then injected until breakthrough while the pressure drop was monitored across the core. The acid was injected at rates of 1, 2, 5, and 7 cm^3/min.

Two more injection rates of 0.5 and 15 cm^3/min were added for some carbonate rock types. At breakthrough for each rate, the acid injection stopped and deionized water was injected until the pressure drop stabilized.

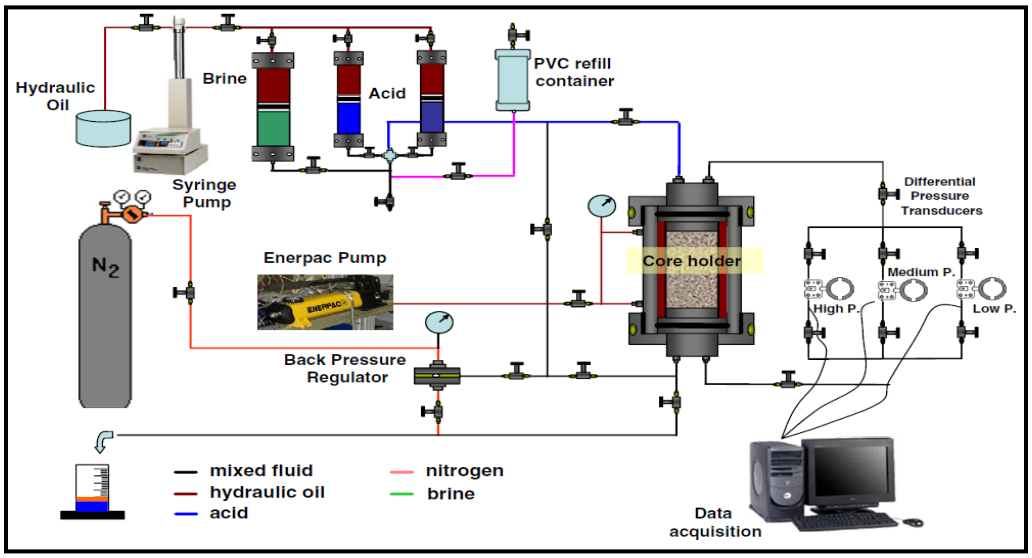

Fig. 4.1—Coreflood setup used in the study.

4.4 RESULTS AND DISCUSSION

4.4.1 Characterization of Carbonate Rock Type

The pore structure and pore scale heterogeneities for carbonate rocks were examined using thin section analysis, nuclear magnetic resonance (NMR), and mercury injection capillary pressure (MICP) measurements.

Indiana Limestone. Fig. 4.2a shows the pore structure image of Indiana Limestone. It is a grainstone composed of predominantly pellets, moderately rounded skeletal grains, ooids, and shell fragments. Skeletal diversity is good with common amounts of crinoids and bryozoans, algal grain, gastropods, and pelecypods.

Equant spary calcite crystals commonly cement the grains. The pore system is dominated by intergranular pores that appear well connected. A few moldic pores are also noted in partially leached grains. **Fig. 4.3a** shows the T2 distribution from NMR measurements. The figure suggests a bimodal pore system which indicates medium to large pores between the grains**. Fig. 4.4a** shows wide pore throat size distribution for Indiana Limestone which reflects the medium to large size intergranular pores. This agrees well with thin section analysis and NMR T2 distribution. Indiana limestone is characterized by a high storage capacity and good permeability.

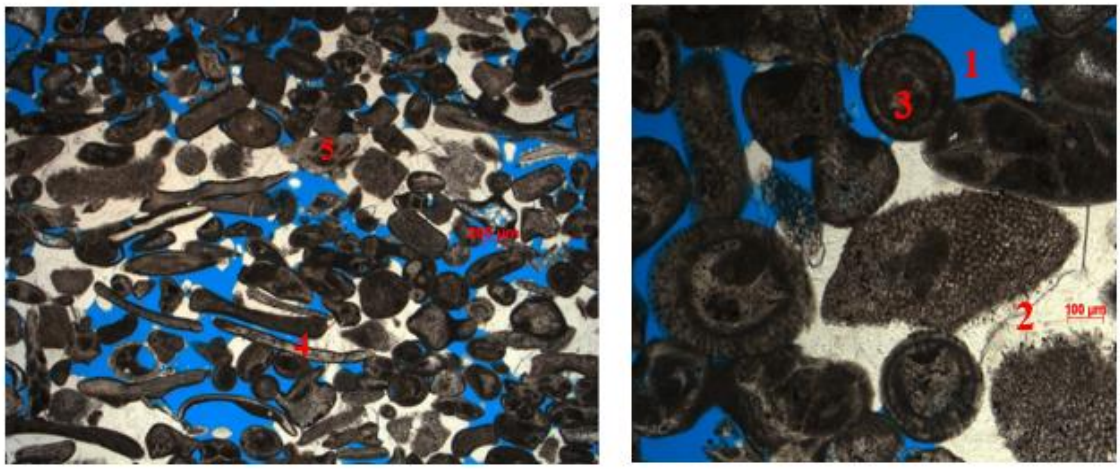

2.5X Magnification 10X Magnification

Fig. 4.2 (a)—Thin section images at 2.5X and 10X magnification for Indiana Limestone. (1) pore openings; (2) calcite cement; (3) ooids; (4) pellets; (5) shell fragment. Thin section shows well connected intergranular pores.

Austin Chalk. Fig. 4.2b shows the pore structure image of Austin Chalk. It is a grainstone composed of pelloids, skeletal grains, and ooids. The grains are cemented by equant calcite spar cement.

Intergranular porosity is the dominant pore system while some moldic and micropores were formed in partially leached grains. **Fig. 4.3b** shows the T2 distribution from NMR measurements. The figure shows a large area under the T2 relaxation curve between 0.01 and 1 sec. This area of faster T2 relaxation time indicates the very small size of the pores between the grains when compared to Indiana limestone carbonate rock type. Austin Chalk has pore throats ranging between 1 to 10 μm with a skewing of smaller pore throat sizes **(Fig. 4.4b)**. This corresponds to very-small-sized intergranular pores with fine and micropores.

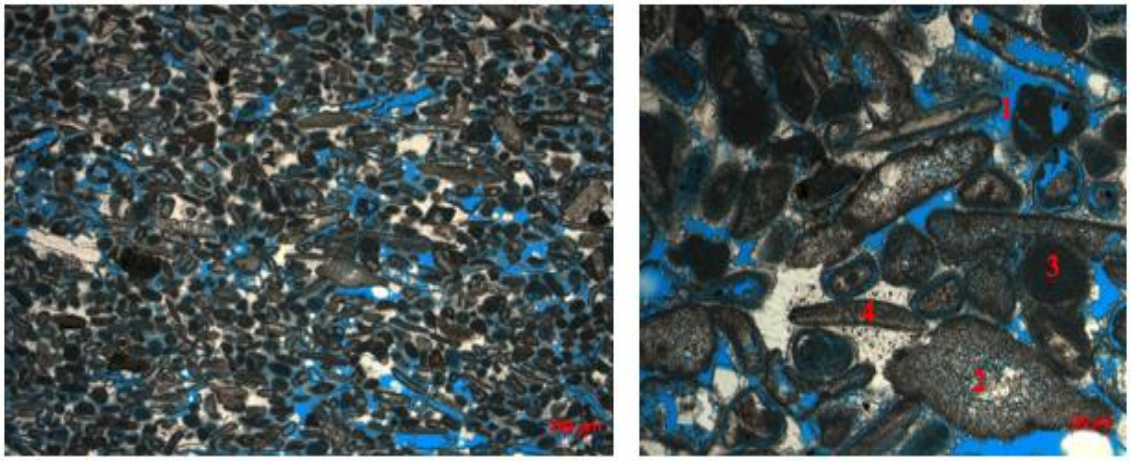

2.5X Magnification 10X Magnification

Fig. 4.2 (b)—Thin section images at 2.5 and 10X magnification for Austin Chalk. (1) intergranular pore openings; (2) moldic pore openings; (3) ooids; (4) pelloids. Dark color indicates grains. White color indicates cement. Thin section shows good connected intergranular pores.

Pink Desert. Fig. 4.2c shows the pore structure image of Pink Desert. It is a good example of mixed fossil grainstone that has undergone moldic dissolution followed by calcite cement fill. The pore structure is dominated by moldic porosity and consequently it is not well connected as in Indiana Limestone. Calcite cement fills the primary intergranular pores and some of the moldic porosity.

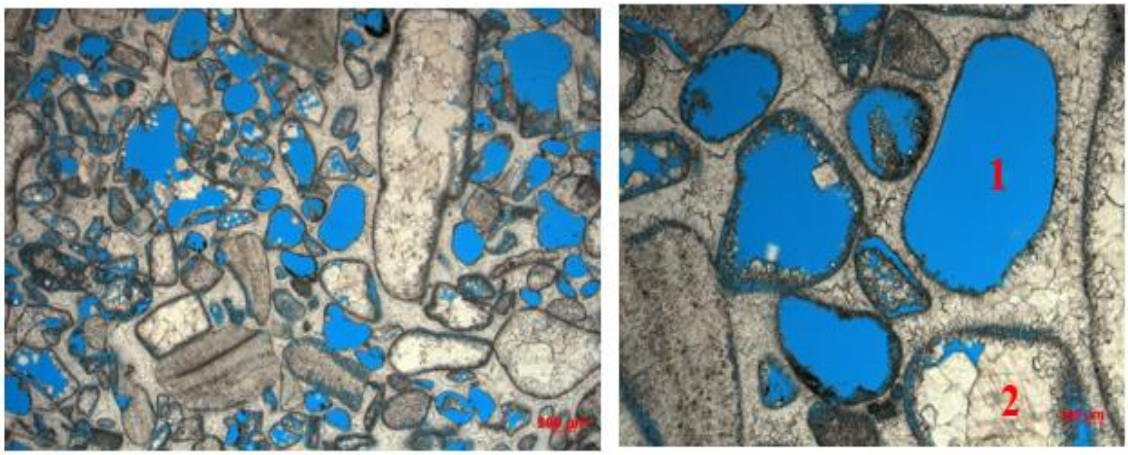

2.5X Magnification 10X Magnification

Fig. 4.2 (c)—Thin section images at 2.5 and 10X magnification for Pink Desert. (1) moldic pore openings; (2) calcite cement fill. Thin section shows moldic pores dominated structure.

Edwards Yellow. Fig. 4.2d shows the pore structure image of Edwards Yellow. It is a skeletal grainstone. The pore system is composed of moldic porosity formed by leaching of fossils and intergranular porosity. Such rock has good moldic-pores connectivity through the intergranular porosity.

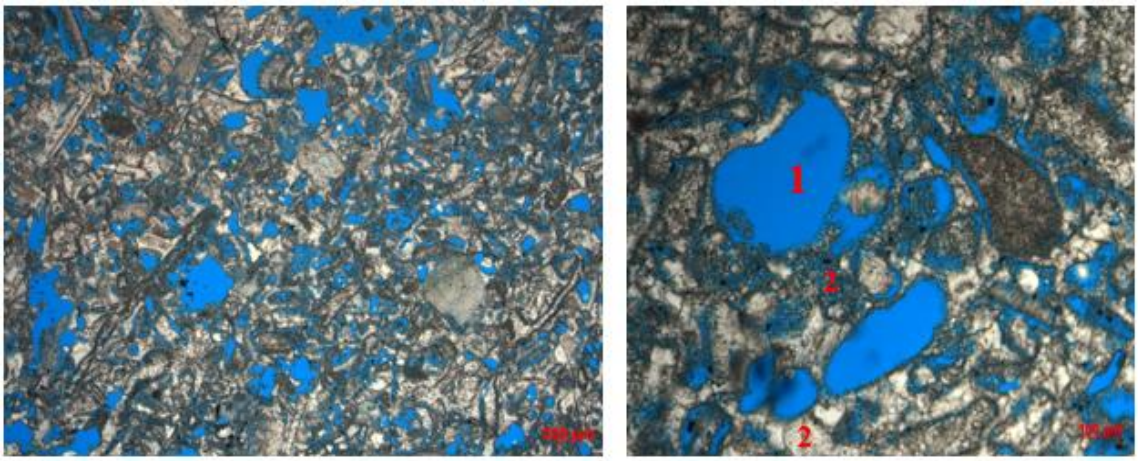

2.5X Magnification 10X Magnification

Fig. 4.2 (d)—Thin section images at 2.5 and 10X magnification for Edwards Yellow. (1) moldic pore Openings; (2) grain fragments. Thin section shows moldic pores connected through intergranular porosity.

Fig. 4.3c and 4.3d shows the T2 distribution from NMR measurements for Pink Desert and Edwards Yellow carbonate rock types respectively. The figure shows that both rocks had unimodal pore system (moldic porosity dominated pore structure). However, Edwards Yellow had larger moldic pores than Pink Desert. The pore throat size distribution dominated by large diameter of pore throats agrees well with thin section analysis and T2 distribution **(Fig. 4c and 4d)**.

Winterset. Fig. 4.2e shows the pore structure image of Winterset. It is an oolitic grainstone that has undergone complete porosity inversion by leaching of original ooids and forming moldic porosity. The diagenesis led to complete filling of the primary intergranular porosity by blocky sparite calcite cement. Although porosity remained high, permeability was substantially reduced because the moldic pores are poorly connected. **Fig. 4.3e** shows the T2 distribution from NMR measurements. The figure

shows broad bimodal pore system. The area of the slow T2 relaxation time corresponds to the presence of large moldic pores. The area of the faster T2 relaxation time indicates the tight intercrystalline pores that connect the large moldic pores. The tight intercrystalline pores dominate the pore throat size distribution measuring slightly higher than 1 μm **(Fig. 4.4e)**. Winterset limestone is characterized by high storage capacity and low permeability.

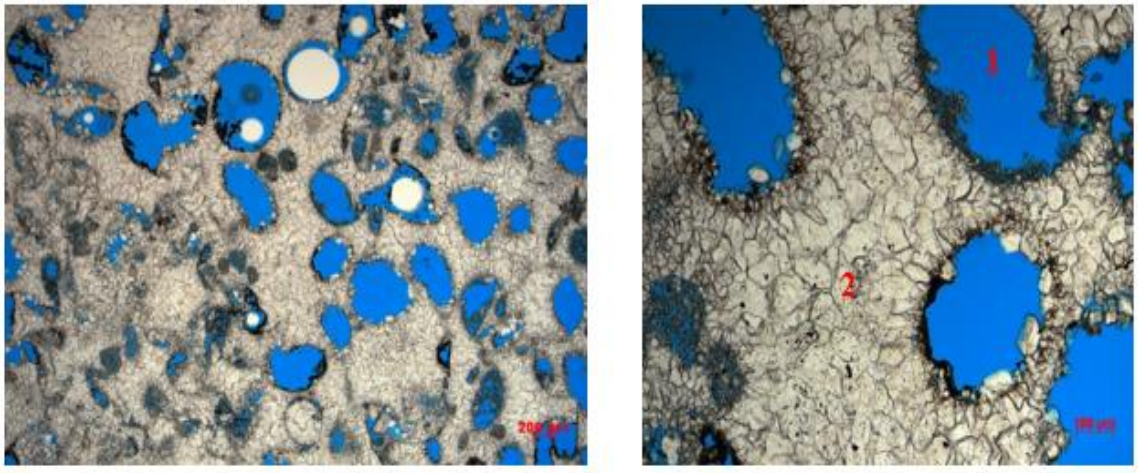

2.5X Magnification 10X Magnification

Fig. 4.2 (e)—Thin section images at 2.5 and 10X magnification for Winterset. (1) moldic pore openings; (2) blocky sparite cement. Thin section shows fairly connected moldic pores.

Edwards White. Fig. 4.2f shows the pore structure image of Edwards White. This is a good example of a planktonic foraminiferal limestone. It has poorly sorted mudstone texture and is predominantly composed of intraclasts, micritized grains, pelecypods, ostracods, ooids and micritized skeletal fragments. Moldic porosity is formed by leaching forams with microporosity within the micritized matrix and fewer intergranular pores. The limestone had a dominant micritic matrix that fills most of the intergranular pores and some of the moldic pores. **Fig. 4.3f** shows the T2 distribution from NMR measurements. The peak on the T2 distribution curve corresponds to the fast T2 relaxation time (around 40 msec) produced by the microporosity within the micritized matrix. The microporosity of Edwards White is reflected by all pore throats measuring around 1 μ **(Fig. 4.4f)**.

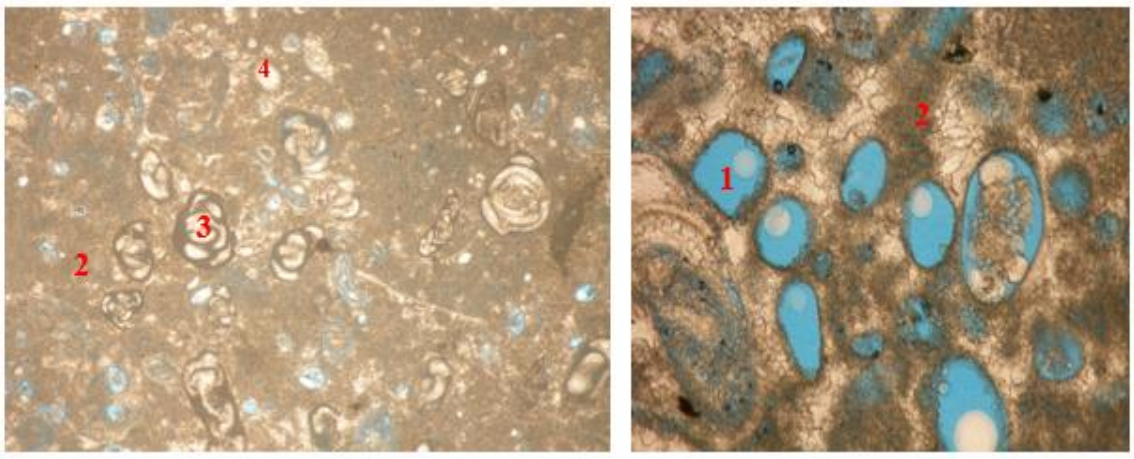

2.5X Magnification 10X Magnification

Fig. 4.2 (f)—Thin section images at 2.5 and 10X magnification for Edwards White. (1) moldic pore openings; (2) micritzed grains; (3) foraminifera; (4) ooids. Thin section shows moldic porosity mudstone rock.

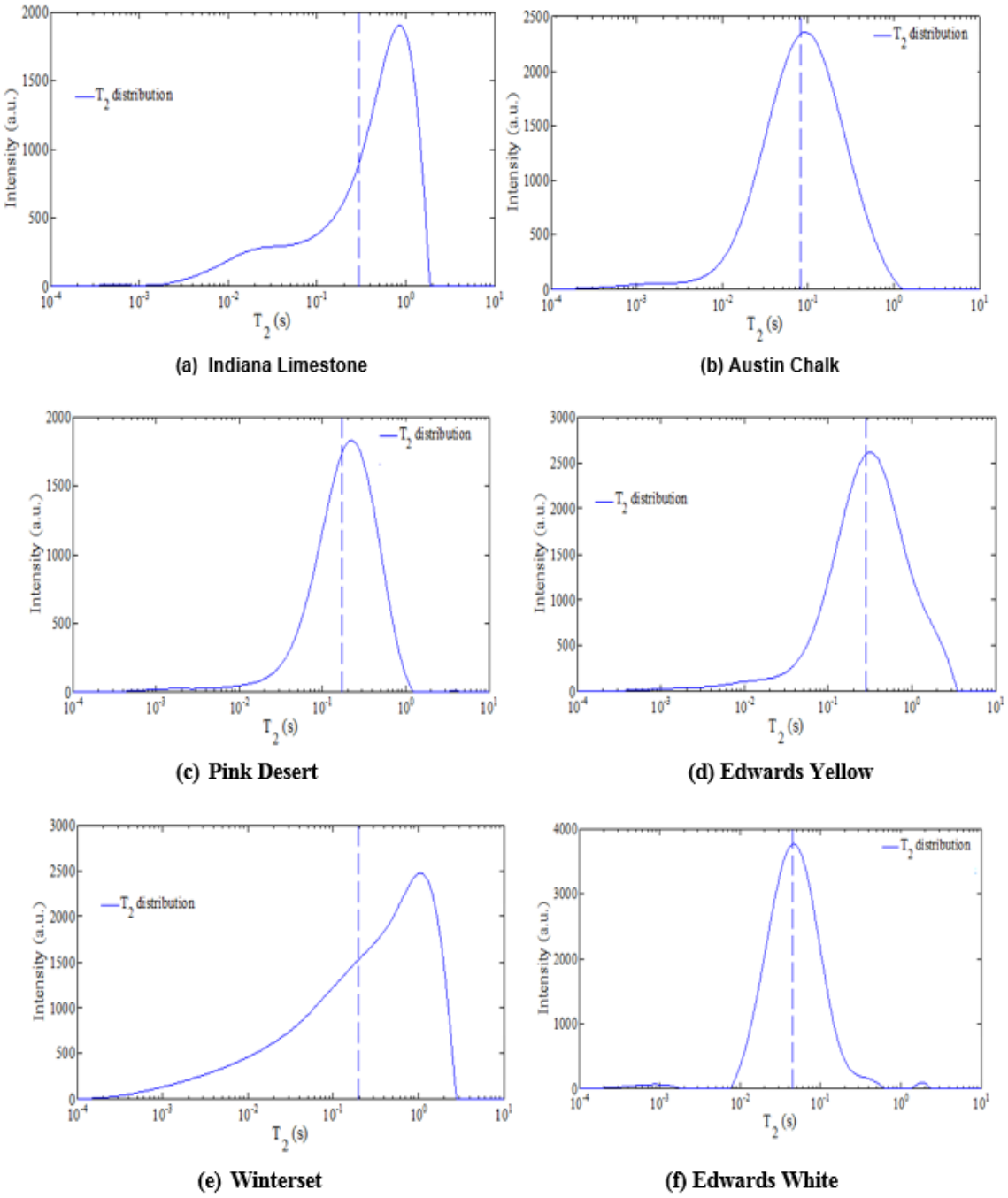

Fig. 4.3—Amplitude of NMR signal plotted against T2 time for (a) Indiana Limestone, (b) Austin Chalk, (c) Pink Desert, (d) Edwards Yellow, (e) Winterset, and (f) Edwards White.

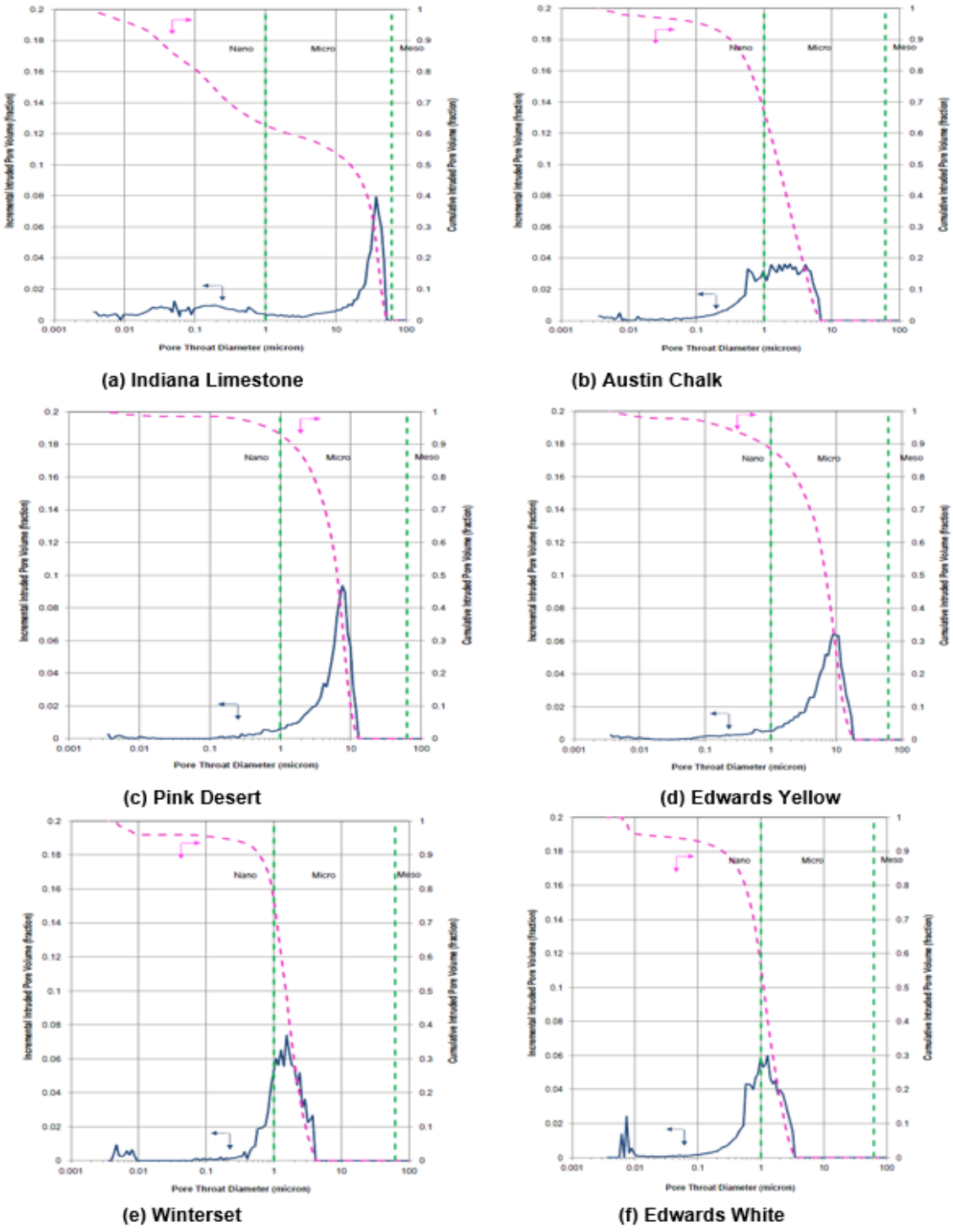

Fig. 4.4—Pore throat size distribution for the carbonate rock types measured using MICP test.

The observations of the thin section supports the existence of preferential flow paths for the tracer fluid in carbonate rock types such as Edward Yellow, Pink Desert and Winterset. The most preferential flow path occurs in Edwards White which led to strongest channeling behavior. Such preferential flow paths do not exist for Indiana Limestone carbonate rock type. Although Austin Chalk exhibits intergranular porosity similar to Indiana Limestone, the pore size is much smaller and the grains are closer to each other. Consequently, it exhibits less connectivity.

4.4.2 Tracer Experiments

The tracer experiments were conducted on each core for each carbonate rock type prior to acid coreflow experiments so that the selected cores to be acidized have almost the same normalized tracer concentration profile. The normalized tracer concentration (C/C_0) in the core effluent samples for different carbonate rock types is plotted as a function of the cumulative pore volume injected **(Fig. 4.5).**

For Indiana limestone carbonate rock type, the tracer concentration profile was found to be symmetrical ($C/C_0 = 0.5$) at one pore volume injected. These results are expected because carbonates of well-connected intergranular pores exhibit a symmetrical profile around 1 PV injection at $C/C_0 = 0.5$ (Skauge et al. 2006). The tracer profile is dominated by a low fraction of inaccessible pores and no capacitance effect (no dead-end pores).

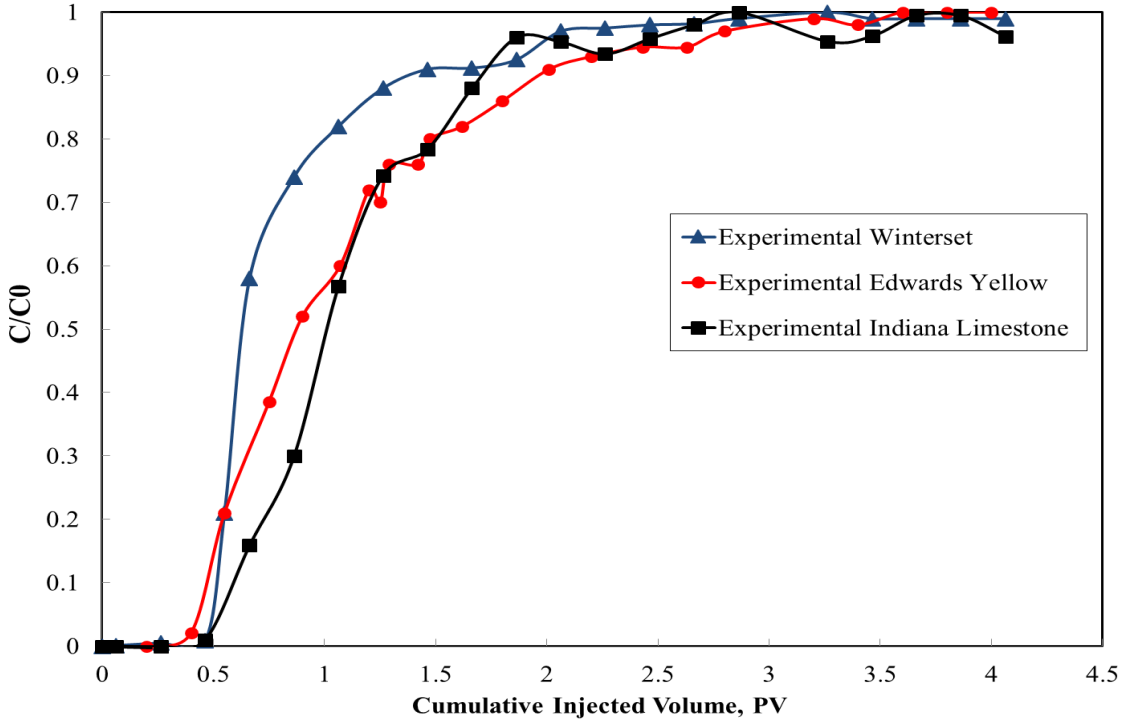

Fig. 4.5 (a)—Tracer concentration profiles for Indiana Limestone, Edwards Yellow, and Winterset carbonate rock types.

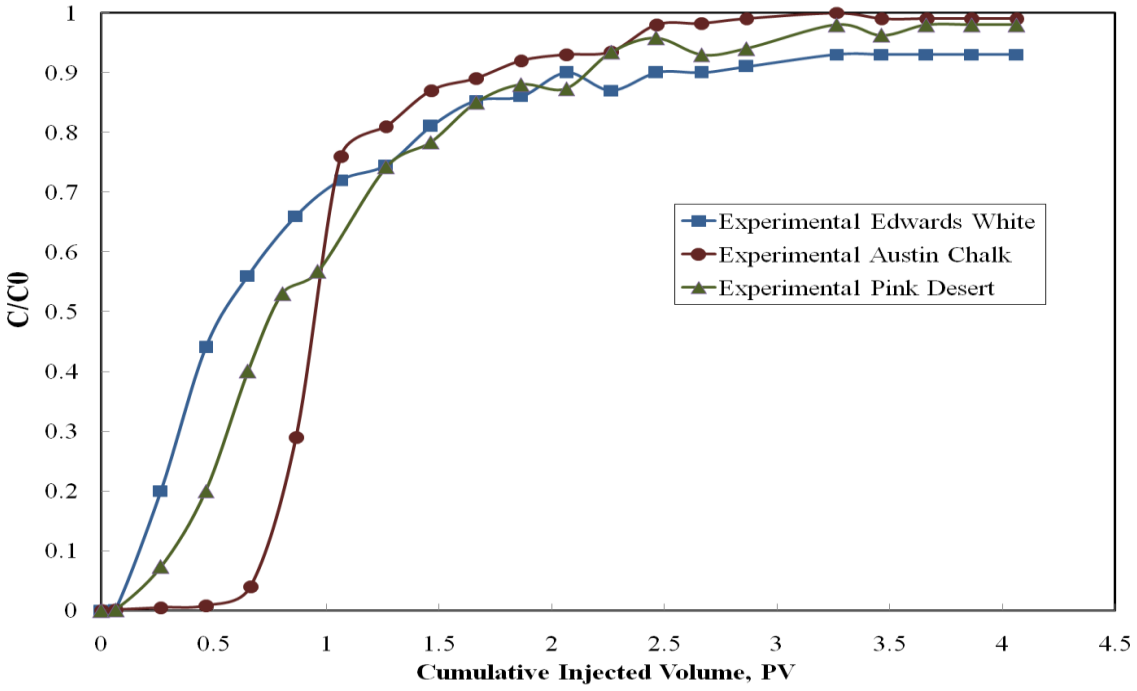

Fig. 4.5 (b)—Tracer concentration profiles for Austin Chalk, Pink Desert, and Edwards White carbonate rock types.

For other carbonate rock types, the pores are not as well connected as for Indiana limestone carbonate rock type. Consequently, it is believed that the fluid flows in a smaller fraction of the pore volume in these carbonates than in well-connected Indiana limestone. The tracer concentration profiles that show an early breakthrough and long tail behavior confirm this hypothesis. The behavior of the tracer concentration profiles is believed to be due to preferential flow paths for the tracer fluid through the porous media. The tracer concentration profiles appear consistent with the observation of thin sections.

4.4.3 Quantification of the Pore-Scale Heterogeneity

As shown in the thin section previously, the pore-scale heterogeneity is introduced as fluctuation in the pores connectivity, variation of porosity types, diversity in the size and shape of pores, and changes in the rock fabric and texture. However, the thin section provides qualitative analysis for the pore-scale heterogeneity. In an attempt to correlate the response of the carbonates to the acid stimulation treatments based on the rock type they belong to, different geological rock typing schemes have been reported in the literature.

For example, Choquette and Pray (1970) emphasize the importance of pore space genesis and the divisions in their classification are genetic, not petrophysical and difficult to correlate to flow properties. Dunham (1962) classification depends on the depositional texture of the carbonate rocks, which is not also appropriate for our study. Lucia (1983) classification may be the most appropriate one as his classification grouped

the carbonates of similar petrophysical properties. However, all these geological classification schemes are still a qualitative analysis.

The magnitude of pore-scale heterogeneity needs to be quantified so that the acid pore volume to breakthrough and the wormhole dissolution pattern can be correlated to the pore-scale heterogeneity. It is believed that the connectivity of the pores, size and shape, rock fabric, and amount of cement strongly affect the flowing fraction of the pore structure measured experimentally from the tracer tests conducted on the carbonate rock types. Hence, the flowing fraction is a practical means to quantify the pore-scale heterogeneity in carbonate rocks. The flowing fraction, in this study, is the cumulative pore volume injected corresponding to the normalized tracer concentration at $C/C_0 = 0.5$ (**Table 4.5)**.

Table 4.5–Flowing Fraction for Different Carbonate Rock Types

Rock Type	Flowing Fraction
Indiana Limestone	1.00
Edwards Yellow	0.91
Austin Chalk	0.92
Winterset Limestone	0.64
Pink Desert	0.73
Edwards White	0.52

4.4.4 Residence Time Distribution

It is expected that the time the tracer remains in each carbonate rock type is different. This time is called the residence time. To obtain the residence time distribution function, we differentiate the normalized tracer concentration as follows:

$$E(t) = \frac{d}{dt}\left[\frac{C(t)}{C_0}\right] \quad \text{(4.1)}$$

Fig. 4.6 shows the computed residence time distribution function for different carbonate rock types. For Indiana limestone, the principal peak occurs at the space time corresponding to one pore volume injected. For other carbonates, the peak occurs at a time shorter than the space time, which indicates early breakthrough for the tracer (i.e., effective pore volume contributing to flow is smaller than the measured pore volume).

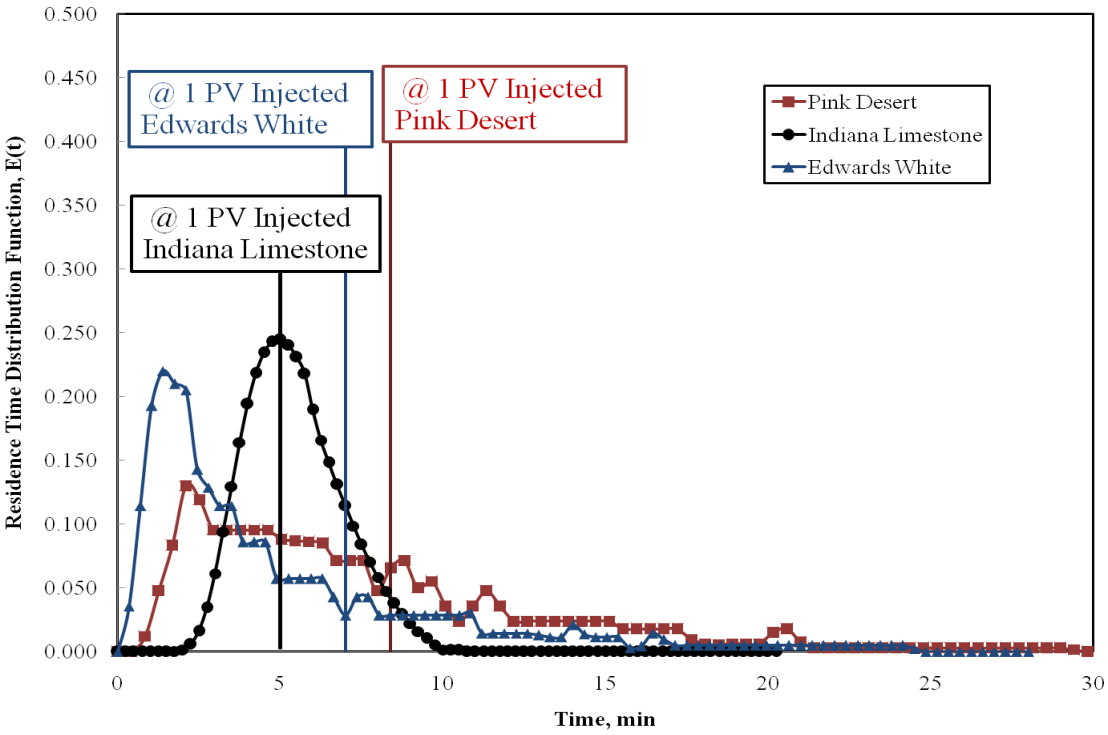

Fig. 4.6 (a)—Residence time distribution function for Indiana limestone, Edwards White, and Pink Desert carbonate rock types.

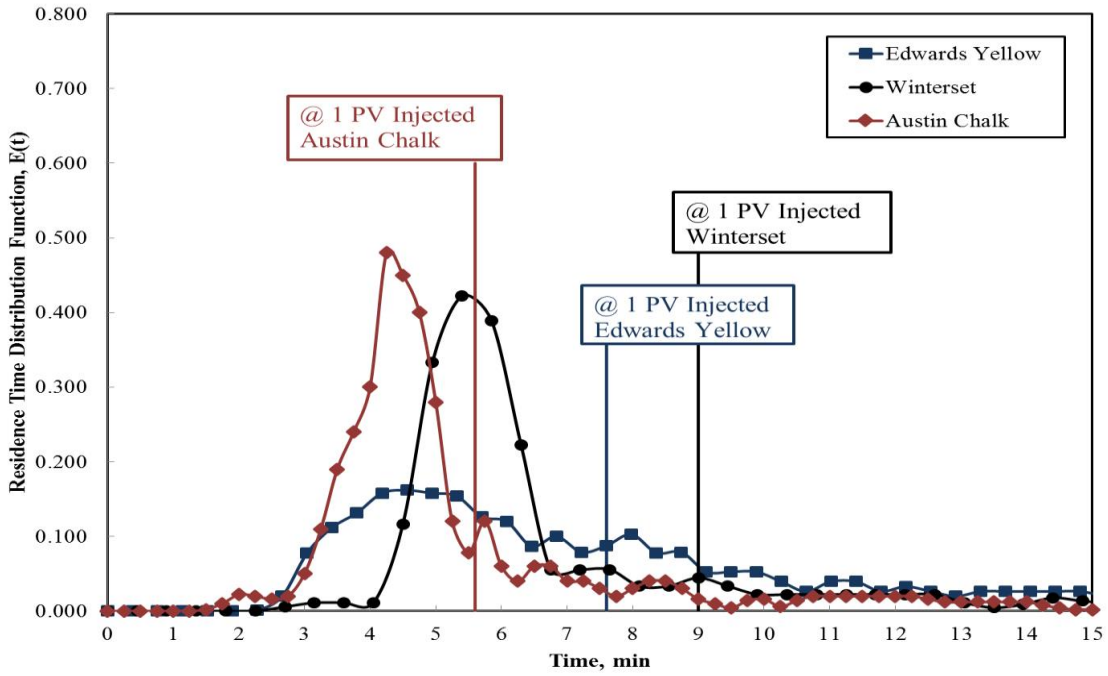

Fig. 4.6 (b)—Residence time distribution function for Austin Chalk, Edwards Yellow and Winterset carbonate rock types.

4.5 FLOWING FRACTION RELATIONSHIP DERIVED FROM MICP AND NMR DATA

The objective in this section is to investigate the correlations between the flowing fraction and the petrophysical parameters obtained from MICP or NMR measurements. The flowing fraction can then be derived from the correlation and the acid stimulation performance can be predicted, if the data from tracer test are not available.

Fig. 4.7a shows a good linear correlation between the median pore throat diameter and the flowing fraction. The correlation suggests that the smaller the median pore throat diameter, the less connectivity between pores and thus the lower the flowing fraction.

It would be more useful to correlate a wire line log measured parameter (NMR T2) than laboratory measured parameter (median pore throat diameter) to the flowing fraction. **Fig. 4.7b** shows a good exponential correlation between the NMR T2 and the flowing fraction. The correlation suggests that the larger T2 (i.e. the larger pore size), the lower the flowing fraction for the carbonate rock type. **Fig 4.7c** shows a poor correlation between the effective to total porosity ratio and the flowing fraction. Effective porosity is estimated from routine core analysis while the total porosity is estimated from NMR measurements. Although the range of data is narrow and it can go beyond this range, for example a vugular carbonate rock type, the slope for the correlation is negative which means that the ratio of the effective porosity to total porosity is no longer a valid parameter to estimate the flowing fraction.

A possible outlier in the correlations is the Austin Chalk sample. This is most likely due to the microporosity in Austin Chalk carbonate rock type.

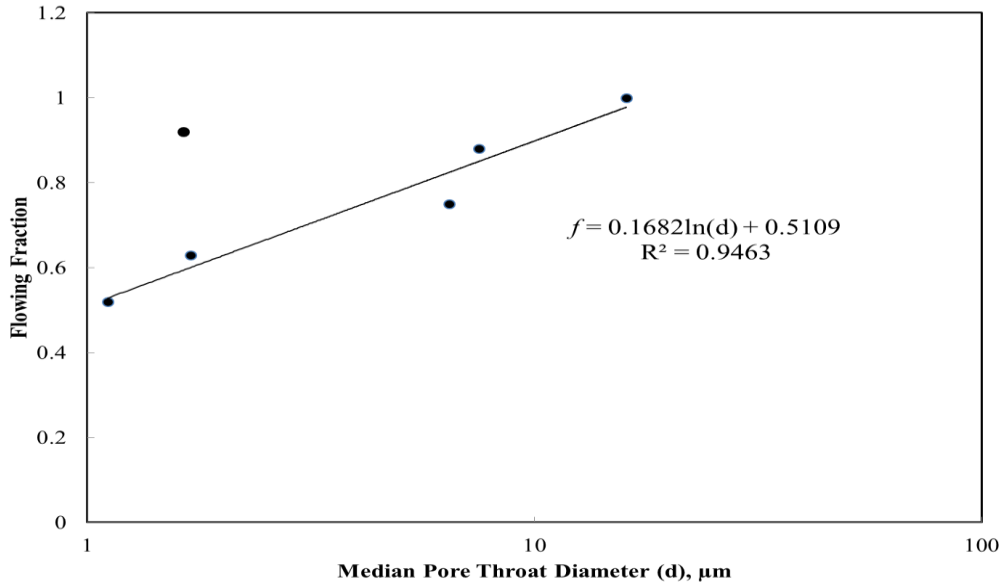

Fig. 4.7 (a)—Crossplot of median pore throat diameter and flowing fraction for six carbonate rock types

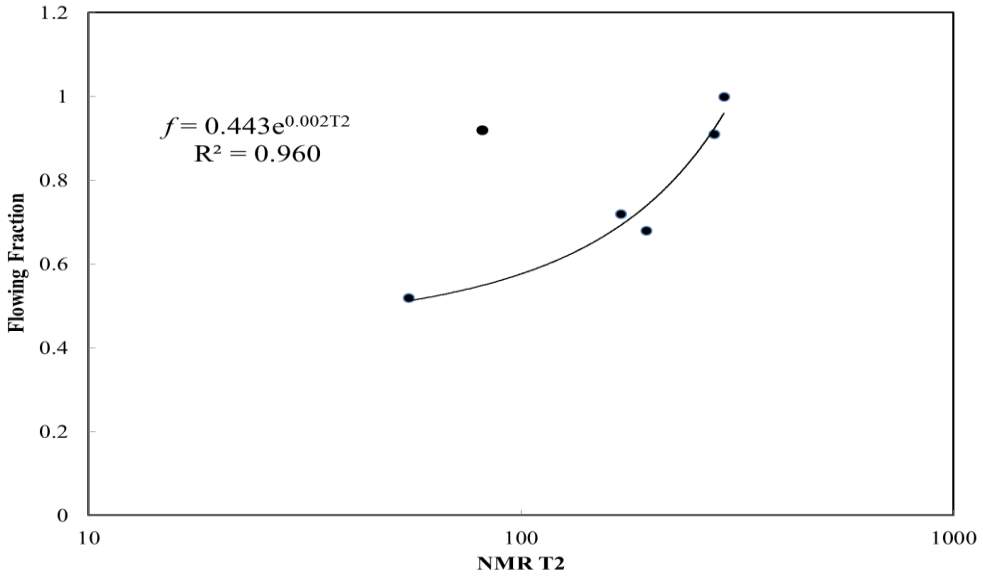

Fig. 4.7 (b)— Crossplot of NMR T2 and flowing fraction for six carbonate rock types.

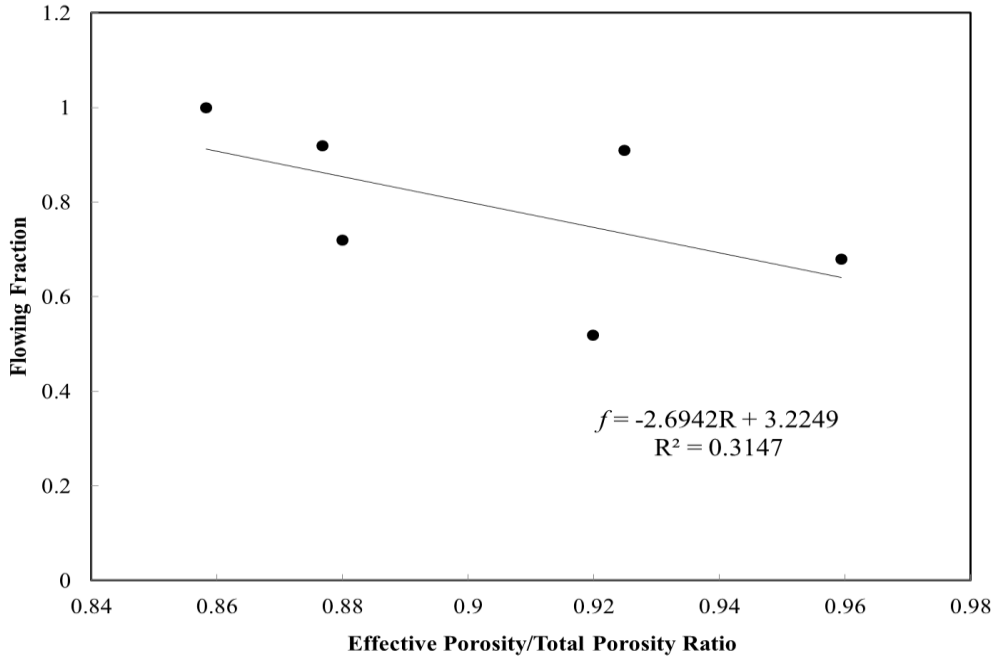

Fig. 4.7 (c)—Crossplot of effective/total porosity ratio and flowing fraction.

4.6 USE OF TRACER TEST TO PREDICT THE ACID PORE VOLUME TO BREAKTHROUGH IN CARBONATE ROCKS

Fig. 4.8 shows the effect of pore-scale heterogeneity on the acid pore volume to breakthrough at different injection rates. For carbonate rock types of higher magnitude of pore-scale heterogeneity, the acid dissolves less rock overall as compared to rock of low magnitude such as Indiana limestone rock type ($f = 1$) which leads to less PV_{bt}. For example, the acid pore volumes to breakthrough for Edwards White carbonate rock type ($f = 0.53$), ranging from 0.6 to 0.38, were observed to be less compared to Indiana limestone carbonate rock type ($f = 1$) with PV_{bt} ranging from 1.4 to 0.82. Acid pore volume to breakthrough strongly depends on how fast the wormhole propagates along the rock. Consequently, the wormhole propagates more rapidly in carbonate rocks of higher magnitude of pore-scale heterogeneity than that in Indiana limestone rock type ($f = 1$).

Fig. 4.9 shows the dependence of the PV_{bt} on the magnitude of the pore-scale heterogeneity at different injection rates. The pore volume to breakthrough decreases with the increase of the magnitude of the pore-scale heterogeneity. The slope of the pore volume to breakthrough-flowing fraction relationship is independent on the injection rate.

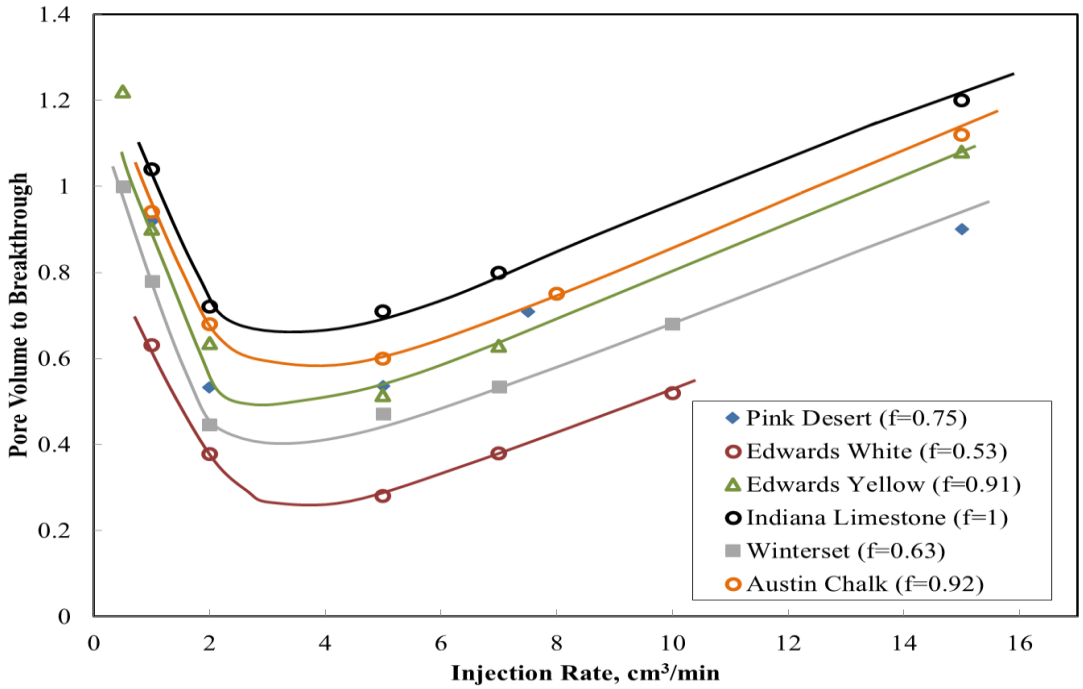

Fig. 4.8—Pore volume to breakthrough as a function of acid injection rate for different carbonate rock types.

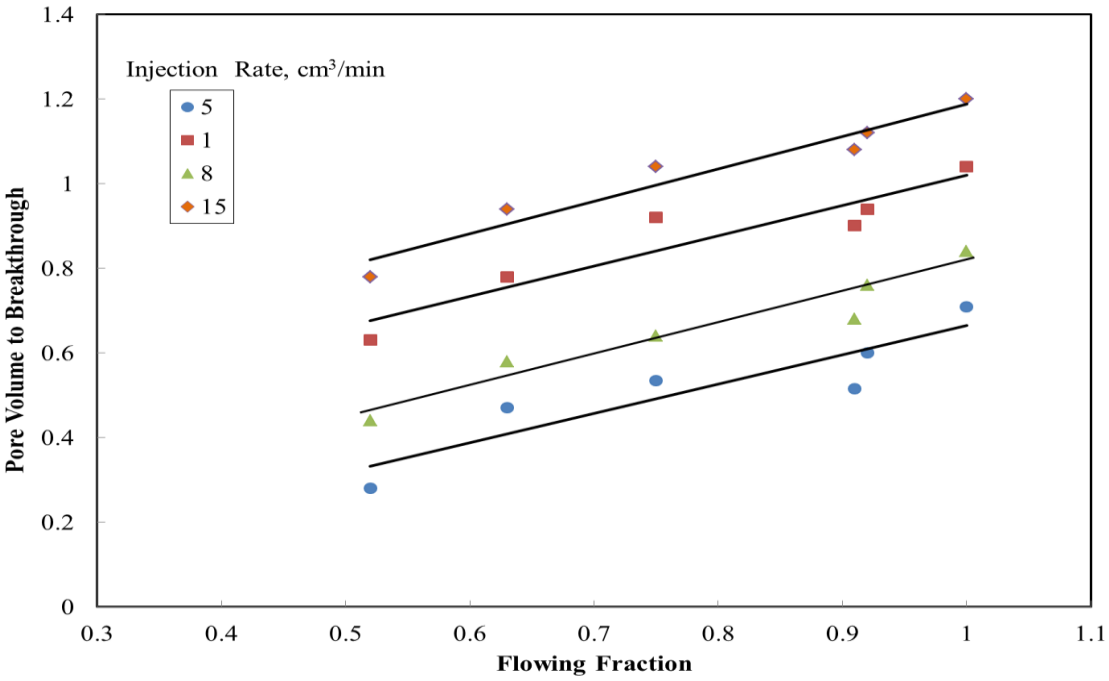

Fig. 4.9—Pore volume to breakthrough as a function of the flowing fraction at different injection rates.

By use of thin section analysis and tracer tests results, one can understand the early acid breakthrough in some carbonate rock types when compared to others. For Indiana limestone carbonate rock type, the observations of thin section show a well-connected intergranular porosity, and thus any preferential flow paths do not exist. The tracer concentration profile shows also a high flowing fraction near unity. In other words, when the acid flows inside the core, it contacts a high fraction of the rock which leads to more acid consumption and a high PV_{bt} curve.

For moldic-porosity-dominated carbonate rock types such as Pink Desert and Edwards Yellow, the thin section shows that the porosity is not as well connected as in grain-dominated rock types such as in Indiana Limestone. It is believed that a smaller fraction of pore volume contributes to the flow, and thus preferential flow paths exist for the fluid flow. Also, the tracer experiments show an early breakthrough and the tracer concentration profile shows a flowing fraction less than unity to support the observations of thin section.

Consequently, when the acid flows inside the core, it contacts lower fraction of the rock where the acid flows at a higher velocity than in the restricted pore fraction (1-f), which leads to less acid consumption and lower PV_{bt} curve.

For further investigation, when the large pores lead the wormhole propagation, a dominant wormhole is formed and the least amount of acid is required to propagate such wormhole. For example, in Pink Desert carbonate rock type, the normalized tracer concentration profile **(Fig. 4.5)** exhibits high dispersion and long tail. The high variation in the microscopic velocity within the flow path from the larger pores to tight flow paths

connecting them is believed to contribute to high dispersion. Also, when large pores are connected to each other through tight flow paths as shown in thin section analysis (Fig. 1c), the stagnant regions, most probably, occur. Following that, large residence times are expected in the stagnant regions because of mass transfer controlled by diffusion, which is the origin of the long tail behavior. Thus, the high dispersion and the long tail observed in the normalized tracer concentration profile confirm that the large pores lead the wormhole propagation.

It is worthy to mention that the existence of large pores in carbonate rocks does not guarantee the low acid pore volume to breakthrough unless these pores could lead the fluid flow through the porous media.

To illustrate this idea, NMR measurements were conducted on each carbonate rock type to measure the pore size. The NMR data for each rock type is presented as T2 distributions **(Fig. 4.2)**. Each figure depicts the portion of porosity (ordinate) associated with the log T2 relaxation time (abscissa). The T2 relates to the pore size: the larger the T2, the larger the pore size. Indiana Limestone carbonate rock type has T2 centered on 1 sec while Pink Desert limestone exhibits lower T2 sec around 0.17 sec. However, the tracer concentration profile for Pink Desert exhibits high dispersion and long tail behavior which means that the pores in Pink Desert lead the fluid flow through porous media, and hence, lower acod pore volume to breakthrough.

The results of the study show that the acid response can be predicted using non-destructive tracer test. The acid pore volume to breakthrough for a wide variety of carbonate rock types correlate with the flowing fraction measured from the tracer tests.

The carbonate rock types with a low flowing fraction have PV_{bt} curve much lower and wormhole velocities much higher than carbonate rock types with high flowing fraction. To collapse the acid PV_{bt} curves of different carbonate rock types into one single curve, the pore volume had to be reduced by the flowing fraction measured experimentally from the conducted tracer tests **(Table 4.5)**. The PV_{bt} for different rocks was recalculated based on the effective pore volume so that the PV_{bt} curves of the carbonate rock types of different flowing fraction combine into a single curve **(Fig. 4.10)**.

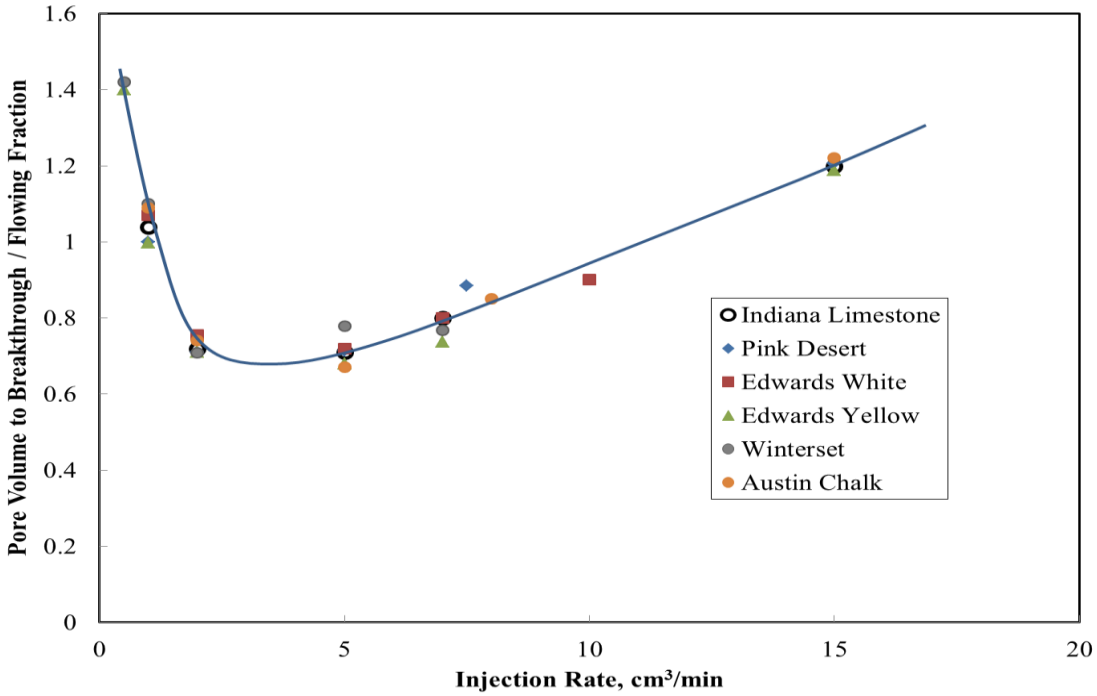

Fig. 4.10—Pore volume to breakthrough curves for different carbonate rock types after collapse at 150°F.

The results reveal a single curve for a wide range of carbonate rock types. This master curve provides a means of estimating the entire pore volume to breakthrough curve from a single non-destructive tracer test (The tracer test is required to determine the flowing fraction). Thus, this master curve eliminates the need for extensive and repetitive coreflood experimentation to determine the PV_{bt} curve for the reservoir carbonate rock. This approach will highly reduce the cost and the time required to sample reservoir cores to perform repetitive and routine experiments. Also, it will be useful when cores are in short supply or when acid experiments cannot be carried out on large blocks as these experiments are prohibitively expensive.

The tracer and acid experiments were repeated at room temperature on Indiana Limestone and Pink Desert carbonate rock types to validate the approach at different conditions. The number of pore volumes to breakthrough is shown as a function of the injection rate in **Fig. 4.11**. The optimum injection rate decreased and the number of pore volumes to breakthrough decreased with decreasing the temperature. **Fig. 4.12** shows the acid PV_{bt} curves for both carbonate rocks after they collapsed into a master curve.

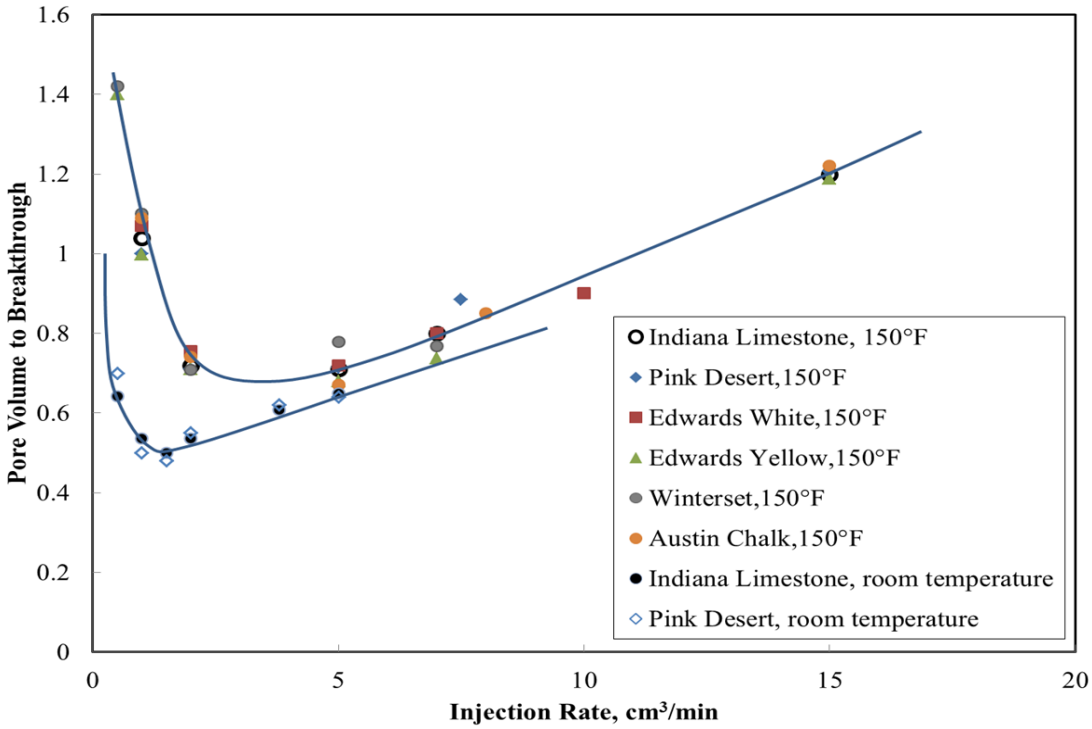

Fig. 4.11—Pore volume to breakthrough curves for different carbonate rock types at 150°F and room temperatures.

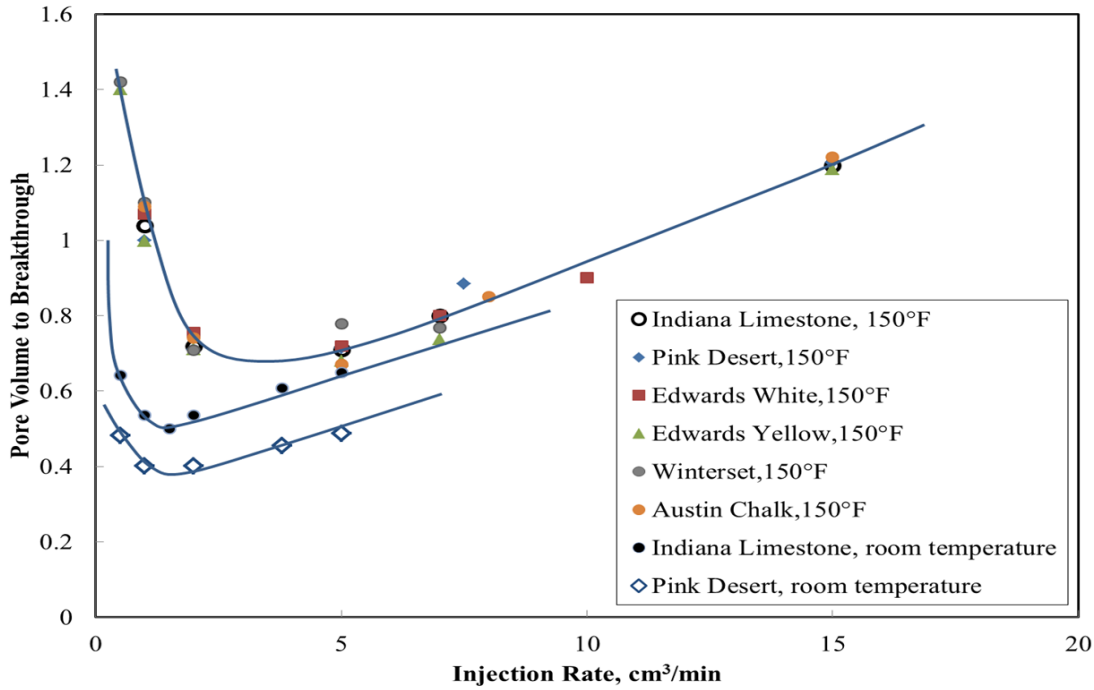

Fig. 4.12—Pore volume to breakthrough curves for different carbonate rock types after collapse.

The two master curves exhibit an optimal Damköhler number at which the number of pore volumes to breakthrough is minimal **(Fig. 4.13)**. To collapse these two master curves, the normalized number of pore volumes to breakthrough are plotted versus the inverse of Damköhler number (Fredd and Fogler 1999) **(Fig. 4.13)**. The normalized number of pore volumes to breakthrough is obtained by normalizing the number of pore volumes to breakthrough by the minimum number of pore volumes to breakthrough for the respective master curve. This approach provides a means of estimating the entire PV_{bt} curve for different combinations of acid system and carbonate reservoir rocks from a single acid experiment on a homogenous carbonate rock ($f = 1$) and a single tracer test on the carbonate reservoir rock.

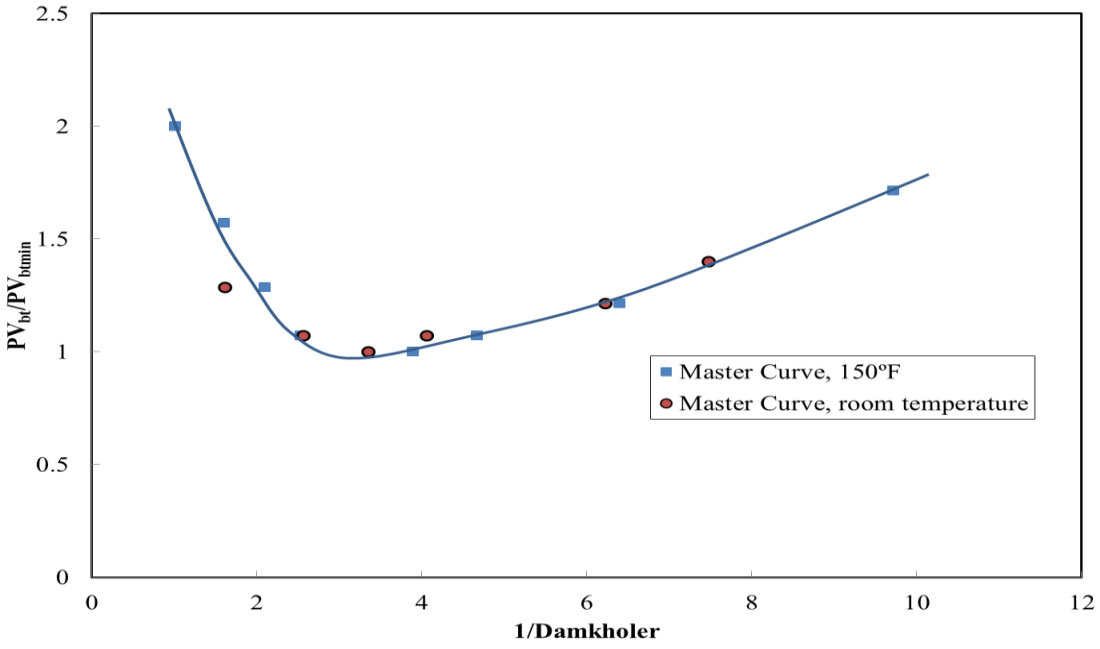

Fig. 4.13—Master pore volume to breakthrough curve for different combinations of acid system and carbonate rock types.

4.7 WORMHOLE DISSOLUTION PATTERN

The wormhole dissolution pattern is important in predicting the post stimulation productivity. The wormhole dissolution pattern for the carbonate rock types is shown in **Fig. 4.14**. Wormhole becomes less branched as the flowing fraction measured experimentally from tracer tests is decreased. For example, for Indiana Limestone carbonate rock type, the tracer test shows a high flowing fraction of 1 so it promotes that the acid will touch a high fraction of rock. CT scan data (Fig. 4.14) shows highly branched wormholes. At intermediate value for the flowing fraction, one dominant wormhole forms with a number of side branches. For carbonate rock types of low flowing fraction measured from the tracer tests such as Winterset rock type, the observations of thin section and tracer concentration profile promote a dominant wormhole. The fractal dimension for each carbonate rock was computed using box counting method. **Fig. 4.15** shows a strong linear relationship between the fractal dimension and the carbonate rock flowing fraction.

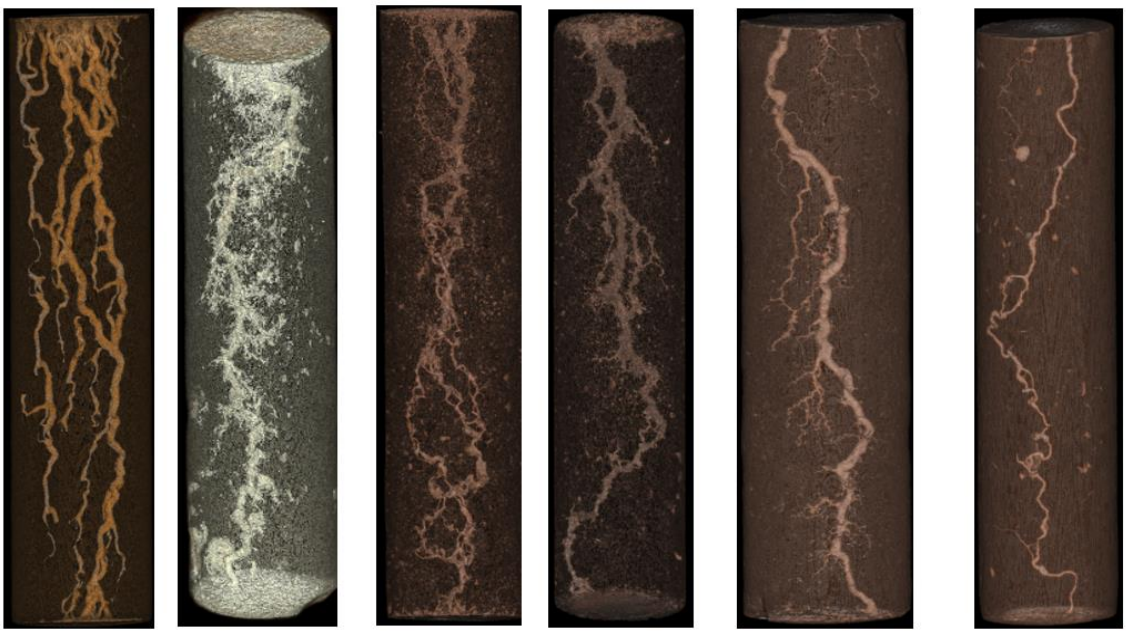

(a) (b) (c) (d) (e) (f)

Fig. 4.14—Wormhole dissolution pattern after 15 wt% HCl acid injection. (a) Indiana Limestone; (b) Austin Chalk; (c) Edwards Yellow; (d) Pink Desert; (e) Winterset; (f) Edwards White.

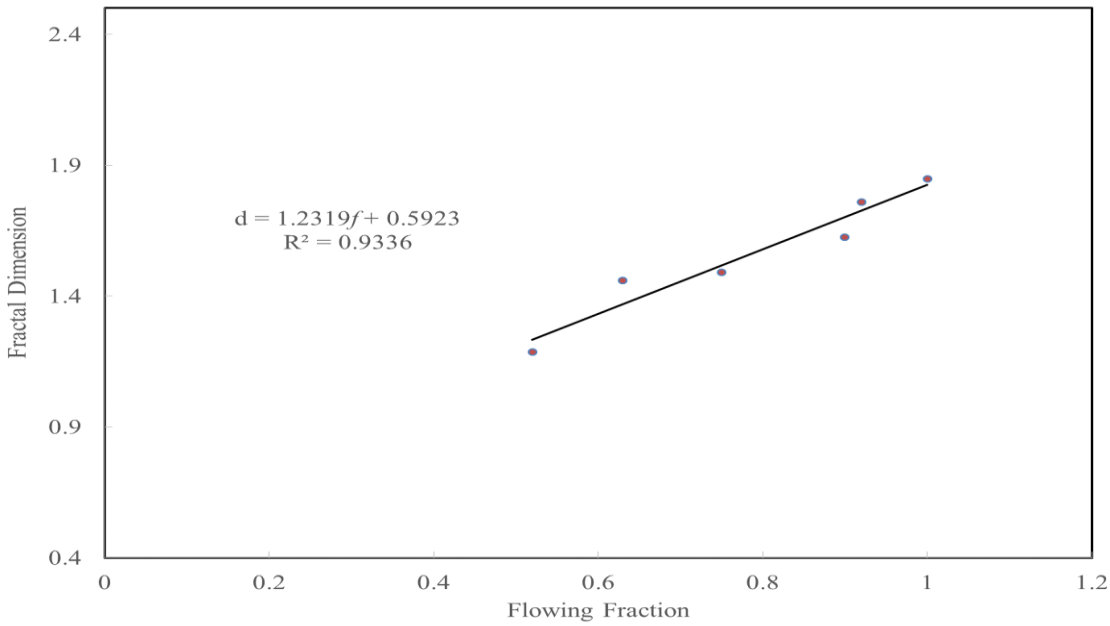

Fig. 4.15—Crossplot of fractal dimension and the flowing fraction.

4.8 APPLICATION

The phenomena of acidization involves several orders of length scale, from few microns to a few centimeters. Panga et al. (2005) developed a model that describes the reactive transport of acid as a coupling between Darcy scale (a length scale at which continuum quantities can be defined) and pore scale (at which dissolution is taking place). Different models have been reported in the literature (Kalia and Balakotaiah 2007; Kalia and Balakotaiah 2009; Ratnakar et al. 2007; and Maheshwari et al. 2013) used the same concept to simulate the acidization process.

To initialize these models, information about average pore radius, pore size distribution, pores connectivity, interfacial area, and structure-property relation parameters are needed. Unfortunately, this information is difficult to obtain directly. Instead, it is common practice to calibrate the acidization model with the experimental data to obtain this information. The PV_{bt} curves and the petrophyscial data obtained by various methods such as thin section analysis, NMR, and mercury injection capillary pressure test, reported in this study can be used to calibrate the acidization models. These models can be then used for rigorous simulation of acid treatment at well scale (Thomas and Nasr-El-Din 2003).

This study primarily focused on pore-scale heterogeneity. However, acid field treatments are dominated by large scale heterogeneities such as fractures, permeability variation, and laminations. Large-scale heterogeneities can be accounted in matrix acidizing models by a reasonably gridding scheme. However, to account for pore-scale heterogeneity, a gridding scheme finer than the pore scale would have to be employed.

This will result in enormous computational time and practically limits the domain size to a few inches on even the most powerful computers available today. Therefore, it is much more efficient to investigate the influence of pore-scale heterogeneity experimentally and represent it by an average PV_{bt} curve (Ziauddin and Bize 2007). The approach and data reported in this study can be used for this purpose. A single tracer test can be conducted with non-destructive fluid on a reservoir core sample without significant core-scale heterogeneity and the flowing fraction can be then measured. The measured flowing fraction and the acid pore volume to breakthrough for a homogenous outcrop core at the desired acid concentration of the field treatment and formation temperature at the optimal Damköhler number can be then used to derive the average pore volume to breakthrough curve using the approach reported in this study. This curve can be used to incorporate the influence of pore-scale heterogeneity of the carbonate reservoir rock in the numerical simulator. The resulting simulator, in which the pore-scale heterogeneity is represented by average PV_{bt} curve and large scale heterogeneity is represented by reasonable gridding scheme can then be used for the design, monitoring and evaluation of reservoir treatments.

The significance of incorporating the effect of pore-scale heterogeneity in the numerical simulators for the design of real treatments is illustrated by two acid diversion experiments. In the first experiment, two cores, one represents Indiana Limestone carbonate rock type and the other is Pink Desert, were acidized together using 15 wt% HCl at 5 cm^3/min and a temperature of 150°F. Both cores have the same initial permeability of 71 md and the same dimensions. Tracer tests were conducted on both of

them prior to acid treatment to show a flowing fraction of 1 for Indiana limestone core and a flowing fraction of 0.75 for Pink Desert one. **Fig. 4.16** shows the acid flow distribution in both cores during the acid treatment.

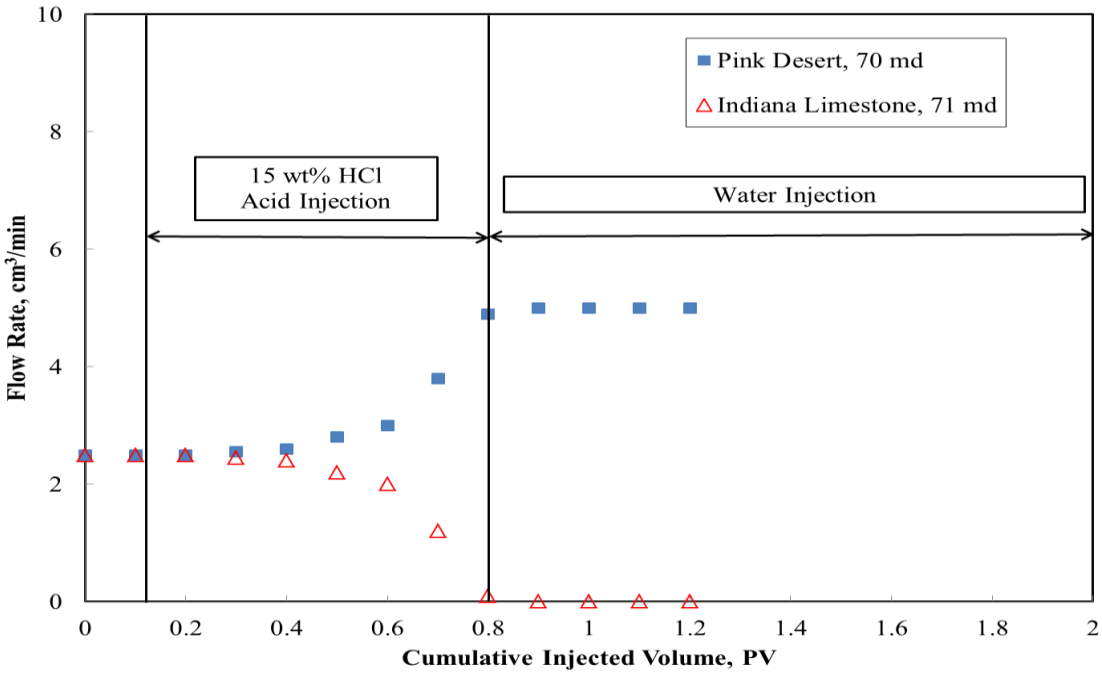

Fig. 4.16—Acid injection flow rate distribution across Indiana Limestone and Pink Desert cores; 15 wt% HCl at flow rate of 5 cm^3/min and 150°F.

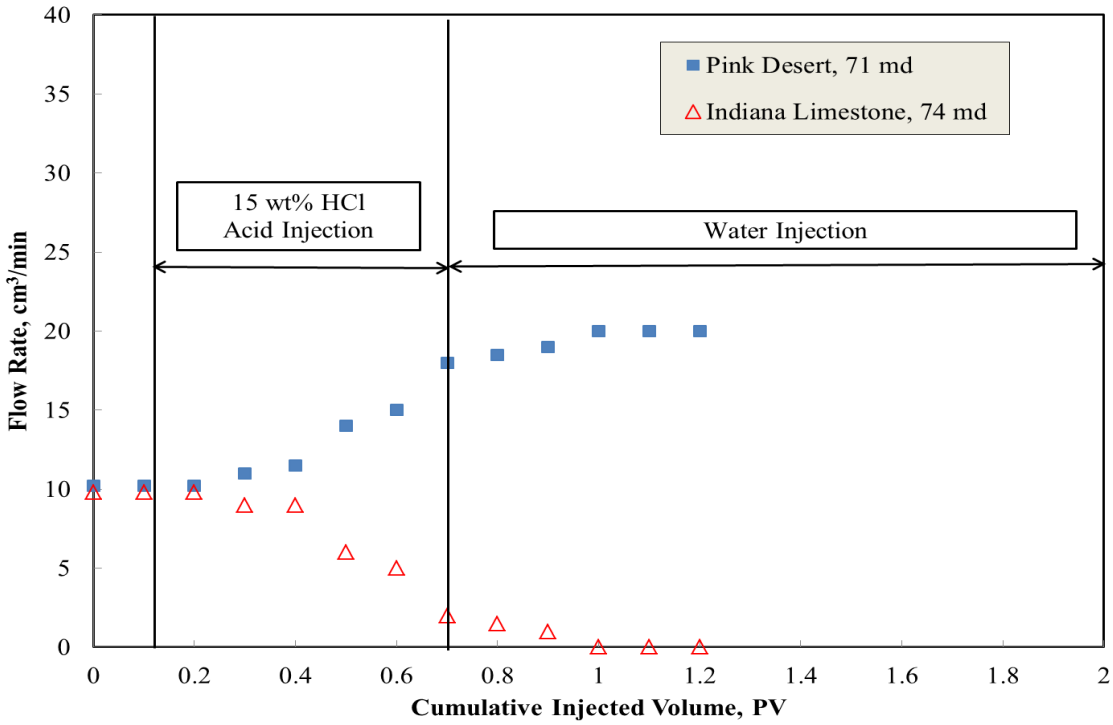

Fig. 4.17—Acid injection flow rate distribution across Indiana Limestone and Pink Desert cores; 15 wt% HCl at flow rate of 20 cm^3/min and 150°F.

In the second experiment, the flow rate was increased to 20 cm^3/min. Both cores were selected to have almost the same initial permeabilities of 74 md for Indiana Limestone and 71 md for Pink Desert. Tracer tests were conducted on both of them prior to acid treatment to show a flowing fraction of 1 for Indiana limestone core and a flowing fraction of 0.75 for Pink Desert one. **Fig. 4.17** shows the acid flow distribution in both cores during the acid treatment. In both experiments, it is noted that uneven acid distribution occurs as the acid flows preferentially in the rock of lower flowing fraction.

As a result, the acid breakthrough is much faster in Pink Desert core than in Indiana Limestone one.

It is generally assumed that the contrast in permeability along the treated interval leads to uneven acid distribution. The results show that in the presence of carbonates of different rock structure or intervals of low flowing fraction within intervals of high flowing fraction in the reservoir, given the same initial permeability, leads to uneven acid distribution. This shows clearly the effect of pore-scale heterogeneity of carbonate rocks on the acid fluid flow distribution. This information can be useful to optimize acid treatment design or consider the use of diverters.

4.9 CHAPTER CONCLUSIONS

The results of the study showed that the pore-scale heterogeneity has a significant effect on the response of various carbonate rocks to the acid. The number of acid pore volumes to breakthrough can be correlated to the pore-scale heterogeneity using one parameter—flowing fraction. The flowing fraction can be estimated from non-destructive tracer test. Carbonate rocks of high flowing fraction consumed more acid volume than the rocks of lower flowing fraction. In the field, a tracer fluid can be injected and then flowed back to estimate the flowing fraction. The PV_{bt} can be then deduced and used along with other petrophyscial data to validate the numerical simulators used for design, monitoring, and evaluation of reservoir treatments.

The results also showed that the presence of carbonates of different rock types in the formation has a strong influence on the acid flow distribution and thus the outcome of the treatment.

The results reported here are for regular treatment fluid (HCl acid solution). Many treatment fluids are shear thinning or viscoelastic in nature. For these fluids, the pore structure of the carbonate is expected to exert a stronger influence than the observed one. This will be addressed in a later chapter.

CHAPTER V

NEW INSIGHTS INTO THE PROPAGATION OF EMULSIFIED ACID IN CALCITE CARBONATE ROCKS

5.1 INTRODUCTION

As discussed in Chapter IV, it was found that the carbonate pore-scale heterogeneity has a significant effect on the acid stimulation treatment using regular HCl acid. It is expected that the carbonate pore structure exerts stronger influence on the acid stimulation treatment using shear thinning fluids such as the emulsified acid.

Several studies in the literature focused on the performance of the emulsified acid. Buijse and Van Domelen (2000) studied the effect of the injection rate, viscosity, and acid volume fraction on the emulsified acid pore volume to breakthrough in carbonate rocks. Sayed et al. (2012) studied the performance of the emulsified acid in low and high permeability carbonate formation using coreflood experiments. It was found that the high permeability carbonate cores consumed more acid volume to breakthrough than the low permeability ones. Also, an optimum injection rate was observed for the high permeability cores while the acid pore volumes to breakthrough decrease with increasing the injection rate for low permeability formations. Al-Anazi et al. (1998) studied the application of the emulsified acid in tight carbonate rocks using coreflood experiments and the results showed that the emulsified acid can form deep wormholes in tight carbonate cores. Other studies (deRozieres et al. 1994; Navarrete at al. 1998; and Al-Mutairi et al. 2008) focused on the reaction rate of the emulsified acid with carbonate rocks. Navarrette et al. (1998) indicated that the reaction rate of 28 wt%

HCl emulsified acid with limestone is 8.5 times less than that of 28 wt% HCl with limestone.

None of the published data in the literature studied the effect of carbonate pore structure on the emulsified acid performance. So, the objective of this chapter is to understand the physics of the emulsified acid flow through carbonate porous media at pore scale and develop a new theory to predict the effect of carbonate pore structure on the emulsified acid performance using tracer test.

5.2 CHARACTERIZATION OF CARBONATE ROCK TYPE

Six carbonate rock types were used in this study. These carbonates are Indiana Limestone, Austin Chalk, Edwards Yellow, Pink Desert, Winterset, and Edwards White. Characterization study was performed on the six carbonate rock types. This study includes thin section analysis, NMR and MICP measurements. The results of the characterization study is discussed in detail in chapter IV.

Indiana Limestone is characterized by well-connected intergranular pores. Consequently, it is believed that when a fluid is injected in this carbonate rock type, it will contact high fraction of the rock. Edwards Yellow, Pink Desert, and Winterset carbonate rock types are dominated by moldic pores. The connectivity between these pores is less compared to the intergranular pores in Indiana Limestone and hence, when a fluid is injected in these carbonate rock types, it will contact lower fraction of the rock compared to Indiana Limestone. Edwards White was found to have the least connectivity between the pores.

Tracer experiments were also conducted on the six carbonate rock types. The results of the tracer experiments were discussed in detail in chapter IV. For Indiana limestone carbonate rock type, the tracer fluid contacts high fraction of the rock. As the connectivity between pores becomes less for Edwards Yellow, and Pink Desert, the tracer fluid contact lower fraction of the rock. Edwards White carbonate rock types was found to have the least flowing fraction. It is worthy to mention that the flowing fraction is defined in this study as the cumulative pore volume injected corresponding to the normalized tracer concentration at $C/C_0 = 0.5$.

5.3 EMULSIFIED ACID EXPERIMENTS

5.3.1 Emulsified Acid Preparation

The emulsified acid **(Table 5.1)** was first prepared by diluting the concentrated HCl acid solution (36.8 wt%) to 15 wt% by deionized water. Then, the required amount of corrosion inhibitor and inhibitor aid was added to the acid.

Separately, the emulsifier was added to the hydrocarbon external phase (oil) in a blender cup at 500 rpm. The emulsifier was given enough time to mix in the oil thoroughly. By using a separatory funnel, the acid solution was added slowly to the hydrocarbon external phase (oil and emulsifier solution). It is important to add the acid droplets slowly and uniform throughout the blending. The emulsion was blended for 2 minutes at constant speed after the last acid droplet was added to generate a uniform emulsion.

Table 5.1–Formula Used to Prepare the Emulsified Acid		
Deionized Water	265.5	gal/1000
36 wt% HCl	419.5	gal/1000
Corrosion Inhibitor	5	gal/1000
Inhibitor Aid	10	gal/1000
Emulsifier	6	gal/1000
Base Oil	294	gal/1000

5.3.2 Viscosity Measurements

Viscosity measurements for the emulsified acid were all conducted using a high-pressure/high-temperature (HP/HT) viscometer. The rotor and bob of the viscometer were made of Hastelloy C to resist corrosion by the acids. The viscosity was measured as a function of shear rate from 1 to 1020 s^{-1} at room temperature and 150°F. A pressure of 300 psi was applied to minimize the evaporation of the sample at high temperature.

The results showed that the emulsified acid has a non-Newtonian, shear thinning behavior **(Fig. 5.1)**. At a given shear rate, the viscosity of the emulsified acid decreased as the temperature was increased. The viscosity-shear rate relationship for the polymer solution can be described by power-law model as follows:

$$\mu = k\,\gamma^{n-1} \quad \text{(5.1)}$$

where μ is the fluid viscosity, γ is the shear rate, n is the power-law index, and k is the power-law consistency index. **Table 5.2** shows the values of k and n for the emulsified acid at room temperature and 150°F.

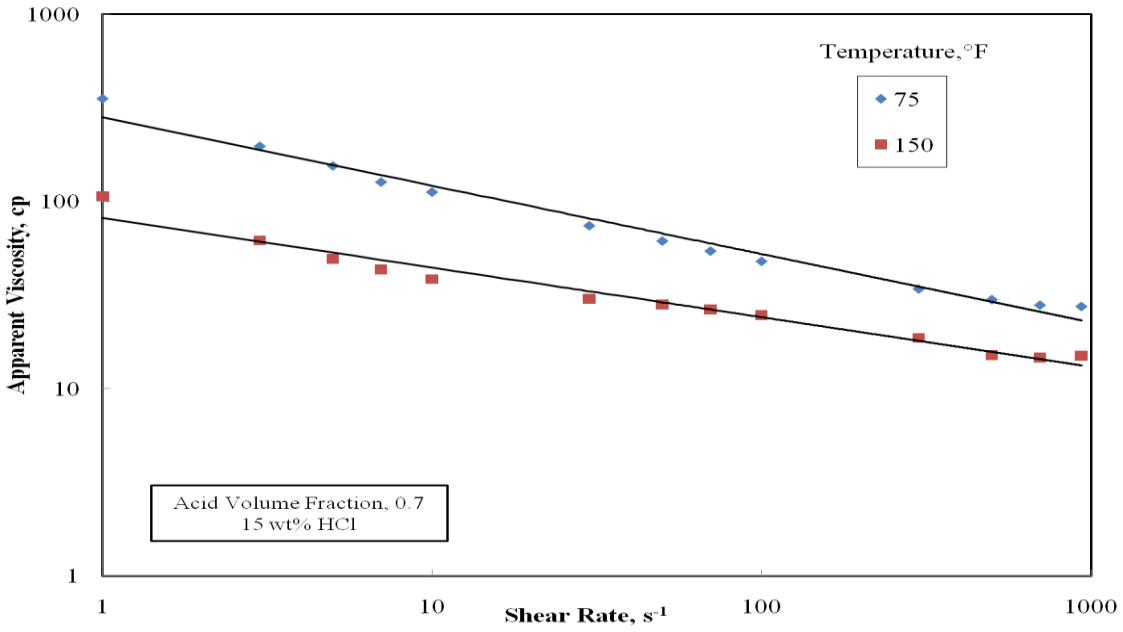

Fig. 5.1—Apparent viscosity of the emulsified acid at room temperature and 150°F as a function of the shear rate.

Table 5.2–Power-Law Model Parameters for the Emulsified Acid				
Sample #	Temperature (°F)	Power-law Consistency, K ($gm/cm.s^{n-2}$)	Power-law Index, n(-)	Correlating Coefficient, R^2
1	75	280.83	0.636	0.98
2	150	81.87	0.631	0.96

5.3.3 Coreflood Experiments

Coreflood experiments were conducted to determine the emulsified acid PV_{bt} for each carbonate rock type at different injection rates. A back pressure of 1100 psi was set to keep most of the carbon dioxide in the solution. Prior to commencing the acid injection, deionized water was injected at different flow rates at room temperature to measure the core permeability **(Table 5.3)**. During injection, an overburden pressure at least 300 psi higher than the inlet pressure was kept to prevent the fluid from bypassing the core. The water injection continues while heating the system to 150ºF. The emulsified acid was then injected until breakthrough while the pressure drop was monitored across the core. The acid was injected at rates of 0.5, 1, 2, 5, and 8 cm^3/min.

Table 5.3–Core Properties for Different Carbonate Rock Types

Rock Type	Pore Volume (cm^3)	Porosity (vol%)	Permeability (md)
Indiana Limestone	23-25	13-15	65-71
Edwards Yellow	33-37	19-21	50-53
Austin Chalk	22-28	13-16	19-22
Winterset Limestone	38-42	22-24	4-5
Pink Desert	41-45	23-26	82-85
Edwards White	31-36	18-21	3-5

5.3.4 Results and Discussion

Fig. 5.2 shows the effect of pore-scale heterogeneity on the acid pore volume to breakthrough at different injection rates. For carbonate rock types of higher magnitude of pore-scale heterogeneity (lower flowing fraction), the acid dissolves less rock overall as compared to rock of lower magnitude (higher flowing fraction) such as Indiana limestone rock type ($f = 1$) which leads to less PV_{bt}. For example, the acid pore volumes to breakthrough for Edwards White carbonate rock type ($f = 0.53$), ranging from 0.3 to 0.35, were observed to be less compared to Indiana limestone carbonate rock type ($f = 1$) with PV_{bt} ranging from 0.6 to 0.7. Acid pore volume to breakthrough strongly depends on how fast the wormhole propagates along the rock. Consequently, the wormhole propagates more rapidly in carbonate rocks of higher magnitude of pore-scale heterogeneity than that in Indiana limestone rock type ($f = 1$).

The carbonate pore structure exerts stronger influence on the emulsified acid performance when compared to regular HCl acid. At a given injection rate, for example 2 cm^3/min, the emulsified acid PV_{bt} for Pink Desert carbonate rock type is 0.61 of the emulsified acid PV_{bt} for Indiana Limestone while it is 0.75 for regular HCl acid.

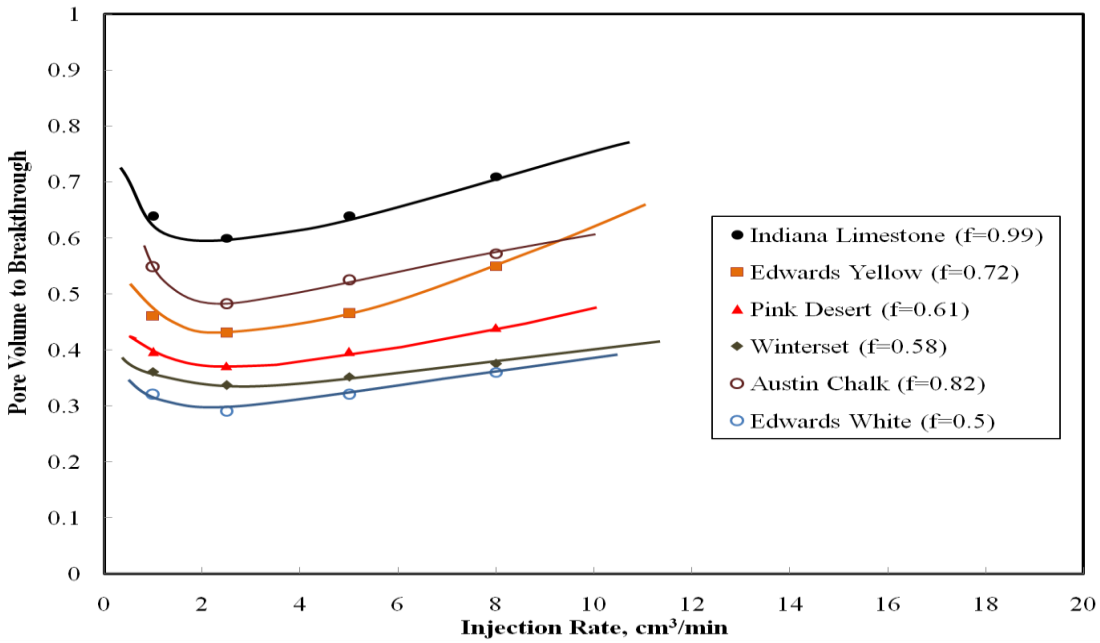

Fig. 5.2—Emulsified acid pore volumes to breakthrough as a function of injection rate for different carbonate rock types.

To collapse the emulsified acid PV_{bt} curves of different carbonate rock types into one single curve, the pore volume had to be reduced by the flowing fraction measured experimentally from the conducted tracer tests. The PV_{bt} for different rocks was recalculated based on the effective pore volume so that the PV_{bt} curves of the carbonate rock types of different flowing fraction combine into a single curve. **Fig. 5.3** shows the attempt to collapse the emulsified acid PV_{bt} curves into a single curve using the flowing fraction estimated from the tracer tests. The curves do not collapse into one single curve, therefore a new formulation for the tracer fluid is needed to predict the emulsified acid performance.

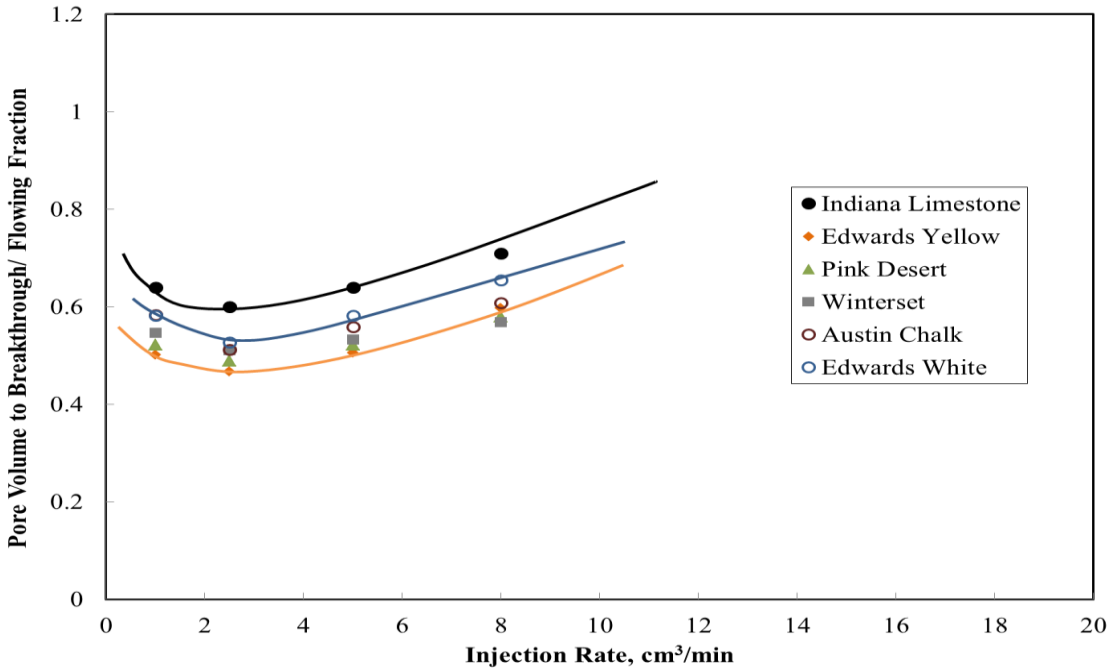

Fig. 5.3— Attempt to collapse the emulsified acid pore volume to breakthrough curves for different carbonate rock types using the flowing fraction measured from tracer experiments using the base tracer fluid.

5.4 NEW THEORY TO PREDICT THE PERFORMANCE OF EMULSIFIED ACID BASED ON TRACER TEST

5.4.1 New Formulation for the Tracer Fluid

A new tracer fluid was developed to understand the effect of carbonate pore structure on the shear-thinning-fluid flow through porous media. Polymer based tracer which is a mixture of polymer and 8 wt% potassium chloride (KCl) (ACS Reagent, >99 wt%) was used. Polymer type and concentration were selected so that the tracer fluid exhibits similar viscosity-shear rate trend to the emulsified acid system. Viscosity

measurements for the tracer fluid were all conducted using a high-pressure/high-temperature (HP/HT) viscometer. The viscosity was measured as a function of shear rate from 1 to 1020 s^{-1} at 150°F. A pressure of 300 psi was applied to minimize the evaporation of the sample at high temperature.

The viscosity of the tracer fluid was measured as a function of shear rate at 150ºF at different polymer concentrations. The results showed a non-Newtonian, shear thinning behavior **(Fig. 5.4)**. The viscosity-shear rate relationship for the polymer-based-tracer fluid can be described by power-law model as follows:

$$\mu = k\,\gamma^{n-1} \quad \text{(5.1)}$$

Table 5.4 shows the values of k and n at 150°F for the fluid at different polymer concentrations. It is observed that at a constant shear rate, the viscosity of the tracer fluid is higher at higher polymer concentration.

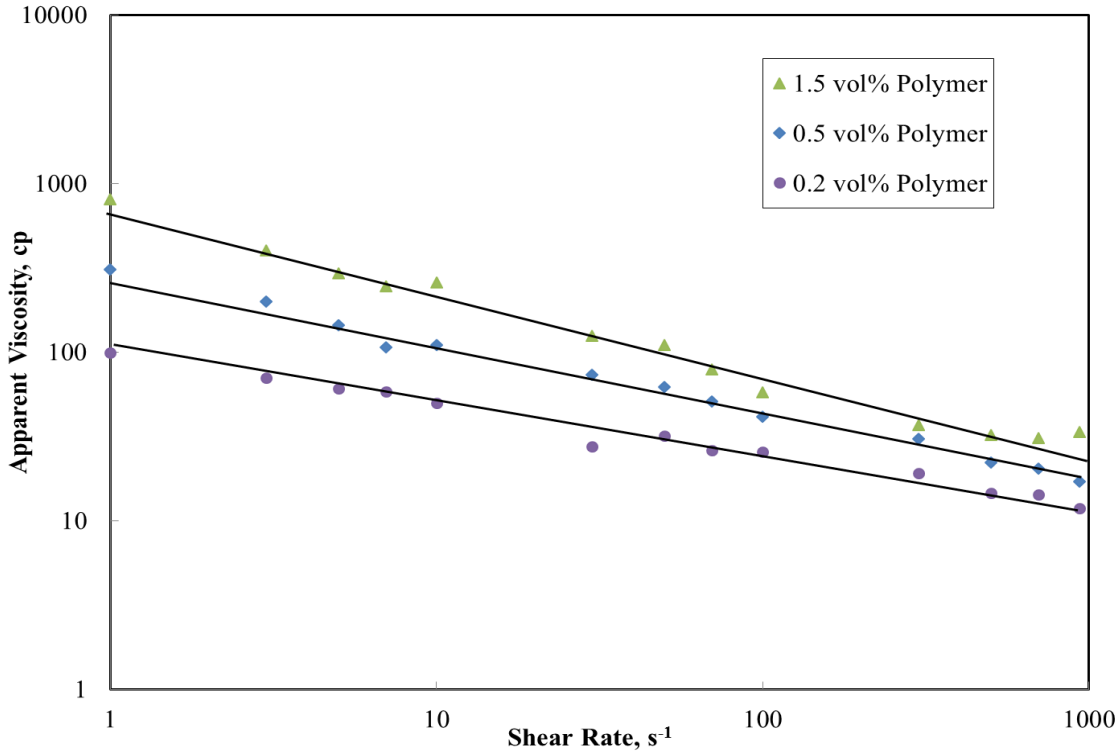

Fig. 5.4—Apparent viscosity of the tracer fluid at different polymer concentrations at 150°F as a function of the shear rate.

Table 5.4–Power-Law Model Parameters for the Tracer Fluid

Sample #	Polymer Concentration (vol%)	Power-law Consistency, K ($gm/cm.s^{n-2}$)	Power-law Index, n(-)	Correlating Coefficient, R^2
1	0.2	98.13	0.641	0.98
2	0.5	288.12	0.591	0.99
3	1.5	684.62	0.515	0.98

Fig. 5.5 shows a comparison between the viscosity measurements for the tracer fluid at different polymer concentrations with the emulsified acid at 150°F. It was observed that the viscosity-shear rate trend for the tracer fluid at polymer concentration of 0.2 vol% is almost the same as the trend for the emulsified acid. Hence, a mixture of 0.2 vol% polymer and 8 wt% KCl was used in the tracer experiments.

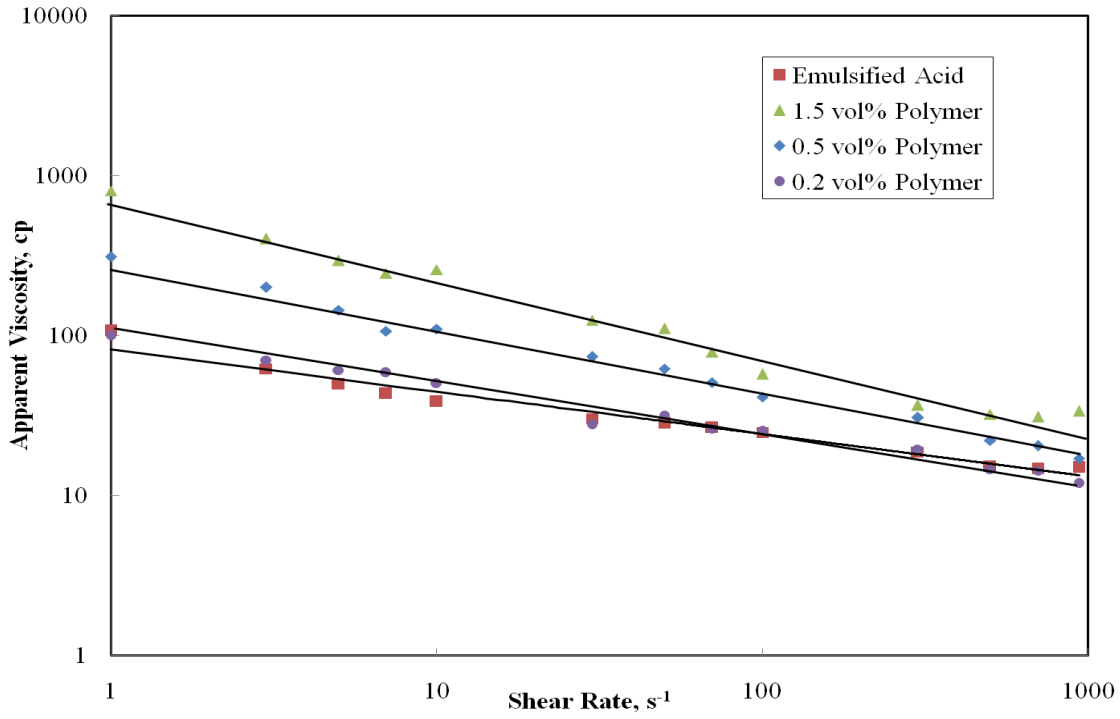

Fig. 5.5—Apparent viscosity of the tracer fluid at different polymer concentrations and emulsified acid at 150°F as a function of the shear rate.

5.4.2 Tracer Experiments

5.4.2.1 Core Preparation

Large set of cores for each carbonate rock type were drilled. Tracer experiments using 8 wt% KCl were conducted on all cores. Two sets of cores were selected so that they exhibit similar tracer concentration profile. Tracer experiments using the new tracer fluid were then conducted on the first set while the emulsified acid experiments were conducted on the second set. This is done in this way to avoid the effect of possible polymer retention or polymer filtercake at the cores inlet on the emulsified acid treatments.

5.4.2.2 Procedure

The tracer fluid was injected for five pore volumes on each core for each carbonate rock type. Prior to commencing the tracer fluid injection, the core was saturated with deionized water under vacuum, and then preflushed with deionized water. Core effluent samples were collected and each sample was analyzed by Inductively Coupled Plasma (ICP-AES) for K^+ ions concentration measurements. The concentration at each point was plotted versus the cumulative pore volume injected.

5.4.3 Results and Discussion

The normalized tracer concentration (C/C_0) in the core effluent samples for different carbonate rock types is plotted as a function of the cumulative pore volume injected of the polymer based tracer **(Fig. 5.6)**.

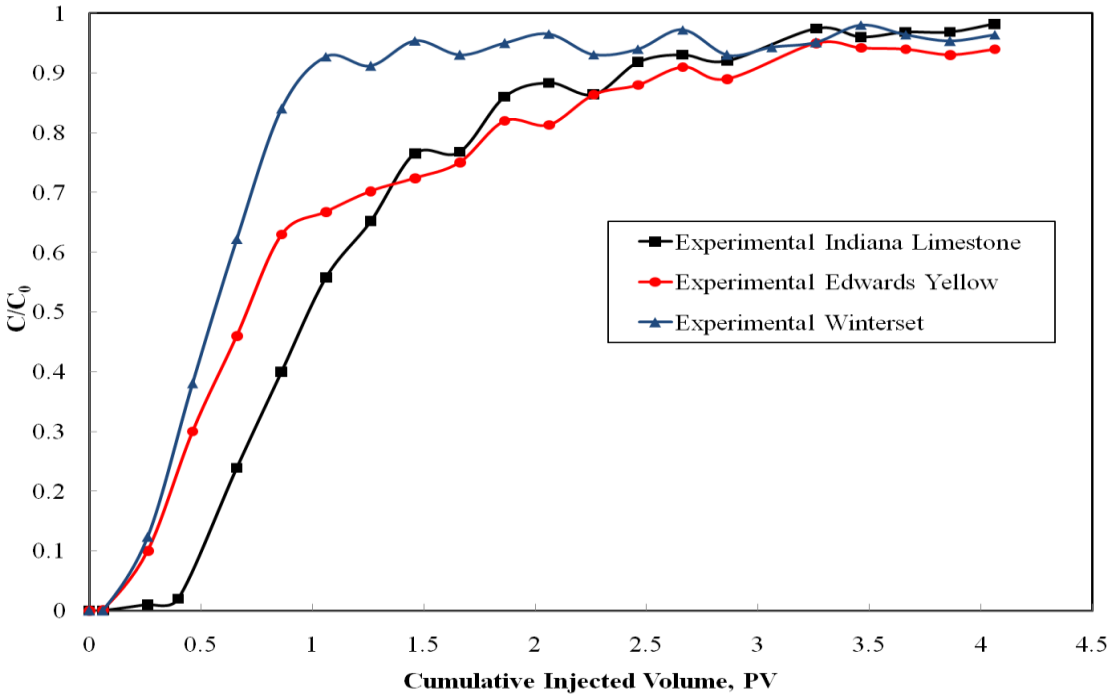

Fig. 5.6 (a)—Tracer concentration profiles for Indiana Limestone, Edwards Yellow, and Winterset carbonate rock types.

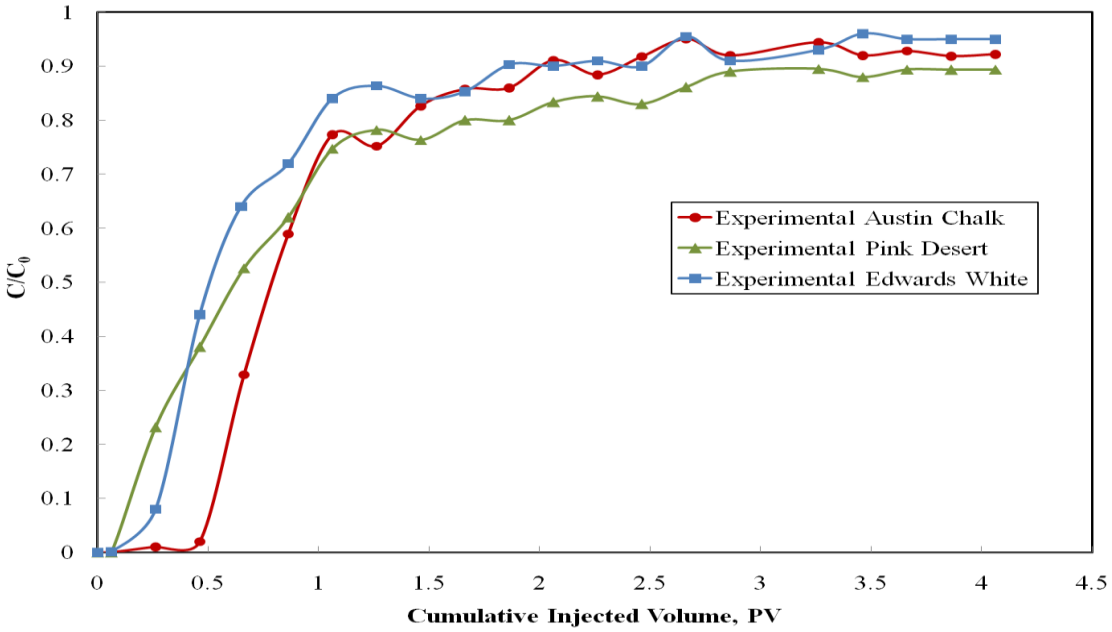

Fig. 5.6 (b)—Tracer concentration profiles for Austin Chalk, Pink Desert, and Edwards White carbonate rock types.

For Indiana limestone carbonate rock type, the tracer concentration profile was found to be symmetrical ($C/C_0 = 0.5$) at one pore volume injected. These results are expected because carbonates of well-connected intergranular pores exhibit a symmetrical profile around 1 PV injection at $C/C_0 = 0.5$ (Skauge et al. 2006). The tracer profile is dominated by a low fraction of inaccessible pores and no capacitance effect (no dead-end pores).

For other carbonate rock types, the pores are not as well connected as for Indiana limestone carbonate rock type. Consequently, it is believed that the fluid flows in a smaller fraction of the pore volume in these carbonates than in well-connected Indiana limestone. The tracer concentration profiles that show an early breakthrough and long tail behavior confirm this hypothesis. The behavior of the tracer concentration profiles is believed to be due to preferential flow paths for the tracer fluid through the porous media. The tracer concentration profiles appear consistent with the observation of thin sections.

As a comparison in **Fig. 5.7**, the normalized tracer profile for polymer based tracer fluid is more flattened than that for base tracer fluid (8 wt% KCl) which indicates more dispersion. Also, the profile for the polymer based tracer fluid is dominated by lower fraction of pore volume contributed to the flow when compared to base tracer fluid.

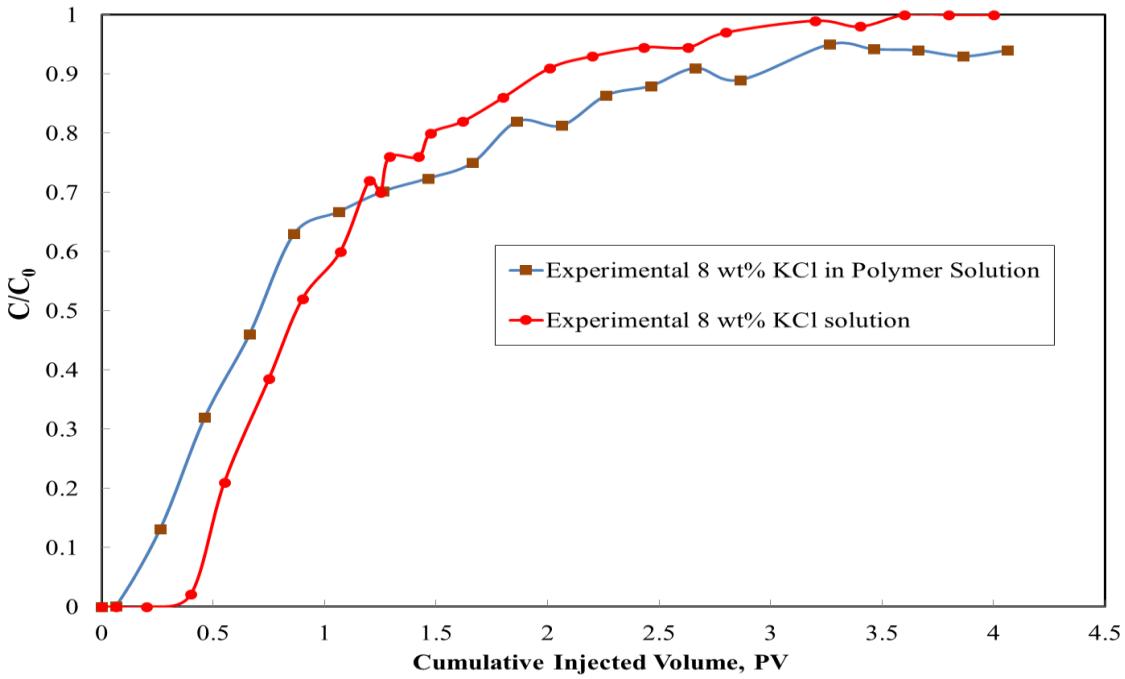

Fig. 5.7—The normalized tracer concentration profiles for Edwards Yellow for both tracer fluids.

Table 5.5 shows the flowing fraction for each carbonate rock type measured from the tracer concentration profile for both tracer fluids. As shown in the table, the polymer based tracer fluid contacts lower fraction of the rock compared to the base tracer fluid.

Table 5.5–Flowing Fraction for Different Carbonate Rock Types for Both Tracer Fluid Types		
Rock Type	Base Tracer Fluid	Polymer Based Tracer Fluid
Indiana Limestone	1	0.99
Edwards Yellow	0.91	0.72
Austin Chalk	0.92	0.82
Winterset Limestone	0.63	0.58
Pink Desert	0.75	0.61
Edwards White	0.52	0.50

The pore volumes for the different carbonate rock types were then reduced by the flowing fraction measured experimentally from the tracer experiments using the polymer based tracer fluid. The emulsified acid PV_{bt} curves for different rocks were recalculated based on the effective pore volume so that the PV_{bt} curves of the carbonate rock types of different flowing fraction combine into a single curve **(Fig. 5.8)**. The figure shows the need for a shear-thinning tracer fluid to collapse the emulsified acid PV_{bt} into a single curve. This validates our approach that the tracer fluid should be selected so that the viscosity-shear rate trend for the fluid is similar to the emulsified acid trend.

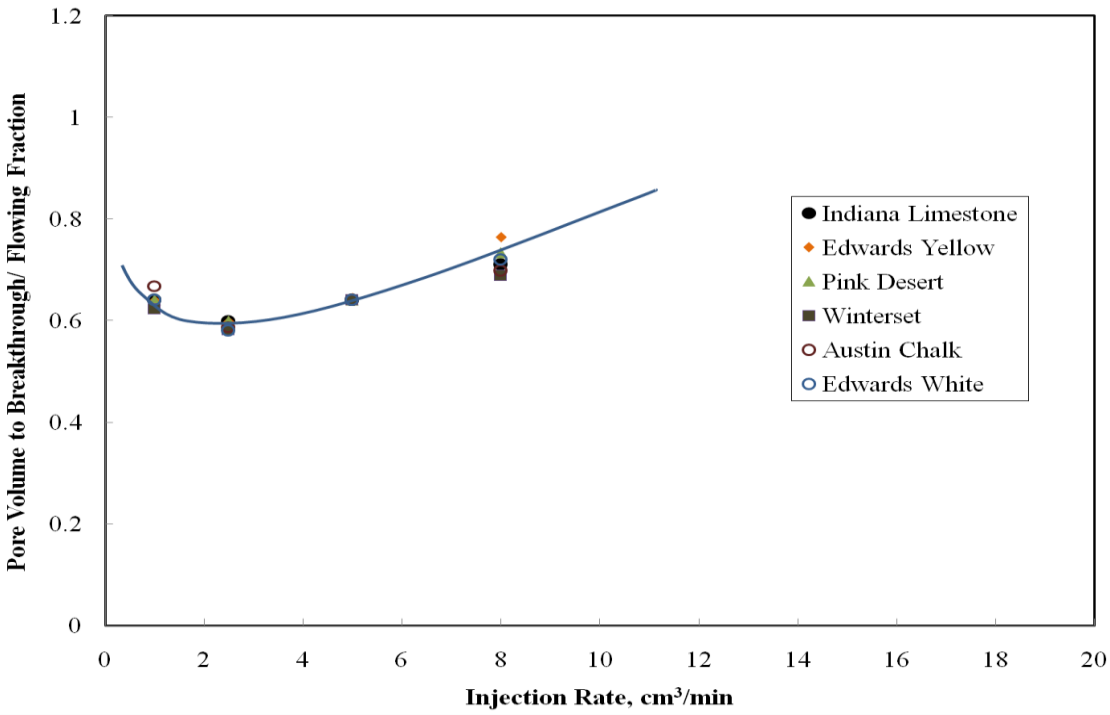

Fig. 5.8— Emulsified acid pore volume to breakthrough curves after collapse into one single curve at 150°F.

5.5 WORMHOLE DISSOLUTION PATTERN

The wormhole dissolution pattern is important in predicting the post stimulation productivity. The wormhole dissolution pattern for the carbonate rock types is shown in **Fig. 5.9**. Wormhole becomes less branched as the flowing fraction measured experimentally from tracer tests is decreased. For example, for Indiana Limestone carbonate rock type, the tracer test shows a high flowing fraction of 1 so it promotes that

the acid will touch a high fraction of rock. CT scan data (Fig. 5.9) shows highly branched wormholes. At intermediate value for the flowing fraction, one dominant wormhole forms with a number of side branches. For carbonate rock types of low flowing fraction measured from the tracer tests such as Winterset rock type, the observations of thin section and tracer concentration profile promote a dominant wormhole.

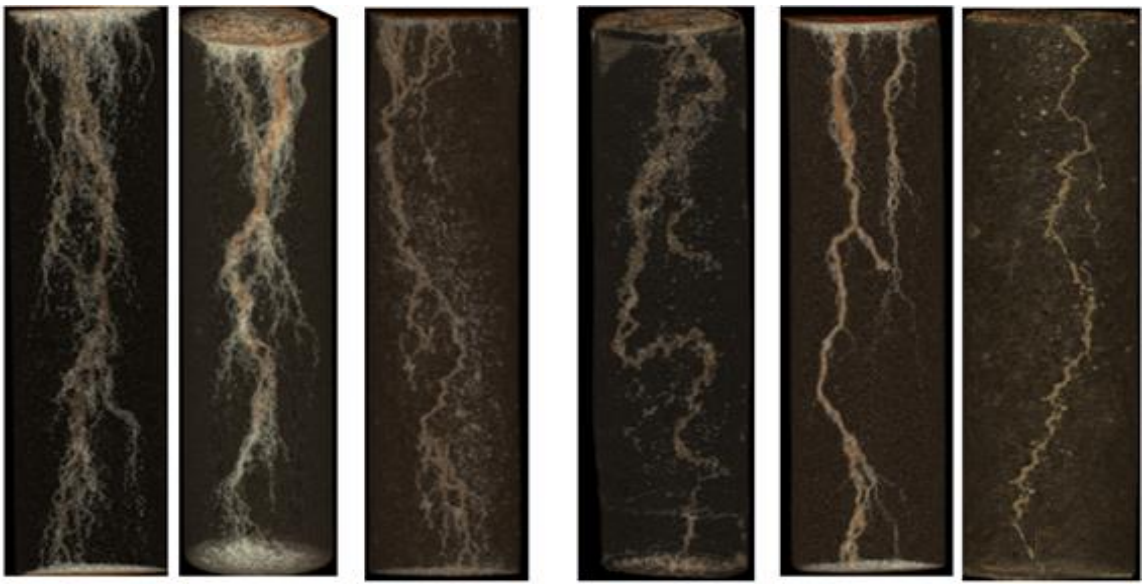

(a) **(b)** **(c)** **(d)** **(e)** **(f)**

Fig. 5.9—Wormhole dissolution pattern after emulsified acid injection. (a) Indiana Limestone; (b) Austin Chalk; (c) Edwards Yellow; (d) Pink Desert; (e) Winterset; (f) Edwards White.

5.6 CHAPTER CONCLUSIONS

The results of the study showed that the pore-scale heterogeneity has a stronger effect on the response of various carbonate rocks to the emulsified acid compared to regular HCl acid. New formulation for the tracer fluid is developed to predict the emulsified acid performance. The number of acid pore volumes to breakthrough and the wormhole dissolution pattern were correlated to the pore-scale heterogeneity using one parameter—flowing fraction which can be estimated from tracer tests.

CHAPTER VI

NEW INSIGHTS INTO PROPAGATION OF EMULSIFIED ACIDS IN VUGGY DOLOMITIC ROCKS*

Carbonate formations are very complex in their pore structure and exhibit a wide variety of pore classes, such as interparticle porosity, moldic porosity, vuggy porosity, intercrystalline porosity, and microporosity. Understanding the role of pore class on the performance of emulsified acid treatments and characterizing the physics of the flow inside was the objective of our study.

The study was performed using vuggy dolomite cores that represent mainly the vuggy porosity dominated structure, while the homogenous cores represent the intercrystalline pore structure. Coreflood runs were conducted on 6 x 1.5 in. cores using emulsified acid formulated at 1 vol% emulsifier and 0.7 acid volume fraction. The objective of this set of experiments was to determine the acid pore volume to breakthrough for each carbonate pore class at different injection flow rates.

In this chapter, we examine whether the heterogeneities observable at the thin section scale have a significant influence on the emulsified acid coreflood run results. The heterogeneities were characterized using thin section observations, tracer experiments, SEM, and resistivity measurements.

---

*Reprinted with permission form "New Insights into Propagation of Emulsified Acids in Vuggy Dolomitic Rocks" by A.S., Zakaria, M., Sayed, H.A., Nasr-El-Din 2014. *SPE J.* **19** (1): 150-160, Copyright 2013 Society of Petroleum Engineers. Reproduced with permission of the copyright owner.

Thin section observations provide means to study the vugs size and their distribution, connectivity, and explain the contribution of the pore class in the acid propagation. Relating the rotating disk experiments of emulsified acid with dolomite to our coreflood experiments results were also conducted in order.

The acid pore volume to breakthrough for vuggy porosity dominated rocks, ranging from 0.1 to 0.3, was observed to be low when compared to the homogenous carbonates (intercrystalline pore structure) with PV_{bt} ranging from 2.5 to 3.5. Also, the wormhole dissolution pattern was found to be significantly different in vuggy rocks than that in homogenous ones. Thin section observations, tracer results, and the coreflood experiments indicated that the vugs are distributed in a manner that creates a preferential flow path which can cause a rapid acid breakthrough and effective wormholing than those with a uniform pore structure. Rotating disk experiment results also showed that the reaction kinetics played a role in determining the wormhole pattern.

6.1 INTRODUCTION

Most carbonate formations are diverse, and exhibit multiporosity systems in terms of vugs, inter- and intragranular porosities which introduce some sort of heterogeneity. On the other hand, emulsified acid has been widely used with carbonate formations. Therefore, a better understanding has recently been gained of the application of emulsified acids in matrix acidizing for complex structured carbonate formations.

Lucia (1983) showed that the most useful division of carbonate pore type was between pore space located between grains or crystals, called interparticle porosity, and

all other pore space, called vuggy porosity. Vuggy pore space is further subdivided into two groups based on the connectivity of vugs. Vugs that are interconnected only through the interparticle pore network are termed separate vugs, and vugs that form an interconnected pore system independent of the interparticle pores are termed touching vugs such as fractures and dissolution channels. Ziauddin and Bize (2007) studied the effects of pore-scale heterogeneities on carbonate stimulation. In their study core samples from eight different carbonate rocks were studied and classified into a Reservoir Rock Type (RRT) based on the results obtained from different characterization techniques. They showed how only using PV_{bt} curves can be misleading in the characterization of acid-rock interactions.

There have been several attempts to understand the flow behavior in vuggy rocks, including the works of Xu et al. (1998); Moctezuma-Berthier and Fleury (2000); Hidajat et al. (2004); Arbogast et al. (2004); and Zhang et al. (2004; 2005). Zhang et al. (2005) conducted a number of "chunk-flow" experiments using vugular rocks to understand the flow characteristics of vuggy rock. All the previous studies focused on the non-reactive flow in vuggy rocks. Only one published study on the reactive flow in vuggy carbonates was found. Izgec et al. (2010) conducted experimental and theoretical studies to investigate the flow of regular 15 wt% HCl acid in vuggy carbonates. They studied the acidization of vuggy carbonates with high resolution computerized tomography imaging, image processing, geostatistical characterization, acid coreflood experiments with 4 in. by 20 in. cores, and numerical simulation. Their experiments showed that the acid propagates more rapidly in vuggy carbonates compared to

homogenous ones.

This is the first study to address the propagation of emulsified acid in vugular-structured dolomitic rocks. The objectives of the present study are to: 1) determine the emulsified acid pore volume to breakthrough in vuggy carbonates and compare it with that in homogenous carbonates; 2) understand the physics of the flow of the emulsified acid in vuggy porosity dominated rocks through a characterization study using tracer experiments, thin section analysis and electrical measurements; and 3) compare the dissolution pattern or the wormhole geometry created by emulsified acid in vuggy carbonates with that created in homogenous ones.

6.2 CHARACTERIZATION OF VUGGY CARBONATE CORES

6.2.1 Selection of Cores

Dolomite cores were drilled from a large block of carbonate obtained from the Thornton outcrop. Pure vugular structure can be found in carbonate rocks with a high degree of dolomitization where the vugs are created by a random process. The cores were cleaned and dried in an oven at a temperature of 300°F. The cores were then weighed dry and again after saturation with deionized water under vacuum. The pore volume was determined from these measurements. **Table 6.1** lists the properties of the dolomite cores used in this study.

Table 6.1–Properties of Dolomite Cores (1.5 in. diameter and 6 in. length)			
Core ID	**Rock Type**	**Pore Volume, cm^3**	**Initial Permeability, md**
Core 2H	Homogenous	15.3	22.5
Core 1H	Homogenous	17.1	39
Core 5H	Homogenous	15.8	32
Core 7H	Homogenous	20.2	23
Core 0.5H	Homogenous	24	37
Core 5V	Vuggy	18	29.4
Core 7V	Vuggy	17.6	32
Core 2V	Vuggy	15.1	0.96
Core 1V	Vuggy	16.2	22
Core 0.5V	Vuggy	19.3	17

6.2.2 Thin Section

Blue epoxy impregnated thin sections were prepared to obtain a detailed description of the porosity distribution**.** The thin section was viewed under an optical microscope. Two images for each rock sample were captured under a magnification of 2.5X and 10X using a digital camera and then sent via card to a computer. Thin section analysis provides means to identify the average size of vugs, their connectivity, and the vuggy pore types. The relationship between the observations from thin section and the tracer experiments were presented. SEM measurements were conducted to further examine the crystal shape for the dolomite rock in the cores used.

6.2.3 Tracer Experiments

A solution with 8 wt% KCl was injected. KCl (ACS reagent, > 99 wt%) was used as a conservative tracer. Concentration of potassium ions in the tracer solution was measured by inductively coupled plasma spectrometer and the measurement was repeated three times to give an average concentration of 36.70 ± 0.05 g/l. Prior to commencing the tracer experiments, the cores were saturated with deionized water under vacuum, and then preflushed with deionized water. The tracer solution was then injected into the vuggy dolomite cores for six pore volumes. Core effluent samples were collected and analyzed by inductively coupled plasma spectrometer (ICP-OES) for K^+ ions concentration.

6.2.4 Electrical Measurements

Resistivity Index measurements were performed on KCl brine saturated cores, from which tortuosity and vuggy porosity were calculated.

6.2.5 X-Ray Computerized Tomography

The CT scan measurements were conducted on the cores before and after acidizing to characterize the wormhole propagation or dissolution pattern in vugular rocks compared to homogenous ones. The CT scan was performed using Universal systems HD-350 (Picker PQ-6000) CT Scanner applying 130 KV and 200 mA. To cover the whole core, 32 slices with 2 mm thickness and 5 mm separation distance between each slice were taken. In the processing step, the binary image data collected by the CT

scanner were processed on a SUN workstation using the CT scanning ImageJ software. Analysis of ImageJ shows a cross sectional area for each slice along the core length. A powerful 3D visualization tool was used, in combination with ImageJ, to show the wormhole dissolution pattern.

6.3 EXPERIMENTAL STUDIES

6.3.1 Materials

The water used throughout the emulsion preparation was distilled water, obtained from a purification system, which has a resistivity of 18.2 MΩ at room temperature. Hydrochloric acid (ACS grade) was titrated using 0.1 N sodium hydroxide solution and the concentration of the acid was found to be 36.8 wt%. Additives such as corrosion inhibitor and cationic emulsifier, obtained from a local service company, were used to prepare the acid in diesel emulsion.

The emulsified acid **(Table 6.2)** was first prepared by diluting the concentrated HCl acid solution by adding distilled water. Then, the required amount of the corrosion inhibitor was added to the acid solution. Separately using blender cup, the emulsifier was added to the diesel at 500 rpm where the emulsifier was given time to be mixed well with the diesel. Maintaining the fluid vortex, 30% of the acid solution was added to the emulsifier-diesel mixture. Without adding more acid solution, the speed of the mixing was increased to 3000 rpm for 3 minutes. Then, the speed was reduced to a moderate rpm and the remaining amount of the acid solution was added. The emulsion was blended for 2 minutes at 1000 rpm.

Table 6.2–Emulsified Acid Formula Used in this Study	
HCl Concentration, wt%	15
Acid Volume Fraction	0.7
Emulsifier Concentration, vol%	1
Corrosion Inhibitor, vol%	0.3

6.3.2 Properties of Emulsified Acid

A Characterization study of the emulsified acids was conducted using acid droplet size distribution measurements, viscosity measurements, and reaction rate experiments with dolomite. The droplet size distribution was measured using a Zeiss Axiophot microscope and it was found to be 6.9 μm with a standard deviation of 2.0 μm **(Fig. 6.1)**. An HPHT rheometer was used to measure the viscosity of emulsified acids at shear rates up to 1000 s^{-1}. The viscosity measurements indicated that the emulsified acid is a non-Newtonian shear thinning-fluid (Sayed and Nasr-El-Din 2012). The emulsified acid has been shown a diffusion coefficient more than two orders of magnitude lower than that of plain acid (Buijse and Van Domelen 2000). Also, from the rotating disk measurements at 230ºF, it was found that the diffusion coefficient of emulsified acid in presence of dolomite was less than that measured with calcite by two-order of magnitude (Sayed and Nasr-El-Din 2012).

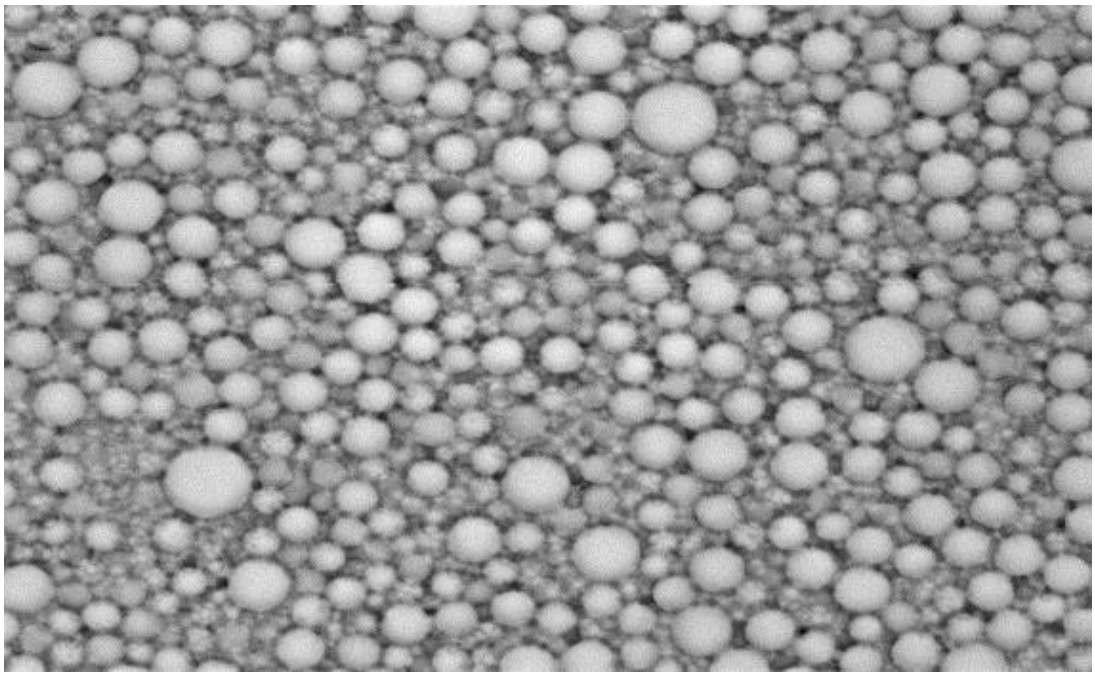

Fig. 6.1—(a) Microscopic image for acid droplets at 40 X magnification.

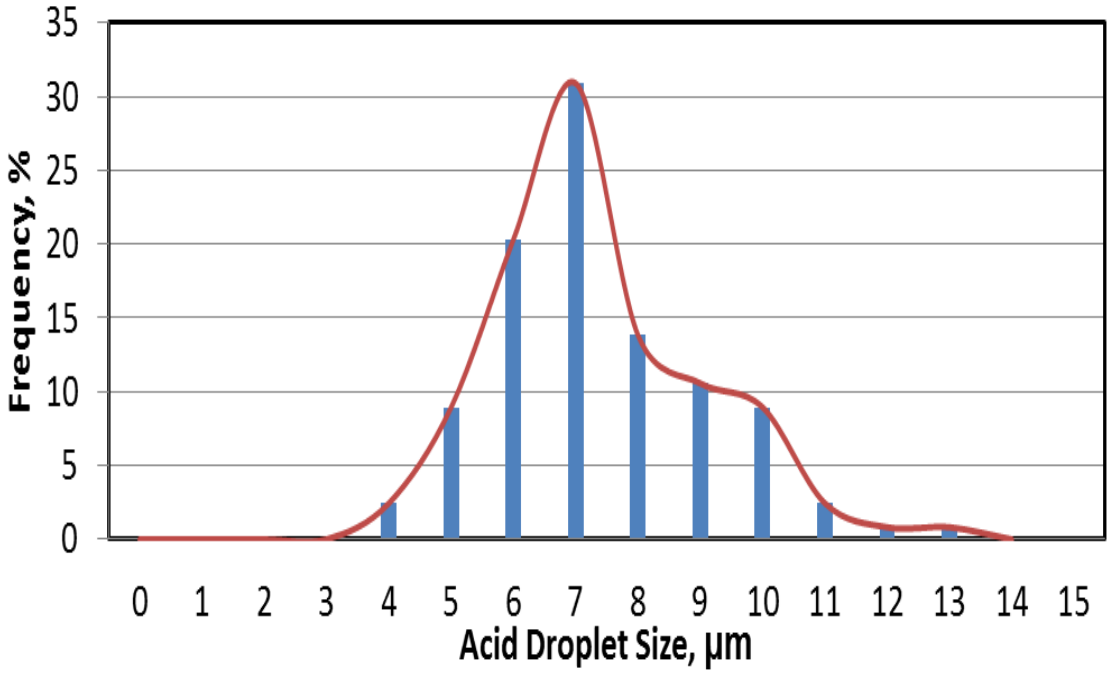

Fig. 6.1—(b) Droplet size distribution for the emulsified acid at 1 vol% emulsifier.

6.3.3 Coreflood Setup and Procedure

Fig. 6.2 shows a schematic diagram of the coreflood setup used in this study. The cores were weighed dry and saturated for porosity calculation. Then, they were CT scanned before acid injection. The coreflood setup included a core holder, two accumulators, a syringe pump, a hydraulic pump, and a differential pressure transducer to monitor the pressure drop across the core. A back pressure of 1100 psi was set to keep most of CO_2 in the solution. Prior to commencing the acid injection, distilled water was injected at different flow rates at room temperature to measure the core permeability. During injection, an overburden pressure at least 300 psi higher than the inlet pressure was kept to prevent the fluid bypass the core. The water injection continues during heating the system to 230°F. The emulsified acid was then injected until breakthrough while the pressure drop across the core was monitored. At breakthrough, the acid injection was stopped and water was injected until reaching the stabilization.

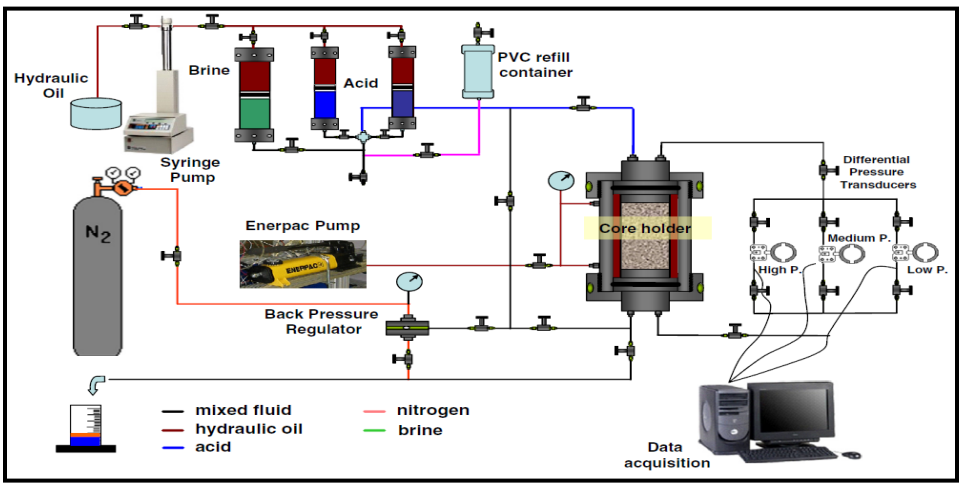

Fig. 6.2–A schematic diagram of the coreflood setup.

For each acid coreflood test, the core effluent samples were collected and analyzed for calcium and magnesium concentrations using Inductively Coupled Argon Plasma Optical Emission Spectroscopy (ICP-OES). The effluent pH was also measured to determine when an acid breakthrough occurred. To measure pH, an Orion model 720A meter and Cole Parmer Ag/AgCl single junction pH electrode were used.

6.4 RESULTS AND DISCUSSION

6.4.1 Description of Pore Structure Using Thin Section and SEM

The pore structure for Core 2V is shown in **Fig. 6.3**. The rock is a dolostone that contains over 95 wt% tightly euhedral dolomite crystals of approximately 90-μm in size. The rock shows a little inter-crystalline porosity. The pore size distribution is wide due to the existence of medium and large vugs among matrix micro-intercrystal pores. The average vug size varies from 0.75 to 1.6 mm. The vugs are connected only through tight inter-crystalline porosity and the microporosity, hence, controls the fluid movement to and from the vugs. Such pore structure promotes the existence of a preferential flow path for the flowing fluid.

Similarly, Core 5V exhibits a double porosity system: primary little intercrystalline porosity and secondary toughing vug porosity system **(Fig. 6.4)**. Dissolution, pressure solution and fracturing have combined to create larger pores (vugs), which are directly connected through microfractures and stylolites. It was observed that the vugs-microfracture system was surrounded by regions of micro-intercrystal pores. In this case, the preferential flow path from and to vugs through

microfracture exist and such pore structure acts as a delivery system.

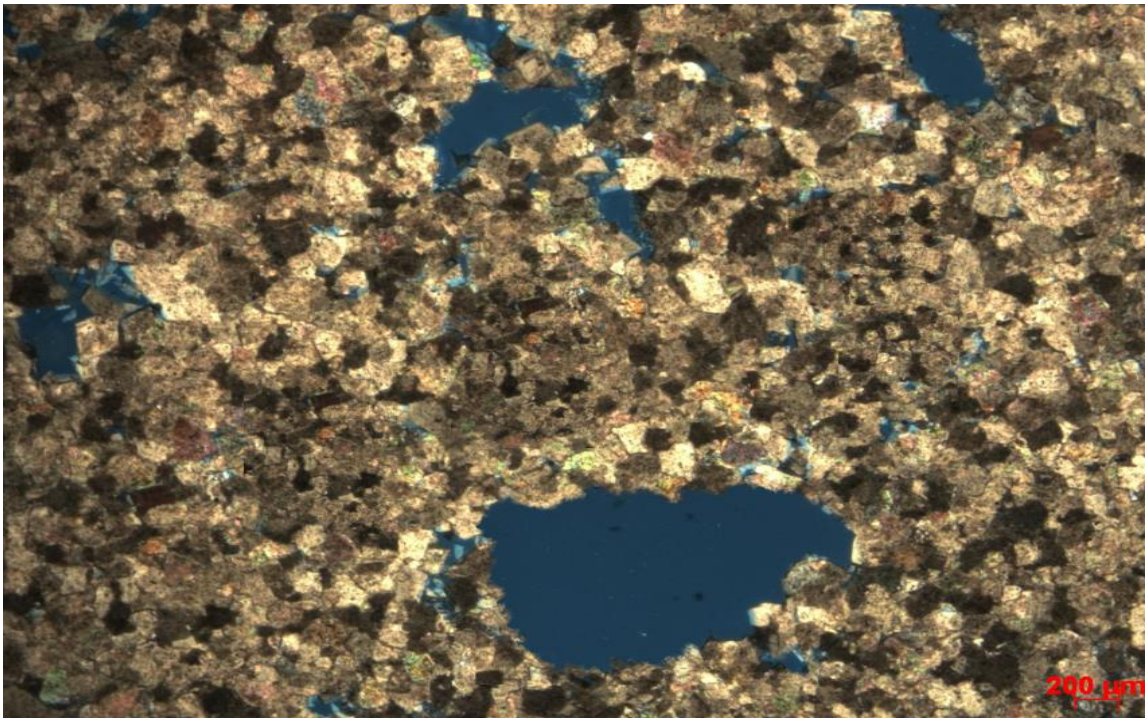

Fig. 6.3–Thin section image at 2.5 X magnification for vuggy Core 2V showing vugs are connected through a microporosity system.

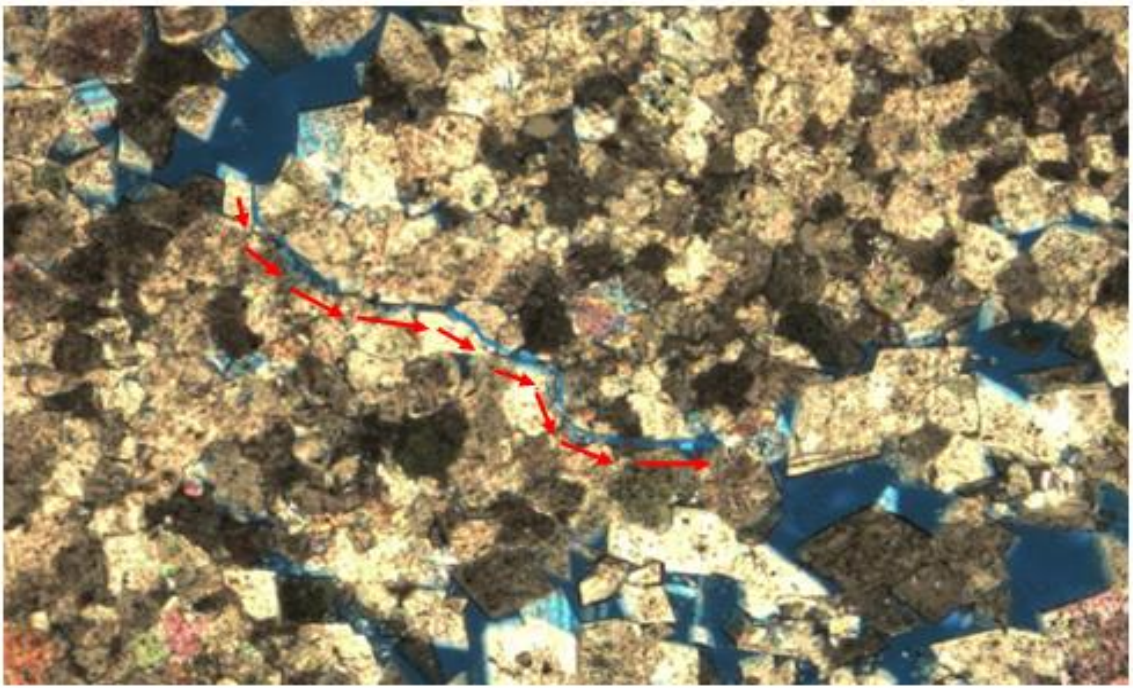

(a) 2.5X Magnification.

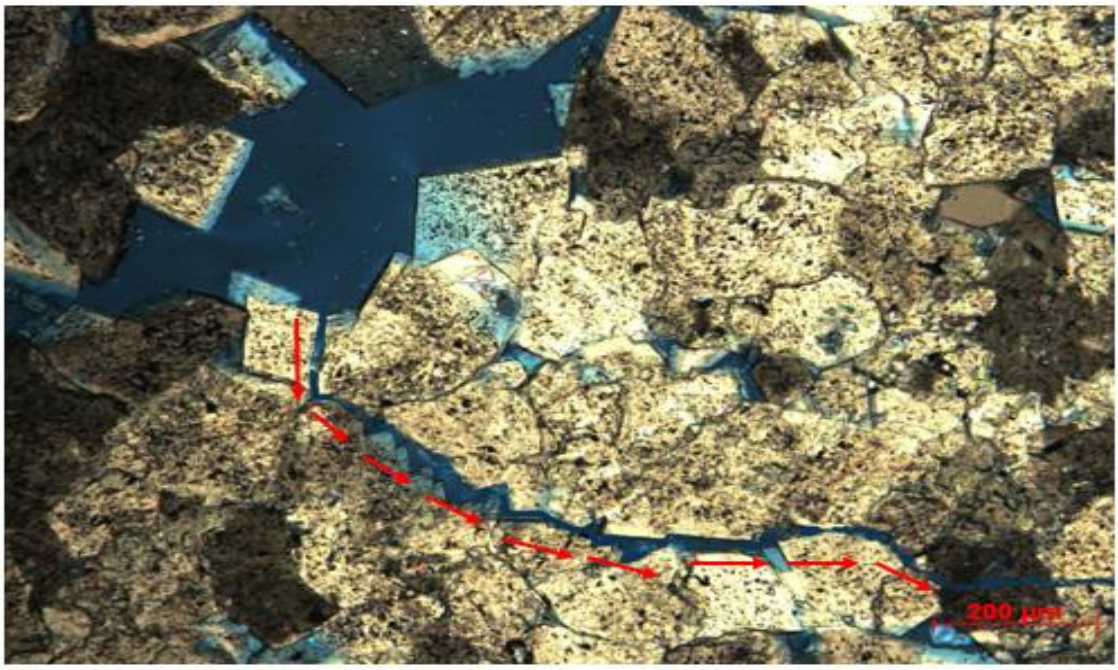

(b) 10X Magnification.

Fig. 6.4–Thin section image for Core 5V showing vugs are connected through a microfracture. Red line shows the preferential flow path.

In contrast, the homogenous carbonate rock samples are dolostones composed only of primary intercrystalline porosity with fine to rare medium crystals. They exhibit diagenetic texture produced by complete dolomitization of precursor limestone. **Fig. 6.5** shows a uniform pore size distribution for Core 2H. In such pore structure, the preferential flow paths do not exist.

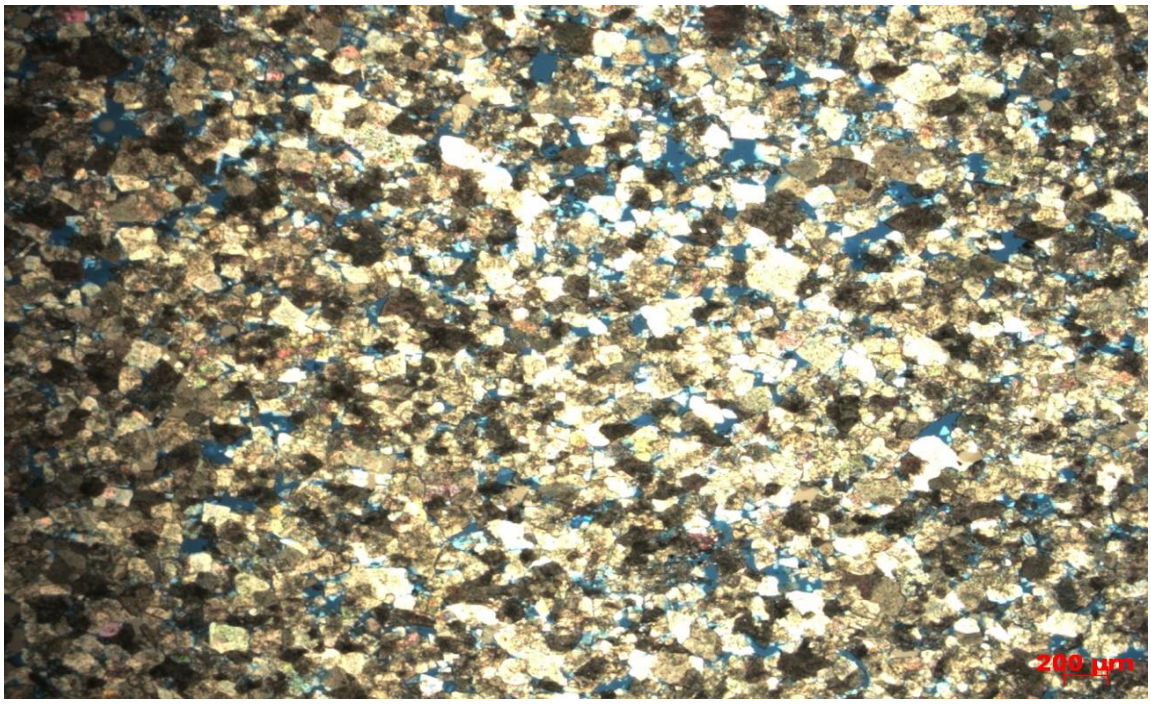

Fig. 6.5–Thin section image for Core 2H showing uniform distribution for the pore openings at 2.5X Magnification

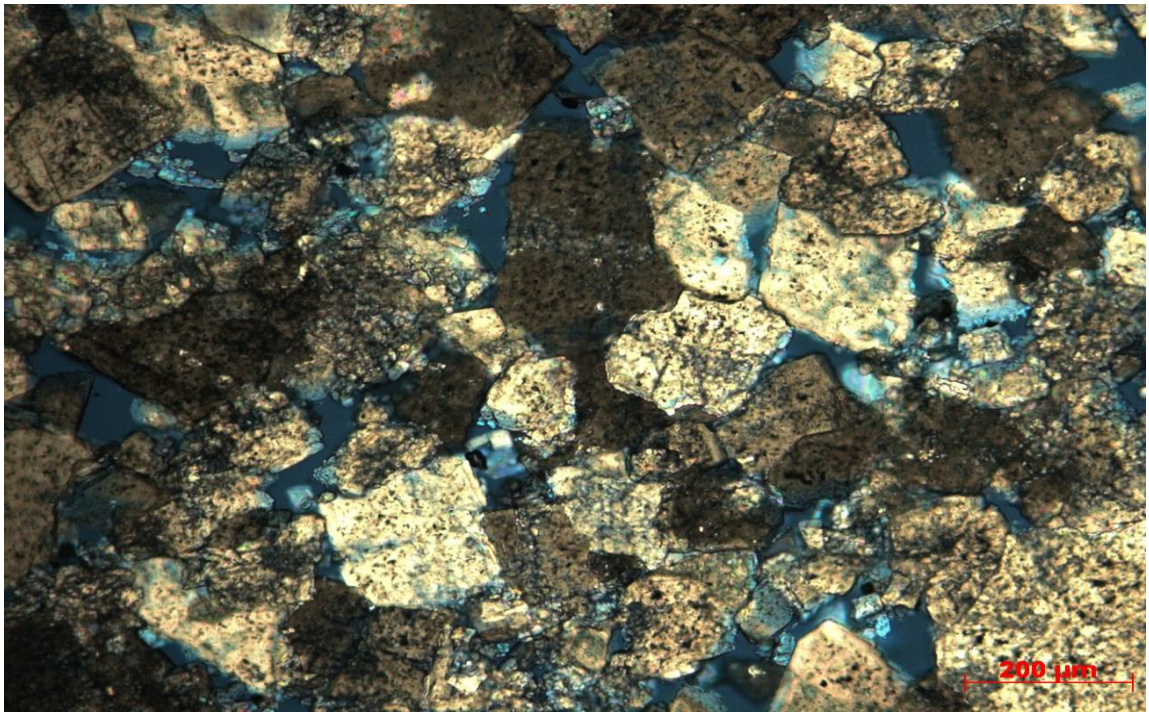

Fig. 6.5–Thin section image for Core 2H showing uniform distribution for the pore openings at 10X Magnification

6.4.2 Tracer Experiments

The normalized tracer concentration (C/C_0) in the core effluent samples is plotted in **Fig. 6.6** as a function of the cumulative pore volume injected. For homogenous carbonates, Core 2H showed a symmetrical tracer concentration profile about $C/C_0 = 0.5$ at one pore volume injected. These results are expected because carbonates of the intercrystal pore class exhibit a symmetrical profile around 1 PV injection at $C/C_0 = 0.5$ (Skauge et al. 2006). In contrast, the normalized tracer concentration profiles for vuggy

porosity dominated carbonates are characterized by early breakthrough and long tail behavior. This behavior, often referred to the existence of preferential flow path, which acts as a highly conductive streak in a low permeability matrix (Hidajat et al. 2004). The tracer results appear to be consistent with thin section observations.

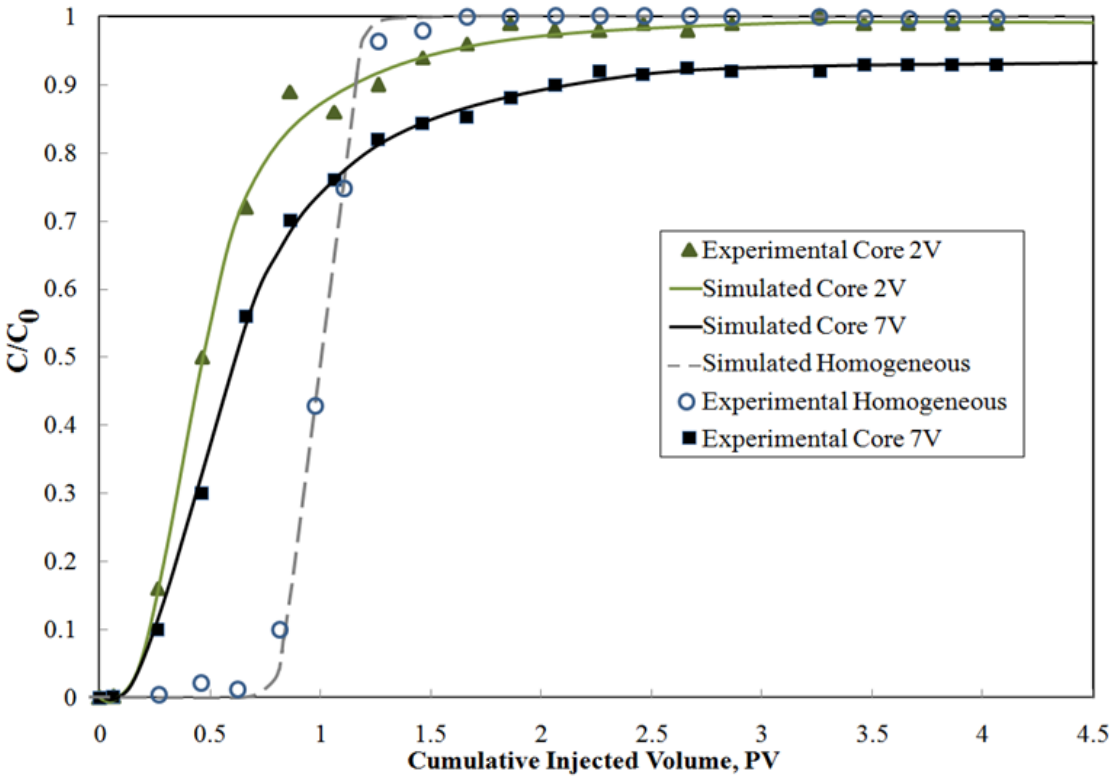

Fig. 6.6 (a)–Experimental and simulated normalized tracer concentration profiles.

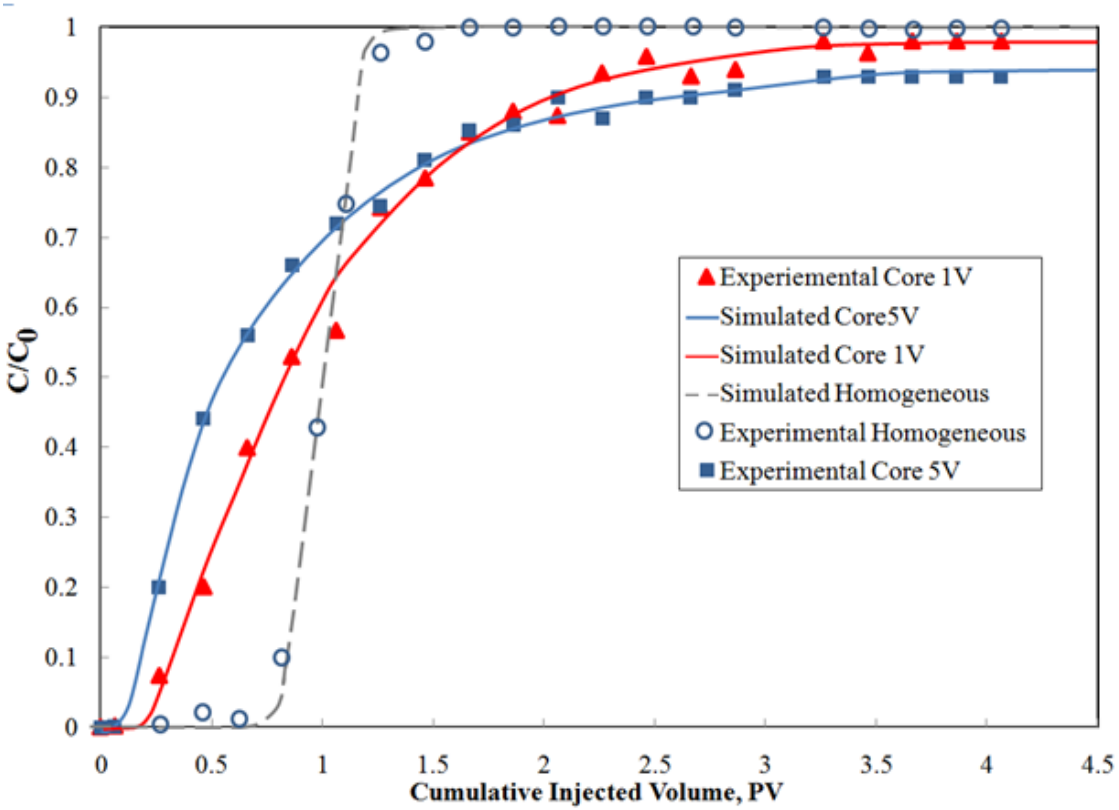

Fig. 6.6 (b)–Experimental and simulated normalized tracer concentration profiles.

The Coats and Smith (1964) dead-end pore model was used to simulate the normalized tracer concentration profiles, **Fig 6.6**. The model equations in a differential form are given in equations 6.1 through 6.4:

$$D\frac{\partial^2 C}{\partial x^2} - v\frac{\partial C}{\partial x} = f\frac{\partial C}{\partial t} + (1-f)\frac{\partial C^*}{\partial t} \quad \text{(6.1a)}$$

and

$$(1-f)\frac{\partial C^*}{\partial t} = M(C - C^*) \quad \text{(6.1b)}$$

Initial and boundary conditions should be defined to solve the differential equations:

Initial condition

$$C(x,0) = 0 \quad \text{for } x \geq 0 \quad \text{(6.2)}$$

Boundary Conditions

$$x = 0,\ vC_0 = v\,C - D\,(\partial C/\partial x) \quad \text{(6.3)}$$

$$x \to \infty,\ C(\infty, t) = 0 \quad \text{(6.4)}$$

The model is characterized by three parameters: (1) the dispersion coefficient (D); (2) the flowing pore volume fraction (f); and (3) the mass transfer coefficient (M). The normalized tracer concentration profile depends strongly on these three parameters (Batycky et al. 1982). A search technique based on a genetic algorithm was used to fit the experimental data with the model solution and obtain the three parameters (Zakaria et al. 2011).

The normalized tracer concentration profile for homogenous carbonates was modeled by a high flowing fraction of 0.98 in the C-S model. The normalized tracer concentration profiles for vuggy carbonates were simulated in the C-S model by flowing fraction significantly less than 1, measureable mass transfer coefficient, and higher dispersion coefficient, as the data in **Table 6.3** shows. This indicates the large variations in the local velocity gradient along the preferential flow path.

Table 6.3–Coats and Smith Simulated Parameters			
Core ID	**Flowing Fraction**	**Dispersion Coefficient, cm^2/s**	**Mass Transfer Coefficient, $cm.s^{-1}$**
Core 2V	0.47	1.45E-02	6.24E-05
Core 7V	0.5	7.09E-02	1.2E-04
Core 5V	0.49	1.22E-02	9.32E-05
Core 1V	0.52	9.34E-02	8.73E-05
Homogenous	0.98	-	-

6.4.3 Electrical Measurements

The resistivity index of the brine saturated cores was measured, from which the formation factor was calculated. The formation factor was obtained by measuring the resistivity of the brine saturated cores and comparing it with the resistivity of the brine itself, as given in Eq. 6.5:

$$F = R_{rock+brine}/R_{brine} = \tau/\varphi \quad \text{(6.5)}$$

In the case of multi-porosity carbonate rock type, Myer's pore combination model (PCM) (Myers et al. 1991) divides the pore space of the carbonate rocks into intergranular and vuggy porosity. The model is described as:

$$F = (1/\varphi_{int})^{1.91}(\varphi_{int}/\varphi)^{1.11} \quad \text{(6.6)}$$

Table 6.4 gives the calculated formation factor, the tortuosity, and the vuggy porosity fraction. The vuggy porosity fraction, as defined by Lucia (1983), is the fraction of pore space that is within grains, crystals, or significantly larger than grains or crystals; that is not interparticle pore space. The measured tortuosity values agree with those reported in the literature for vuggy carbonates (e.g., Hidajat et al. 2004).

Table 6.4–Formation Factor, Tortuosity, and Vuggy Porosity

Core ID	Formation Factor	Tortuosity	Vuggy Porosity, vol%*
Core 1V	192	17.7	58
Core 5V	149	15.5	57
Core 7V	128	13.3	48
Core 2V	233	20	59

*Vuggy Porosity = total porosity - intergranular porosity

6.4.4 Coreflood Experiments

Coreflood experiments were performed to assess the response of emulsified acid in vugular dolomitic rocks compared to that of the homogenous ones. Ten coreflood experiments with an emulsified acid system were conducted using homogenous and vugular dolomitic cores. All experiments were conducted at 230°F, while the pressure drop was recorded across the core. The results of all coreflood experiments are summarized in **Table 6.5**. The pH of all core effluent dropped to zero, indicating that

acid breakthrough did occur in all coreflood experiments. The pressure response curves for experiment #1 and experiment #2 can be found in **Fig. 6.7** and **Fig. 6.8**, respectively.

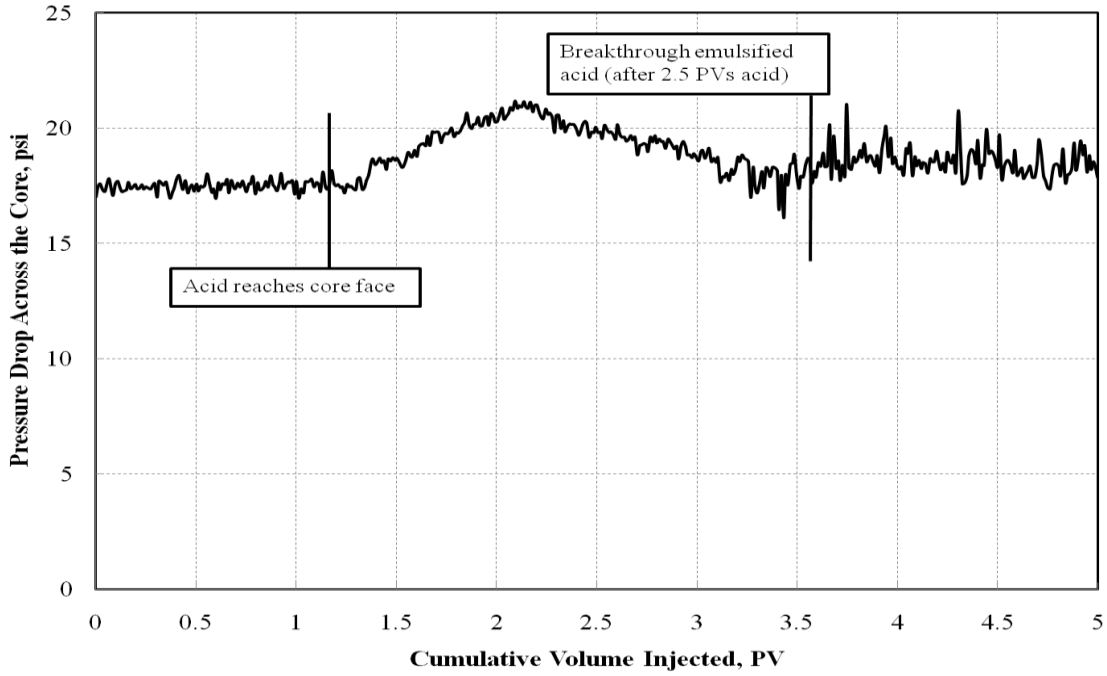

Fig. 6.7–Pressure drop across Core 2H. Emulsified acid was injected at 2 cm^3/min and T= 230ºF.

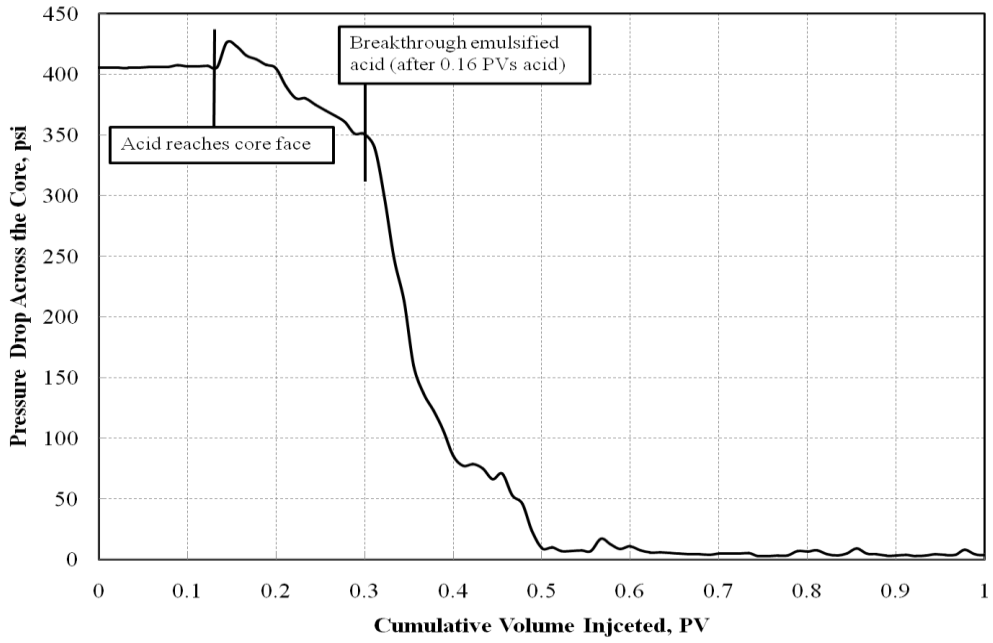

Fig. 6.8–Pressure drop across Core 2V. Emulsified acid was injected at 2 cm^3/min and T= 230ºF.

The emulsified acid was injected at a flow rate of 2 cm^3/min into Core 2H, where acid breakthrough was observed after 2.5 PV's of acid injection. **Fig.6.7** shows a typical pressure drop as a function of the cumulative pore volume injected. As the acid entered the core, the pressure drop increased because of the acid viscosity. Following this, the pressure drop started to decrease gradually in a constant manner due to wormholing until acid breakthrough. No sudden decrease in the pressure drop was observed when acid breakthrough. This may be attributed to: 1) Emulsified acid formed many narrow wormholes and the friction of such viscous solution in these narrow channels was high (wormhole geometry will be discussed in CT scan section) and, 2) An amount of

residual emulsion, retained inside the core, caused a damage that compensated the permeability improvement caused by the narrow wormholes (this will be discussed in the next section).

Table 6.5–Summary of Coreflood Results

Core ID	Core Flood No.	Rock Type	Flow Rate, cm^3/min	Acid PVBT	Initial Permeability, md	Final Permeability, md
Core 2H	1	Homogenous	2	2.5	22.5	80
Core 2V	2	Vuggy	2	0.16	0.96	90
Core 1V	3	Vuggy	1	0.2	22	400
Core 5H	4	Homogenous	5	2.4	32	90
Core 1H	5	Homogenous	1	2.7	39	70
Core 7V	6	Vuggy	7	0.14	32	598
Core 7H	7	Homogenous	7	3	23	100
Core 5V	8	Vuggy	5	0.32	29.4	394
Core 0.5V	9	Vuggy	0.5	0.1	17	423
Core 0.5H	10	Homogenous	0.5	3.2	37	115

Fig. 6.8 shows the pressure drop across Core 2V during the injection of

emulsified acid at a flow rate of 2 cm^3/min. In contrast to coreflood #1, the pressure drop behavior during flooding the vuggy dolomite core with emulsified acid is characterized by three trends. In the first trend, the pressure drop increased due to the higher viscosity of the emulsified acid than that of the injected water. The pressure increase was less than would be expected from the emulsion viscosity. Thin section observations for Core 2V **(Fig. 6.3)** showed that the vugs were connected through a tight matrix and microporosity network. On the other hand, the emulsified acid was a shear thinning fluid. The shear rate that the acid was subjected in porous media is directly proportional with the Darcy velocity and inversely proportional with the core permeability (Rojas et al. 2008) as given in Eq.6.7:

$$\dot{\gamma} = u/\varphi l \quad \text{(6.7)}$$

where u is the Darcy velocity, m/s; φ is total porosity, volume fraction; l is a characteristic length representative of the pore scale velocity, $l = 0.05\,D$; where D is the average pore throat diameter. Dick et al. (2000) stated that the pore size is a function of the square root of the permeability. Thus, the shear rate that the emulsified acid was subjected to in Core 2V was high due to the low permeability of the core, which led to lower viscosity of the emulsified acid.

In the second trend, the pressure declined rapidly due to wormholing and any pressure drop exists because of the matrix flow ahead of the propagating wormhole. Finally, a sudden decrease in the pressure drop was observed when acid breakthrough

occurred after only 0.16 PV's of acid injection (compared to 2.5 PV's of acid in experiment # 1, with the homogenous core).

Interpreting the acid coreflood results using the tracer experiments and thin section observations, demonstrating that the vuggy dolomite cores showed a preferential flow path and early breakthrough, gives an explanation of the low acid pore volume to breakthrough observed in vuggy porosity dominated rocks when compared to homogenous carbonates. In other words, the volume fraction of the pores available for the injected fluid to flow is low. Therefore, as the acid enters the core, it channels the preferential flow path and dissolves low fraction of the core, leaving most of the rock untouched. This leads to a rapid pressure decline and low acid volume to breakthrough.

6.4.5 Permeability Evolution in Vugular Rocks

The pressure drop response during the acid injection is an indicator of the manner in which the permeability evolves due to dissolution in the vugular rocks. The evolution of permeability due to dissolution in vuggy cores differs than that in the homogenous case **(Figs. 6.9 and 6.10)**. For homogenous carbonates, the permeability slightly reduced after acid treatment. This reduction in permeability indicates that the damage caused by residual emulsions compensates for the improvement caused by the branched narrow wormholes. In vuggy rocks, the permeability increases rapidly and the permeability improvement due to the formation of a single dominant wormhole is much greater that any damage maybe encountered from the residual emulsions. This indicates that an effective wormholing in vugular rocks was achieved when compared to

homogenous ones. In other words, a single dominant wormhole was formed for vugular cores compared to many narrow branched wormholes in the homogenous core.

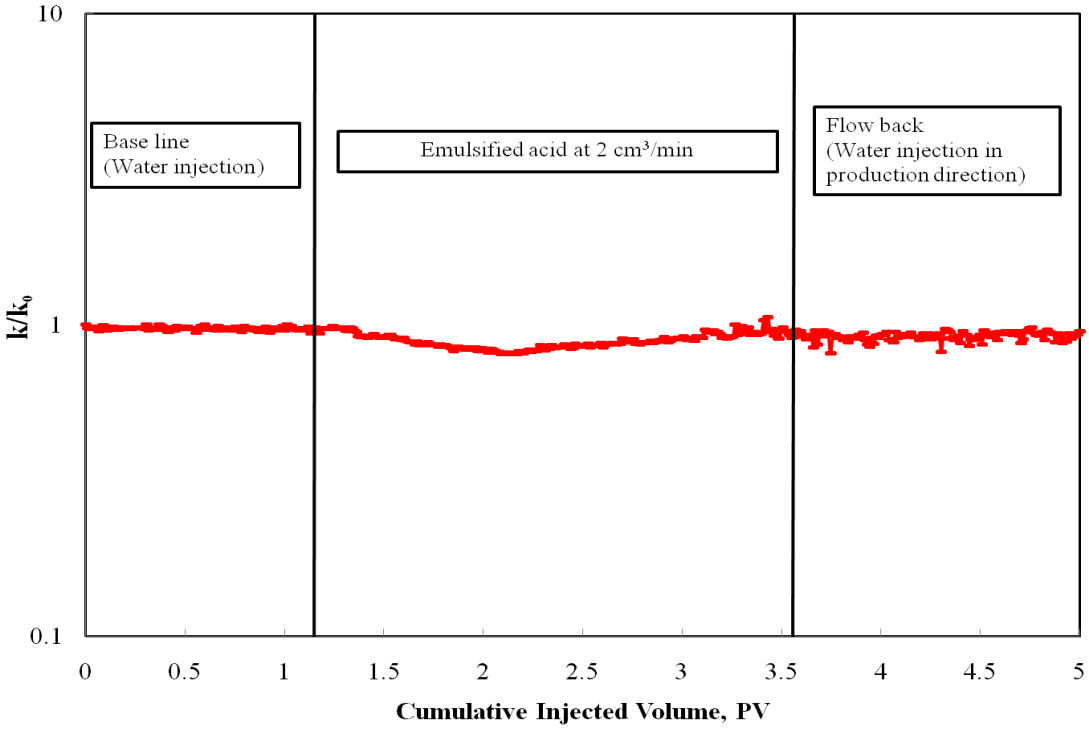

Fig. 6.9–Evolution of permeability for coreflood experiment #1.

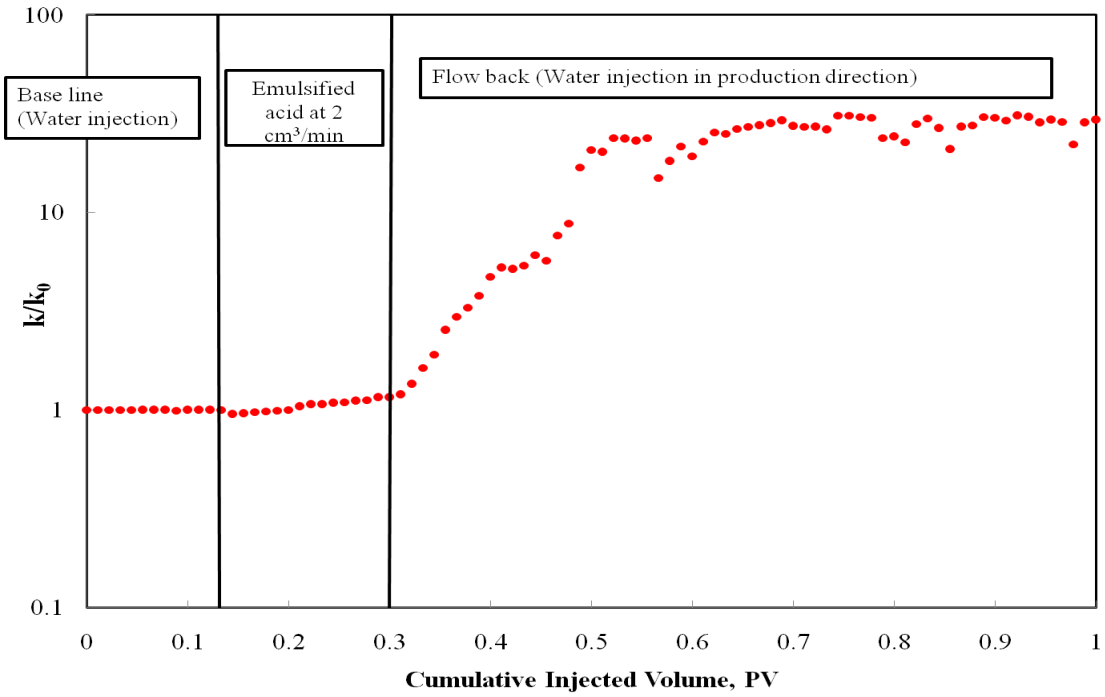

Fig. 6.10–Evolution of permeability for coreflood experiment #2.

Flowback experiments were done to evaluate the cleanup characteristics in both carbonate types (**Fig. 6.11**). In homogenous carbonates, flowback the cores with water in the opposite direction (production direction) did not reduce the encountered damage caused by the residual emulsions. Ethylene glycol monobutyl ether solution at 10 vol% was used to aid in the cleanup and permeability improvement, hence, was achieved.

In contrast, vuggy carbonates show better cleanup characteristics. In terms of acidizing practices, no need to back flow the wells when emulsified acid systems are used to stimulate the vuggy dolomitic reservoirs. This could reduce the rig time and the cost of the stimulation job.

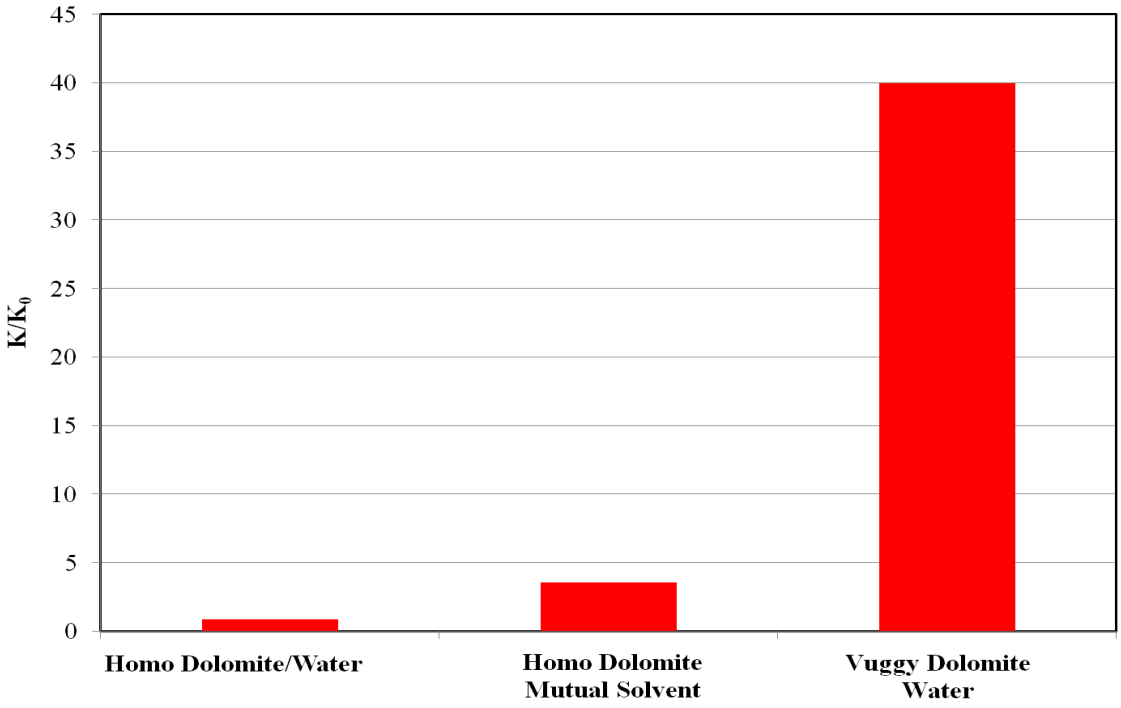

Fig. 6.11–Regained permeability of cores after acid injection in homogenous and vuggy carbonates.

6.4.6 Analysis of Core Effluent Samples

The emulsified acid did react with both homogenous and vuggy cores and released calcium and magnesium in the core effluent samples as shown in **Fig. 6.12**. In coreflood Experiment # 1, the pH reached zero when acid breakthrough occurred after 2.5 PV's injected **(Fig. 6.13)**. With the vuggy dolomite core in Experiment # 2, the initial pH value was nearly 7 and after injecting only 0.16 PV's of acid solution, it dropped to zero. At this point, the injection was switched from emulsified acid to water and the pH started to increase after 1.6 PV's of water injection.

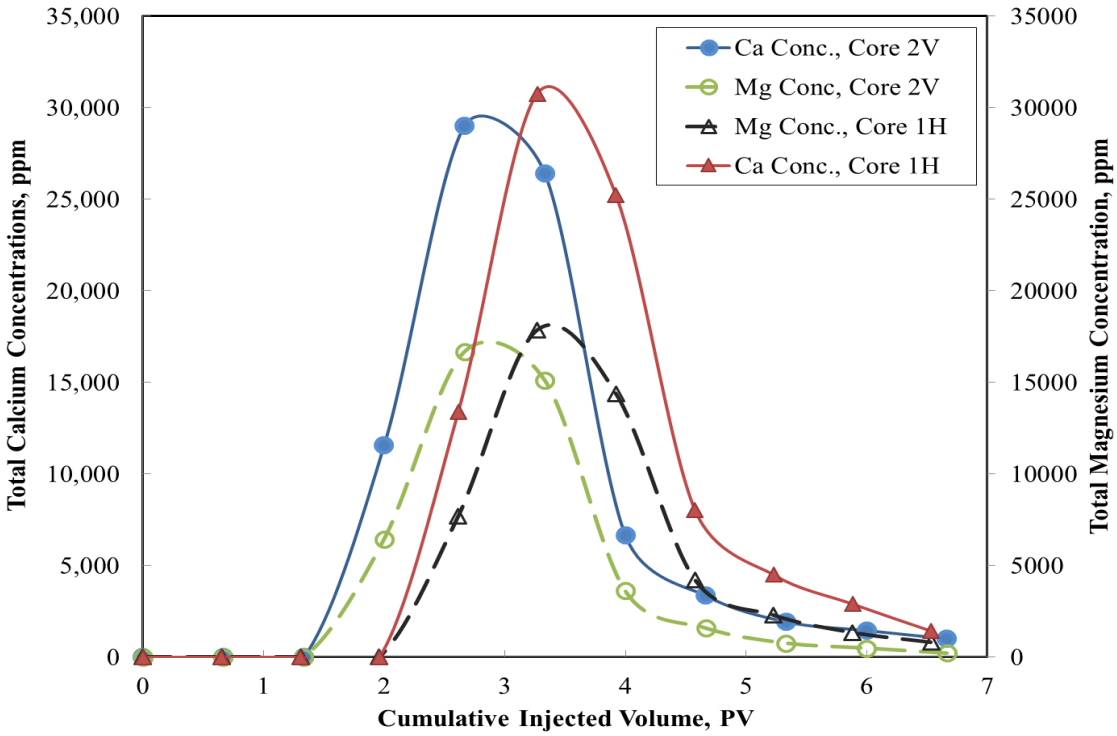

Fig. 6.12–Calcium and magnesium concentrations in the core effluent samples.

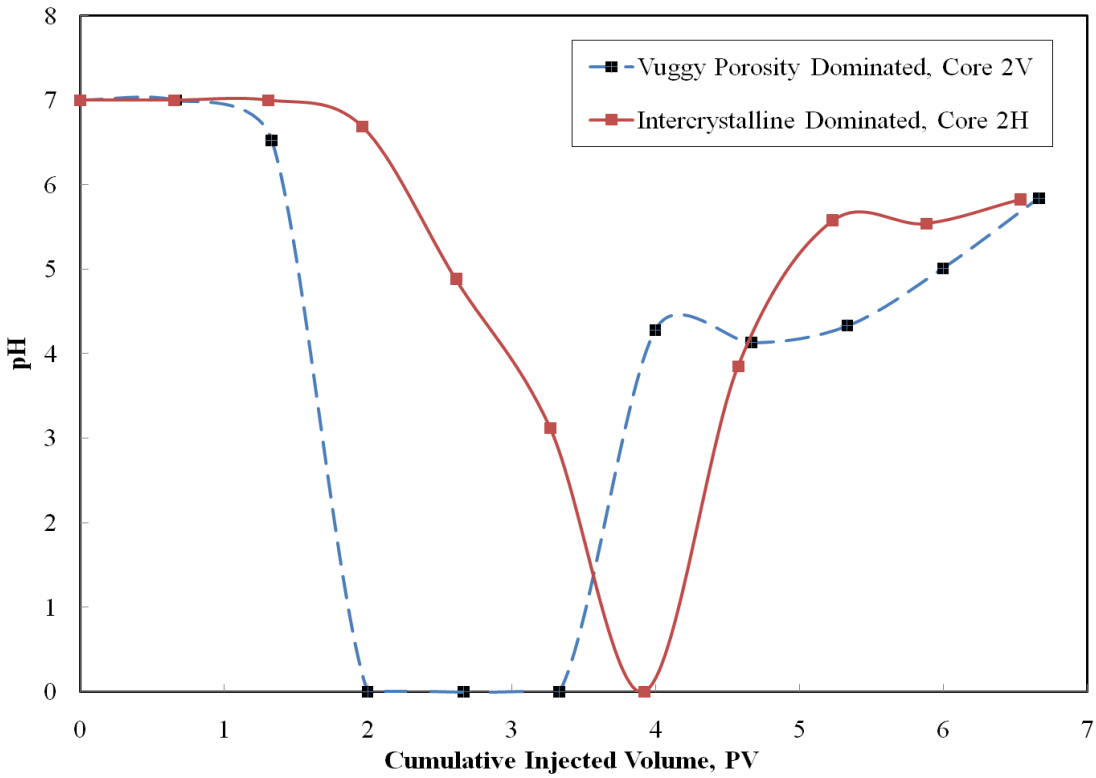

Fig. 6.13–Measured pH in the core effluent samples.

It was noted that pH took a longer time to start rising in coreflood experiment # 2 than that in experiment # 1. This indicates that more live acid was available for deeper wormhole penetration in vugular pore structured formations than that in homogenous carbonates, thus, a more effective acid treatment was achieved with less volume of acid.

6.4.7 Pore Structure and Pore Volume to Breakthrough

Fig. 6.14 suggests that the acid pore volumes to breakthrough observed in vuggy porosity dominated rocks are much lower than that in the homogenous carbonates (intercrystalline porosity dominated) by a factor of 15 to 20 times. Acid pore volume to breakthrough strongly depends on how fast the wormhole propagates along the rock. This is clearly illustrated in **Fig. 6.15**, where the wormhole propagation rate is plotted against the interstitial velocity. It is noted that the wormhole propagates more rapidly in vuggy porosity dominated rocks than that in homogenous carbonates. In the next paragraphs, this finding was investigated.

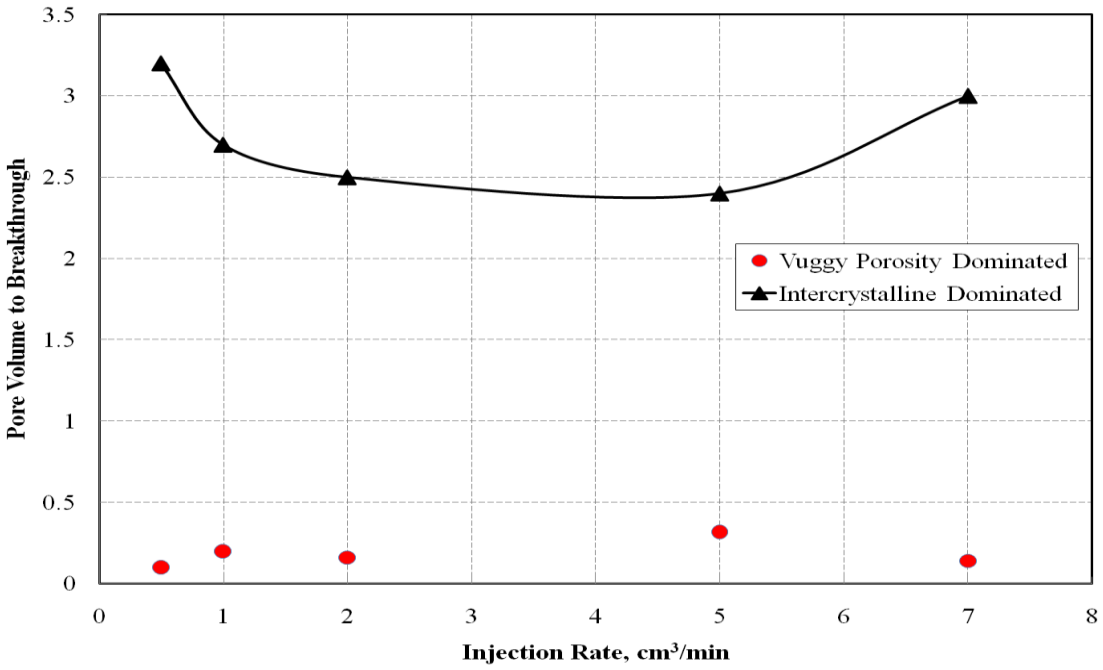

Fig. 6.14–Experimental observed pore volume to breakthrough.

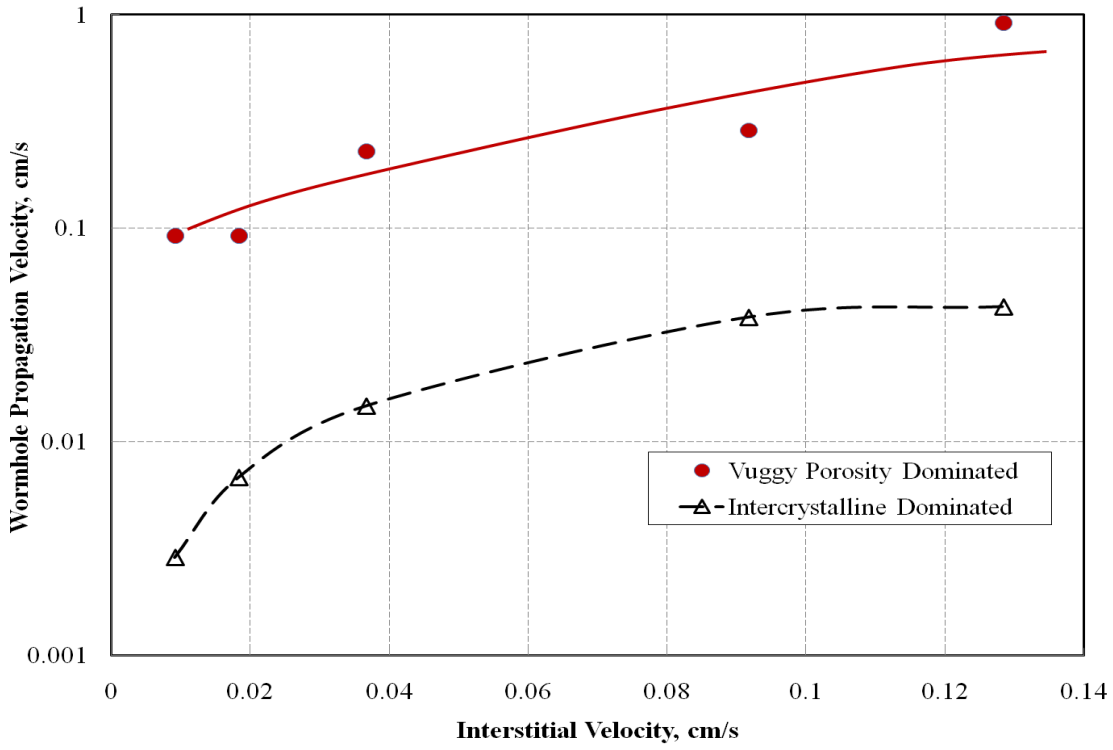

Fig. 6.15–Wormhole propagation velocity.

For vuggy porosity dominated rocks, if the acid channeled the preferential flow path through which it moves at higher velocity than in the restricted pore fraction (1-*f*), corresponding to faster wormhole propagation rate, this leads to a rapid acid breakthrough and very low PV_{bt}. In other words, the acid flows in a small volume fraction of the core guided by the distribution of the vugs and leaves most of the rock untouched. Thin section observations, tracer experiments and CT scanning (discussed in details in CT section) all support such conclusion.

The thin section observations on vuggy cores demonstrate that the vugs were distributed in a manner that creates a preferential flow path for the flowing fluid, which

contributes to the early breakthrough observed in the tracer experiments **(Figs. 6.3 and 6.4)**.

The normalized tracer concentration profiles were simulated in the C-S model by flowing fraction significantly less than unity. In other words, the volume fraction in vuggy cores available for the injected fluid to flow is low.

We will further investigate how the acid propagates in the vuggy porosity dominated rocks until acid breakthrough. Our hypothesis is that "the variation in the local velocity gradient at the pore scale guides the propagation of acid in vuggy porosity dominated rocks". The normalized tracer concentration profiles for vuggy carbonates **(Fig. 6.6)** are well simulated in the C-S model by a high dispersion coefficient. The variation in the microscopic velocity within the flow path from one pore to another is believed to contribute to high dispersion. The enlargements (vugs) and constriction (narrow channels connecting vugs) in the pore channel leads to a high variation in the local velocity gradient. Also, when large pores are connected to narrow channels, the stagnant regions, most probably, occur. Following that, large residence times are expected in the stagnant regions because of mass transfer controlled by diffusion, which are the origin of the long tail behavior. Thus, the high dispersion coefficient modeled in the C-S model and the long tail observed in the normalized tracer concentration profiles confirms that the path drawn from vug to other through the connecting channel between them is the main flow path in the vuggy porous media which the acid will follow until breakthrough **(Fig. 6.4).**

One more important observation, it is clear from the coreflood experiment results that no optimum injection rate was identified for vuggy carbonates within the tested injection flow rates range. The wormhole dissolution pattern is widely discussed in the literature and it was found to be strongly dependent on the injection rate. Daccord (1987) found that at high injection rates, the branched wormhole structure may be fractal. This study focused on virgin area: the effect of vuggy porosity structure on the optimum injection rate.

The optimum injection rate marks the transition from diffusion limited wormholing to fluid loss wormholing. In other words, at injection rates higher than the optimum one, the fluid loss at the wormhole face is the dominating factor in branching the wormhole pattern. In our case, vuggy carbonates, when the acid propagates in the vuggy pores, the wormhole diameter will be equal to the vug size. The acid, then, tends to flow in the narrow channels connecting the vugs where the velocity of the acid is at a maximum rate and the fluid loss at the wormhole face is minimal. Thus, in vuggy porosity dominated rocks, no transition exists between the diffusion limited and fluid loss limited wormholing, and thus, no optimum injection rate is noted.

For homogenous carbonates, the thin section observations do not promote any preferential flow paths **(Fig. 6.5)** and the normalized tracer concentration profile was simulated by a high flowing fraction near 1 in the C-S model. In other words, the acid, when it flows inside the core, contacts a high fraction of the rock leading to branched wormhole and more acid consumption.

The rotating disk measurements demonstrated the much retarded emulsified acid

spending rate especially with dolomite. This leads to a slow increase in the wormhole width and one would expect narrow wormholes were formed. Combining the thin section observations, tracer experiment results and the rotating disk measurements, one would expect branched narrow wormholes to be formed in the homogenous carbonates (interscrystalline porosity dominated rocks). Thus, more acid consumption and high acid pore volumes to breakthrough.

6.4.8 CT Scan Study

6.4.8.1 Vuggy Carbonates

Fig. 6.16 shows the cross sectional area for slices 3, 10, 18, and 25 taken from Core 2V before emulsified acid injection. Observing the slices for the studied core, the vugs are the main characteristic of the porosity system. At this scale, the average vug size varies from 3 to 14 mm. A yellow colored region indicates the matrix porosity while the dark and violet colored regions indicate clean and filled vugs, respectively.

All of these observations (pressure response, PV_{bt}, thin section, tracer experiments, and permeability evolution trend) promote a single dominate wormhole along the core that follows the preferential flow path. **Fig. 6.16** shows the wormhole dissolution pattern for Core 2V after acid injection, which appears consistent with the promotion. The cross sectional slices for Core 2V after acid injection was shown to the left of the figure. It was shown that the acid propagates in a selective manner, in other words, the acid propagates through the vuggy porosity region along the core, and no wormholes were observed in the matrix porosity regions.

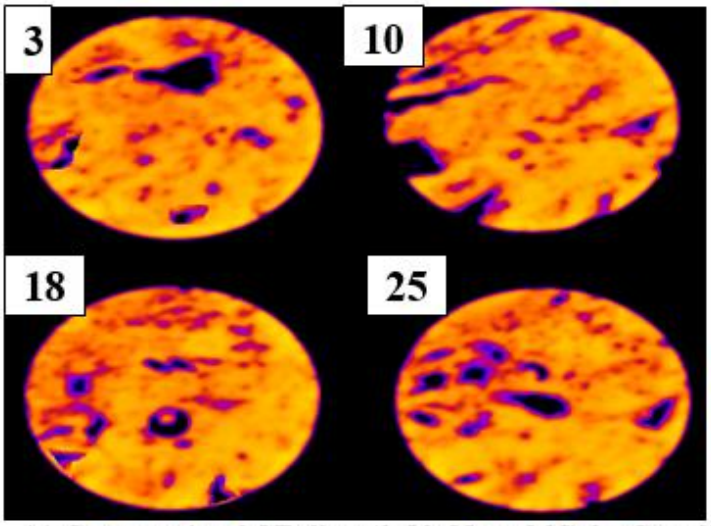

(a) Cross-sectional CT slices (3, 10, 18, and 25) for Core 2V before acid injection. Separation distance between each slice is 5 mm

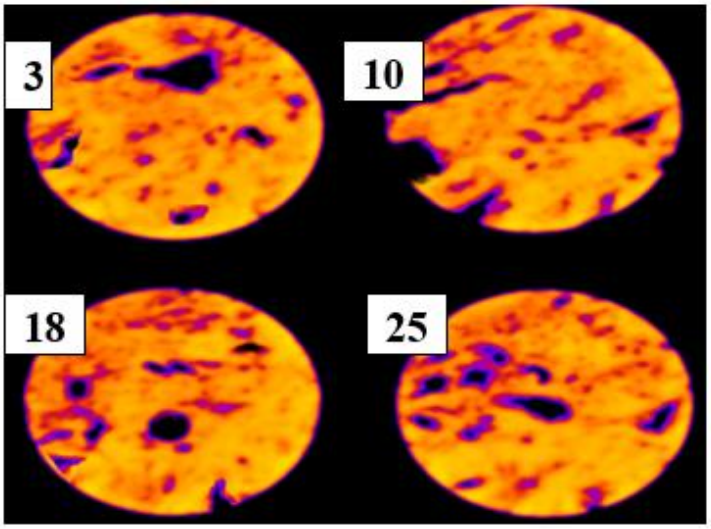

(b) Cross-sectional CT slices (3, 10, 18, and 25) for Core 2V after acid injection. Separation distance between each slice is 5 mm

(c) 3D Wormhole pattern

Fig. 6.16–CT scan study for vuggy Core 2V showing a single dominant wormhole.

An approach to quantifying the difference between the geometry of the main wormhole generated in Core 5V to that in Core 7V. One would examine the variance of the "tortuosity" of the wormholes. Tortuosity is defined as the ratio between the effective wormhole length (Le) and the length of the core (L) and can be calculated as given in Eq. 6.8:

$$\tau = L_e/L \quad (6.8)$$

Effective wormhole length was taken as the line drawn down the center of the wormhole (Lynn and Nasr-El-Din 2001). The wormhole tortuosity for Core 5V was found to be 1.46, and for Core 7V, it is 1.12. These data demonstrate that the acid pore volume to breakthrough in vuggy carbonates is related to the tortuosity of the preferential flow path that the acid follows to breakthrough.

6.4.8.2 Homogenous Carbonates

The rotating disk measurements promote narrow wormholes because of the retarded reacting process between the emulsified acid and dolomite. On other hand, the tracer experiments promote that the acid will touch high fraction of the rock. The CT scan results are consistent with the rotating disk measurements and tracer experiments results.

Fig. 6.17 shows the wormhole dissolution pattern created by the emulsified acid in Core 2H. As shown, the emulsified acid forms narrow branched wormholes and

touches a high fraction of the core during its propagation in the homogenous carbonates. The average wormhole diameter is 2 mm compared to 9 mm for the single dominant wormhole created in vuggy carbonates.

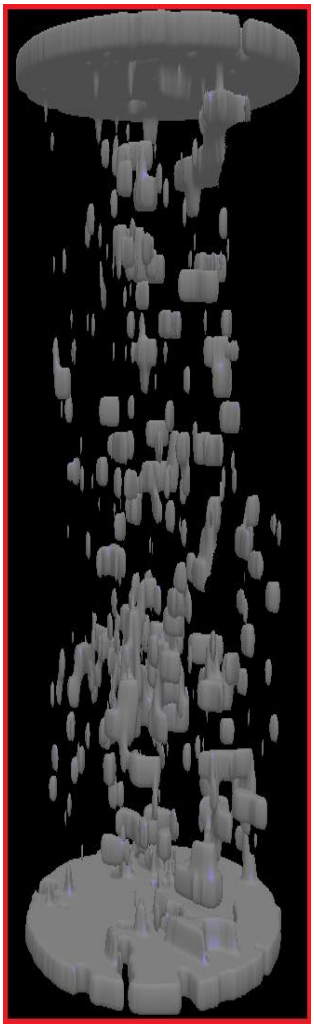

Fig. 6.17–CT scan study for homogenous Core 2H showing branched narrow wormholes.

6.5 CHAPTER CONCLUSIONS

The study demonstrated that the presence of vugs in dolomite cores has a significant effect on the stimulation treatment using emulsified acids. Based on the results obtained in this study, the following conclusions can be drawn:

1) The efficiency of the acid treatment increases in the presence of vugs. The acid volume needed to propagate a wormhole in vuggy porosity dominated rocks, at different flow rates, was less than that in homogenous rocks by a factor of 15 to 20 times.
2) The efficiency of the wormholing process increases in vuggy carbonates when compared to homogenous ones. In vuggy carbonates, a single dominant wormhole will be created with less volume of acid. Examination of wormhole structure in homogeneous carbonates showed that a narrow branched wormhole network is present. Thus, in vuggy carbonates, a better outcome for the acid treatment is expected as characterized by a lower skin factor.
3) Thin section observations for vuggy carbonates show that the vugs are distributed in a manner that creates a preferential flow path for the acid to propagate through until breakthrough. In field, the wide pore size distribution and preferential flow path will lead to deeper acid penetration and better permeability enhancement than expected.
4) Vuggy carbonates show better cleanup characteristics than that in homogenous carbonates. In terms of acidizing practices, no need to flow back the wells in the case of vuggy carbonates. This could reduce the rig time and the cost of the

stimulation job.

5) In acidizing simulations, heterogeneities such as vugs should be included with the large scale heterogeneities such as laminations and fractures, for better design, monitoring, and evaluation of field acid treatments.

CHAPTER VII

NEW INSIGHTS INTO THE ACID FLUID FLOW DISTRIBUTION IN CARBONATE ROCKS

7.1 INTRODUCTION

Uniform distribution of live acids is necessary for the successful matrix acid treatments. When injected, the acid tends to follow the path of least resistance that is to the higher permeability and/or the least damaged zones. Since damage must be removed or bypassed from the entire producing interval, effective diversion techniques must be employed.

Uniform distribution of acids in carbonates is generally more difficult than in sandstones because of the ability of the highly reactive HCl to increase permeability in carbonate rocks as the acid reacts with the rock and generates new flow channels. Apart from particulate diverters, a number of methods and techniques are commonly used for acid diversion in matrix treatments including: mechanical methods (packers, bridge plugs, ball sealers, and coiled tubing); and chemical methods (gelled acids based on polymers or viscoelastic surfactants, emulsified acids and foams).

An extensive literature review showed that most of acid diversion studies focused on studying the effectiveness of different acid systems or different diverting agents against cores of different permeabilities. So, the objective of this chapter is to study the effect of presence of carbonates of different rock structure or pore structure along the formation on the acid fluid flow distribution.

The study was performed using two dolomite rock types. Vuggy dolomite cores that represent mainly the vuggy-dominated-pore structure, while the homogenous cores represent the intercrystalline-dominated-pore structure. Both dolomite rock types were first characterized using thin section analysis and tracer experiments. Following that, the effect of different pore structure on the acid fluid flow distribution was studied using parallel coreflood setup. The coreflood runs were conducted on 6 x 1.5 in. cores using emulsified acid formulated at 1 vol% emulsifier and 0.7 acid volume fraction.

Experimental results showed that even for nearly the same permeability, the emulsified acid preferred to flow through the vuggy dolomite rock type even at low or high injection rates. The results also showed that the presence of carbonate of different pore structure along the treated formation is more severe than the permeability contrast. The results obtained can be used to better design acid treatments in carbonate reservoirs.

7.2 EXPERIMENTAL STUDIES

7.2.1 Cores Selection

Dolomite cores were drilled from a large block of carbonate obtained from the Thornton outcrop. Pure vugular structure can be found in carbonate rocks with a high degree of dolomitization where the vugs are created by a random process. The cores were cleaned and dried in an oven at a temperature of 280ºF. The cores were then weighed dry and after saturation with deionized water under vacuum. The pore volume was determined from these measurements. **Table 7.1 and Table 7.2** lists the properties of the dolomite cores used in this study.

7.2.2 Thin Section

Blue epoxy impregnated thin sections were prepared to obtain a detailed description of the porosity distribution for each dolomite rock type**.** The thin section was viewed under an optical microscope. Two images for each rock sample were captured under a magnification of 2.5 and 10X using a digital camera and then sent via card to a computer. Thin section analysis provides means to identify the pore types and their connectivity.

7.2.3 Tracer Experiments

A solution with 8 wt% KCl was injected in both dolomite rock types. KCl (ACS reagent, > 99 wt%) was used as a conservative tracer. The concentration of potassium ions in the tracer solution was measured by inductively coupled plasma spectrometer and the measurement was repeated three times to give an average concentration of 36.70 ± 0.05 g/l. Prior to commencing the tracer experiments, the cores were saturated with deionized water under vacuum, and then preflushed with deionized water. The tracer solution was then injected into both dolomite rock type cores for six pore volumes. Core effluent samples were collected and analyzed by inductively coupled plasma spectrometer (ICP-OES) for K^+ ions concentration.

7.2.4 Coreflood Setup and Procedure

The parallel coreflood setup was constructed to simulate the matrix-stimulation treatments **(Fig. 7.1)**. A tee connection was used to split the inlet line into two branches. Each branch fed the inlet of one core holder. Each core holder had its own outlet that connected to a different backpressure regulator adjusted to 1,000 psi. To ensure that the two cores were subjected to same condition, the backpressure on the outlet of the two cores had the same value and the lengths of tubing connected to the two core holders were similar. Pressure transducers were connected to a computer to monitor and record the pressure drop across the cores during the experiments every 5 seconds.

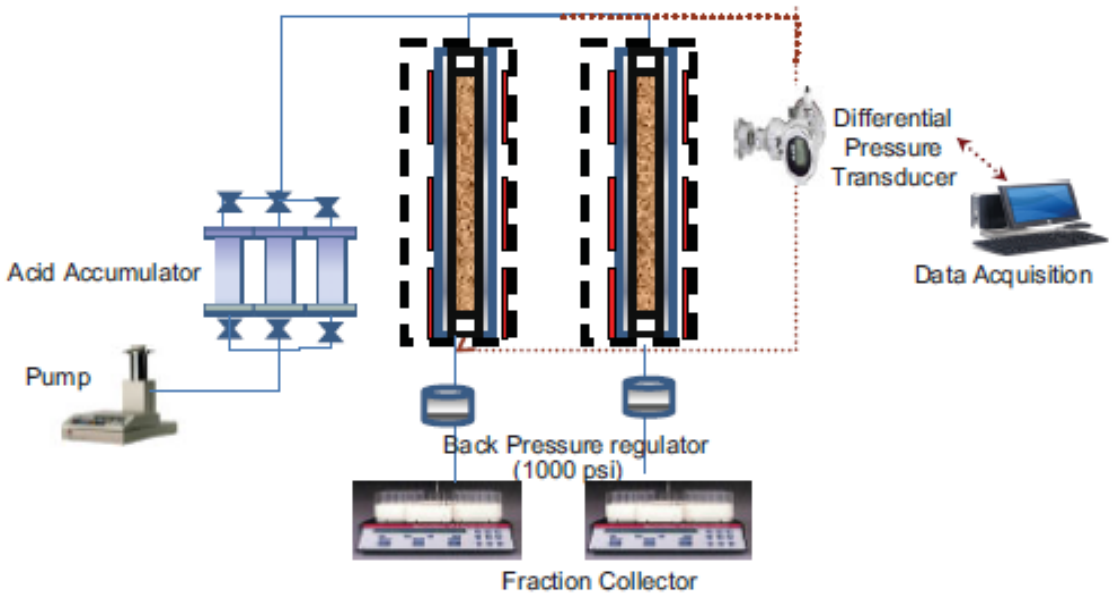

Fig. 7.1—Coreflood setup used for parallel coreflood experiments.

Before starting injection of the emulsified acid, deionized water was injected separately in each core with the selected rate. This ensured that the core was fully saturated with water. Also, the pressure drop required to flow the water in each core was recorded for permeability measurements for each core used for parallel coreflood experiments. After measuring the pressure drop for each core, deionized water was pumped through the two cores. After reaching a stable pressure drop across the cores, a stage of emulsified acid was injected until breakthrough occurred in one of the cores. The pressure drop across the cores was monitored and the flow rate inside each core was determined by collecting effluent volume over a specific period of time. The permeability was then measured separately for the core that did not have a breakthrough.

7.3 RESULTS AND DISCUSSION

7.3.1 Thin Section Analysis

The vuggy dolomite rock samples exhibit double porosity system: primary little intercrystalline porosity and secondary toughing vug porosity system **(Fig. 7.2)**. Dissolution, pressure solution and fracturing have combined to create larger pores (vugs), which are directly connected through microfractures and stylolites. It was observed that the vugs-microfracture system was surrounded by regions of micro intercrystal pores. In this case, the preferential flow path from and to vugs through microfracture exist and such pore structure acts as a delivery system.

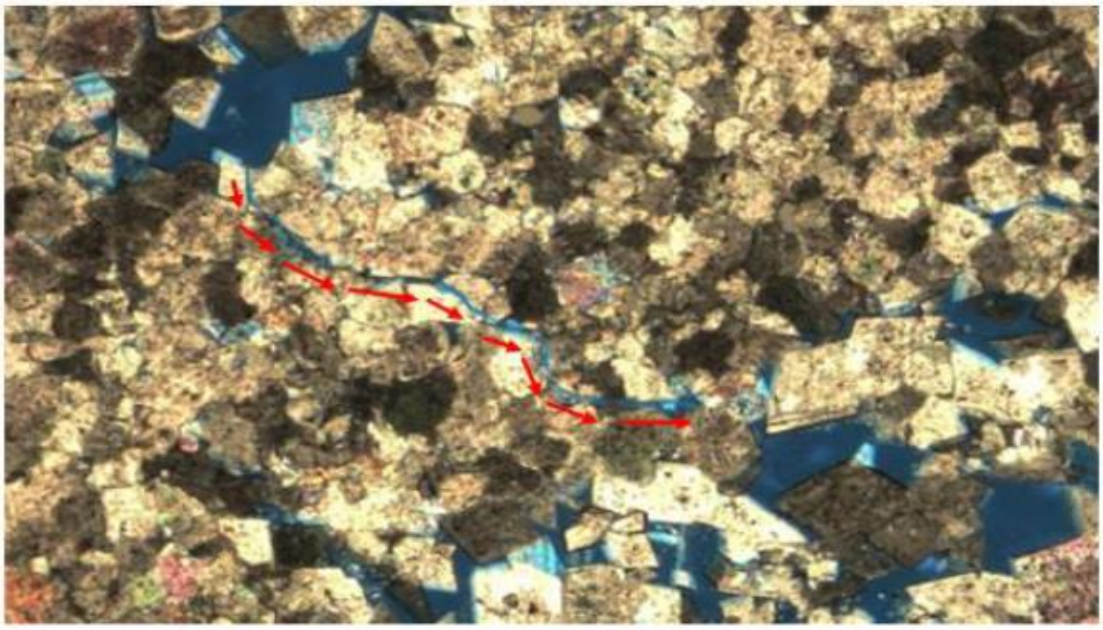

(a) 2.5X Magnification.

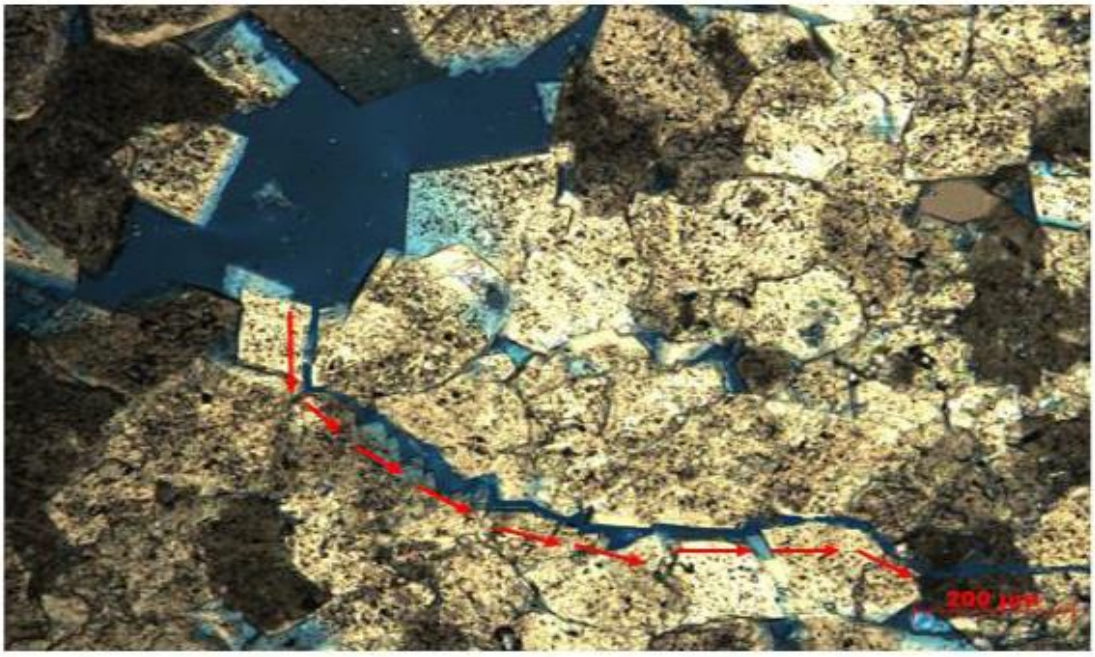

(b) 10X Magnification.

Fig. 7.2–Thin section image for vuggy dolomite rock type showing vugs are connected through a microfracture. Red line shows the preferential flow path.

The homogenous dolomite rock samples are dolostones composed only of primary intercrystalline porosity with fine to rare medium crystals. They exhibit diagenetic texture produced by complete dolomitization of precursor limestone. **Fig. 7.3** shows a uniform pore size distribution for the homogenous dolomite rock type. In such pore structure, the preferential flow paths do not exist and the fluid is expected to flow in a high fraction of the rock.

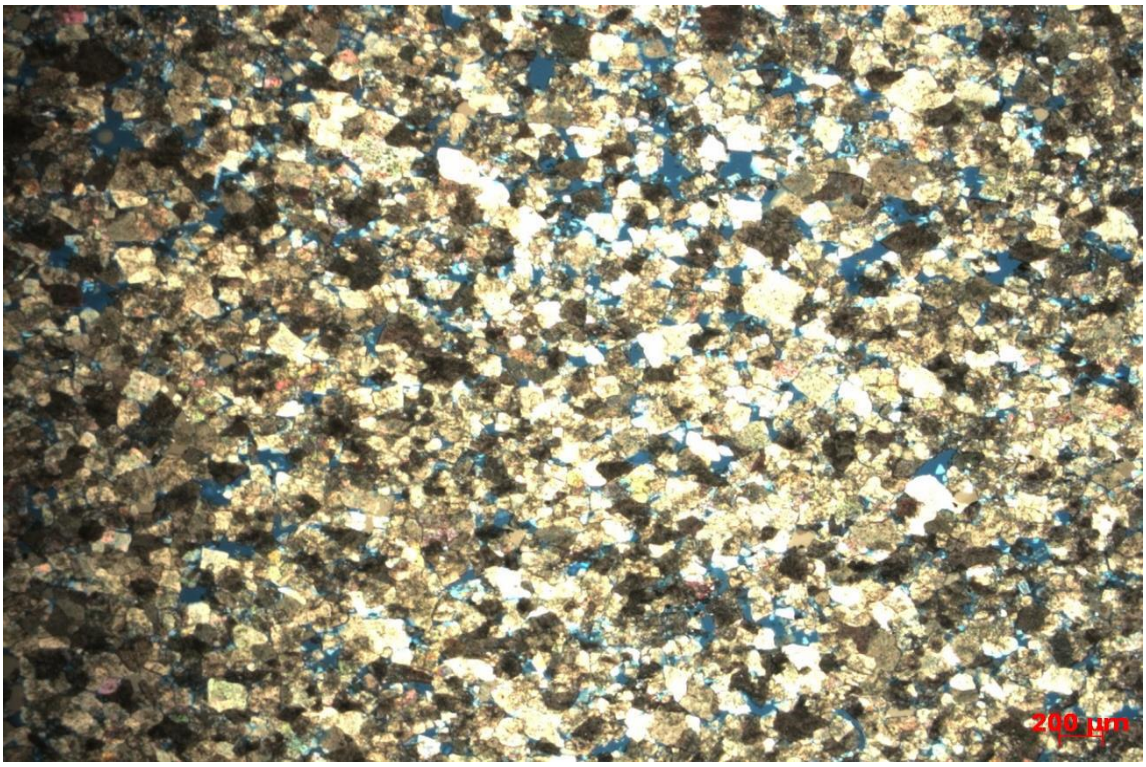

Fig. 7.3 (a)–Thin section image for the homogenous dolomite rock type showing a uniform distribution for the pore openings at 2.5X Magnification

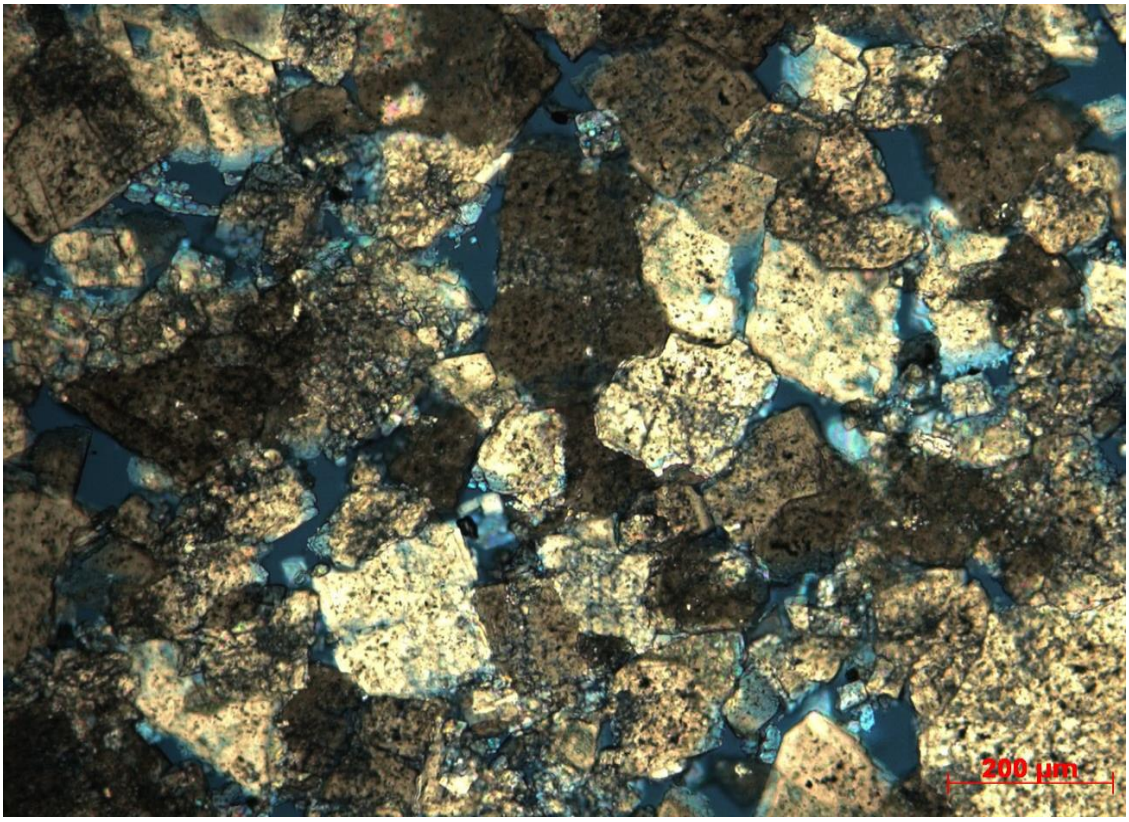

Fig. 7.3 (b)–Thin section image for the homogenous dolomite rock type showing a uniform distribution for the pore openings 10X Magnification.

7.3.2 Tracer Experiments

The normalized tracer concentration (C/C_0) in the core effluent samples is plotted in **Fig. 7.4** as a function of the cumulative pore volume injected. The homogenous dolomite rock type showed a symmetrical tracer concentration profile about $C/C_0 = 0.5$ at one pore volume injected. These results are expected because carbonates of the intercrystal pore class exhibit a symmetrical profile around 1 PV injection at $C/C_0 = 0.5$ (Skauge et al. 2006). These results indicate that when a fluid is injected in the dolomite rock type, it will contact a high fraction of the rock. In contrast, the normalized tracer concentration profiles for vuggy dolomite rock type are characterized by early breakthrough and long tail behavior. This behavior, often referred to the existence of preferential flow path, which acts as a highly conductive streak in a low permeability matrix (Hidajat et al. 2004). This indicates that when a fluid is injected in this dolomite rock type, it will contact a low fraction of rock. The tracer results appear to be consistent with thin section observations.

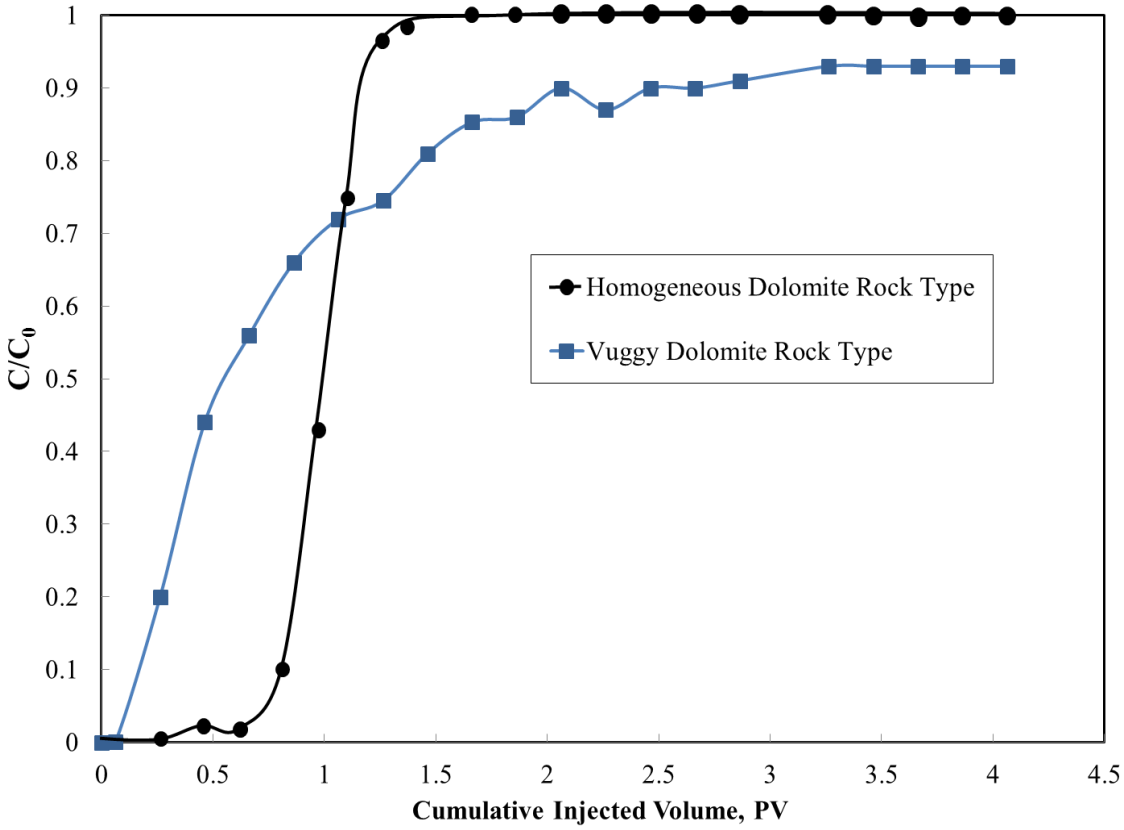

Fig. 7.4—Tracer concentration profile for homogenous and vuggy dolomite rock types.

7.3.3 Impact of Carbonate Pore Structure on Acid Fluid Flow Distribution

In experiment 1 through experiment 4, two parallel cores were used that had different pore structure. The selected injection rates were 1, 2, 5, and 10 cm^3/min. A summary of the experimental results is given in Table 7.1. Experiments at rates of 10 and 2 cm^3/min are discussed in detail.

7.3.3.1 Emulsified Acid Treatment at High Injection Rate

In Experiment 4, Core 7 (vuggy core) and 8 (homogenous core) had an initial permeability of 32.8 and 30 md respectively and they were different only in their rock structure. The cores were used to investigate the effect of the presence of vugs in one of the cores or rock structure heterogeneity along the treated formation on acid fluid flow distribution at a rate of 10 cm^3/min. The initial permeabilities are nearly equal; therefore, the water injected at 10 cm^3/min is divided evenly between the two cores. **Fig. 7.5** shows the pressure drop and the injection rate for both cores as a function of cumulative injected volume. As the emulsified acid entered the cores, the pressure drop decreased significantly indicating a faster wormhole propagation in the vuggy core. The decrease in pressure is accompanied by an increase in the rate in the vuggy core to a value of 10 cm^3/min while the rate drops to zero in the homogenous one. Only 0.34 PVs of acid injection was needed to breakthrough in vuggy core. From rate trend during the acidizing, it was clear that even there is no permeability contrast between the two cores, the heterogeneity in rock structure or the existence of vugs in one of the cores had a significantly effect on acid diversion. **Fig. 7.6** shows the 3D visualization for the created wormhole in both cores after acid injection. Acid breakthrough was achieved only in the vuggy core, while there is no evidence that the flow rate is diverted in the homogenous one to any extent.

Thin section analysis for vuggy dolomite rock type showed a preferential flow path for the fluid to flow through (Fig. 7.2) and this is reflected on the tracer concentration profile (Fig. 7.4) by an early breakthrough and long tail behavior. So, this

preferential flow acts as a permeability streak for the acid to flow when it is injected to both cores leading to breakthrough in the vuggy core and leaves the homogenous dolomite core untouched.

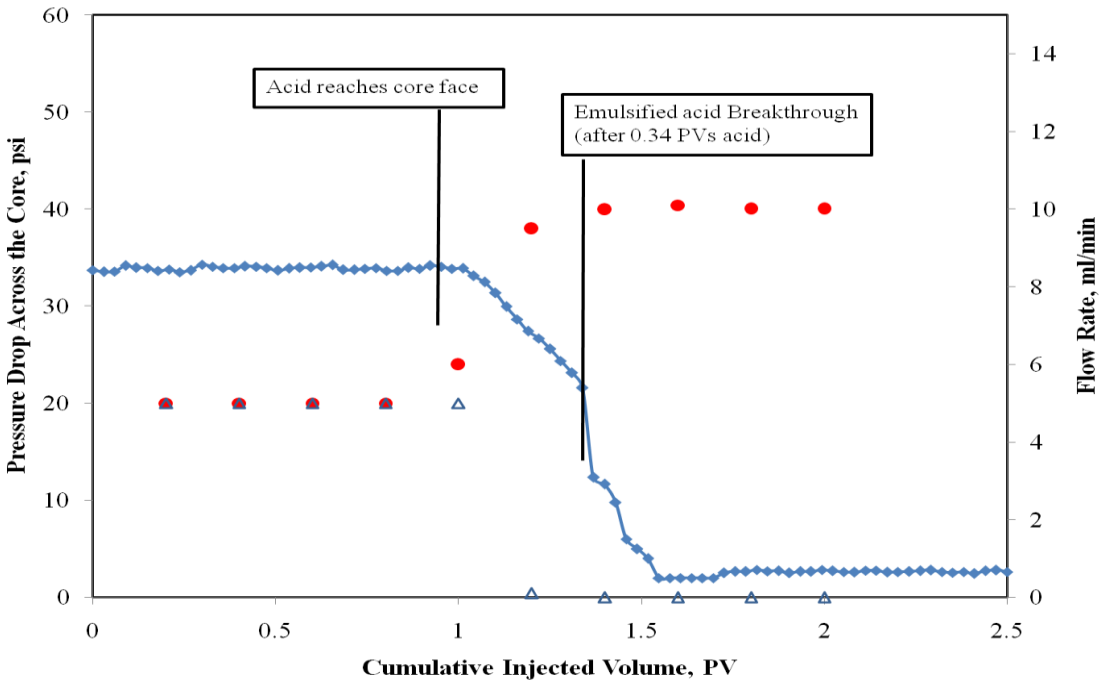

Fig. 7.5—Pressure drop and flow rate distribution in cores 7 and 8, emulsified acid treatment at rate of 10 cm^3/min, and temperature of 200°F.

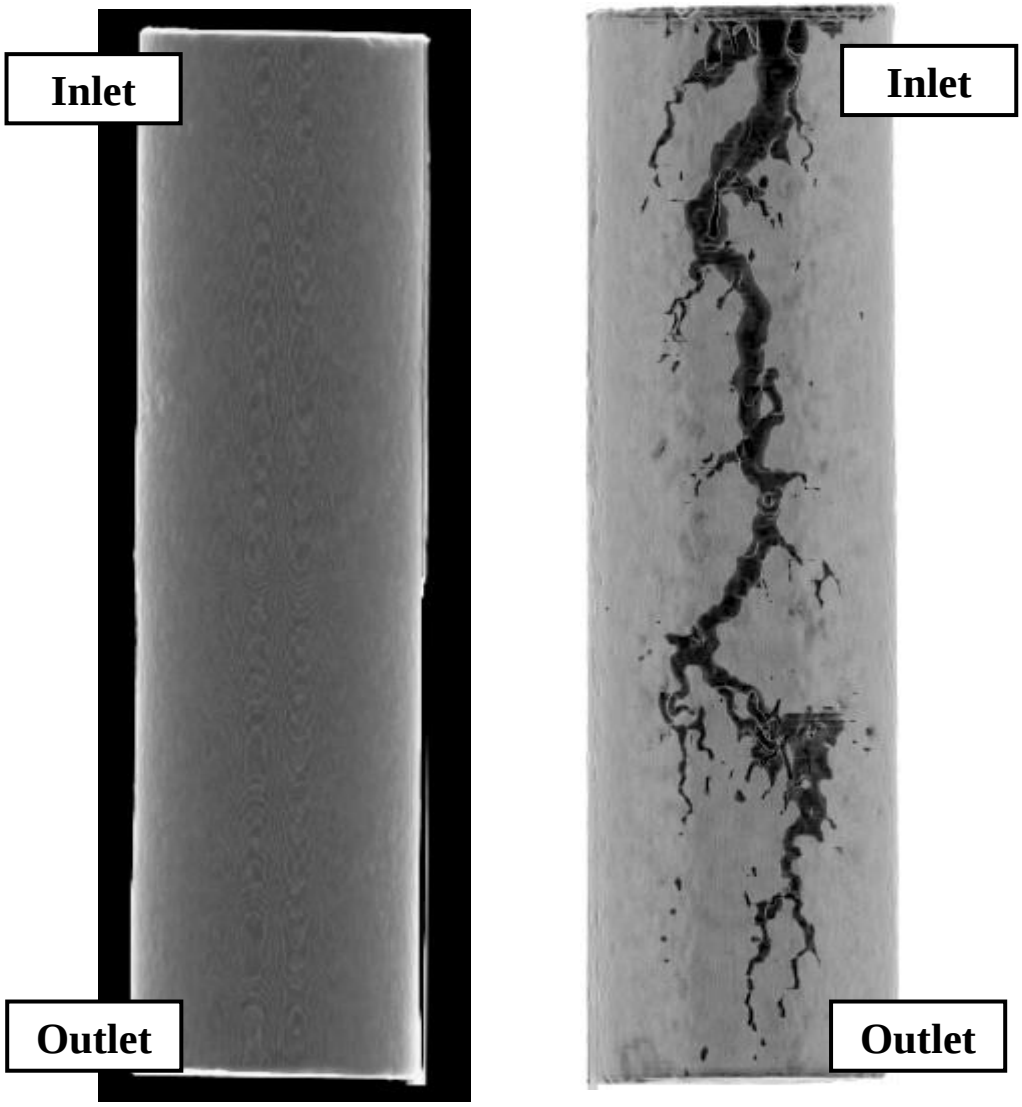

Fig. 7.6—Wormhole dissolution patterns for experiment 4.

7.3.3.2 Emulsified Acid Treatment at Low Injection Rate.

Experiment 2 was conducted using injection rate of 2 cm^3/min through Cores 3 (vuggy core) and 4 (homogenous core). **Fig. 7.7** shows the pressure drop and the

injection rate for both cores as a function of cumulative injected volume. As the acid enters the cores, the pressure drop increased because the emulsion viscosity is higher than that of the water, then the pressure drop declines in two parts with two different slopes. The first part had a pressure drop decline slope equal to 20 psi/PV where the acid injection flow was distributed among both cores. In the second part, most of the acid diverted into the vuggy core after 0.3 PVs of acid injection, the pressure drop decreased rapidly until acid breakthrough from Core 3. An acid breakthrough was achieved only in the vuggy core while the acid did not break through the homogenous core. However, a permeability enhancement in Core 4 was achieved where it was increased from 15.1 to 18 md.

When compared to experiment 4, at low injection rate, the applied shear rate on the emulsified acid is low keeps the viscosity of the acid high. The increased viscosity of the system improves the wellbore coverage and diverts acid into the homogenous core. However, in both experiments, it was found that the presence of carbonates of different pore structure along the treated formation significantly affects the acid fluid flow distribution. Thereby, a diverting agent should be considered even if all the layers within the formation have almost the same permeability.

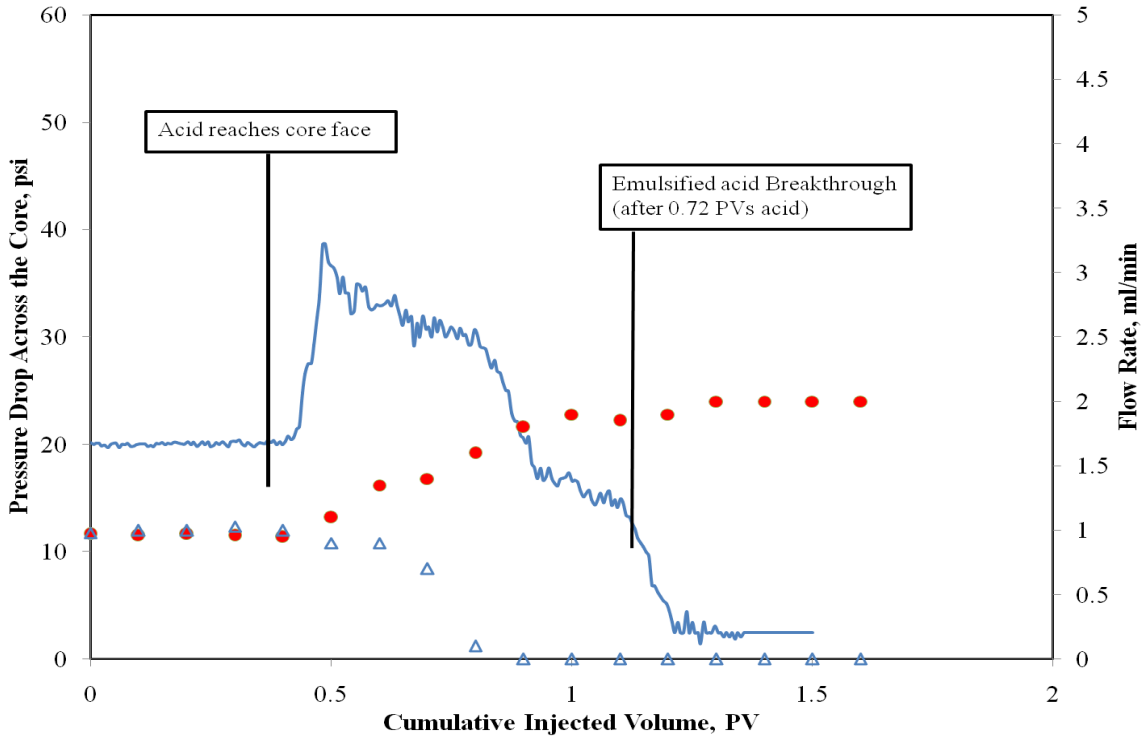

Fig. 7.7—Pressure drop and flow rate distribution in cores 3 and 4, emulsified acid treatment at rate of 2 cm^3/min, and temperature of 200°F.

7.3.4 Impact of Permeability Contrast on Acid Fluid Flow Distribution

In experiment 5 through experiment 8, two parallel cores were used that had a permeability contrast 1:4. The selected injection rates were 1, 2, 5, and 10 cm^3/min. A summary of the experimental results is given in Table 7.2. Experiments at rates of 10 and 2 cm^3/min is discussed in detail.

7.3.4.1 Emulsified Acid Treatment at Low Injection Rate.

In Experiment 6, Cores 11 and 12 had an initial permeability of 7.5 and 30 md respectively. Experiment 6 was conducted at 2 cm^3/min. **Fig. 7.8** shows the pressure

drop and the injection rate for both cores as a function of cumulative injected volume. As the acid entered the cores, the pressure drop increased because of emulsion viscosity and then it decreased slowly while the flow is distributed among both cores. After 0.9 PV's of acid injection, the flow was diverted to the low permeability core and acid breakthrough was achieved after 1.41 pore volumes. The permeability in Core 12 was increased from 30 to 50.5 md. The increased viscosity of the system results in improved the coverage, diverting more fluid to the low permeability core. The fluid velocity may still be low in the low permeability core but the retarded nature of the emulsified system provides efficient wormholing, even at low rates.

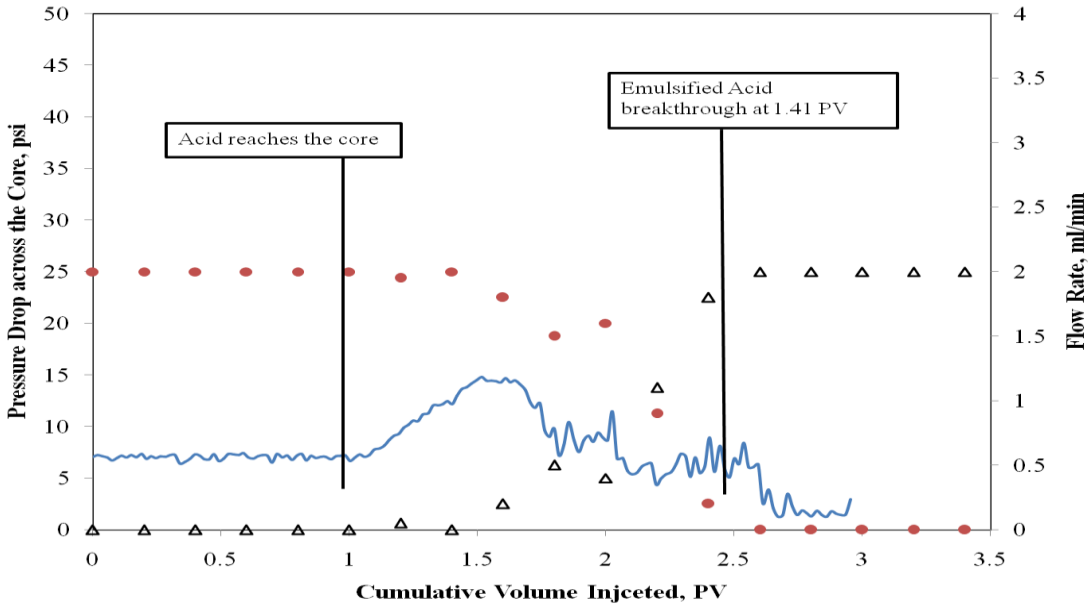

Fig. 7.8—Pressure drop and flow rate distribution in cores 11 and 12, emulsified acid treatment at rate of 2 cm^3/min and temperature of 200°F.

7.3.4.2 Emulsified Acid Treatment at High Injection Rate

In Experiment 8, Cores 15 and 16 had an initial permeability of 18 and 82 md respectively. The experiment was conducted at 10 cm^3/min. **Fig. 7.9** shows the flow rate distribution for both cores as a function of cumulative injected volume. After injection of 1.81, the acid breakthrough was achieved in the high permeability core and a permeability improvement was achieved in the low permeability core from 18 to 22 md.

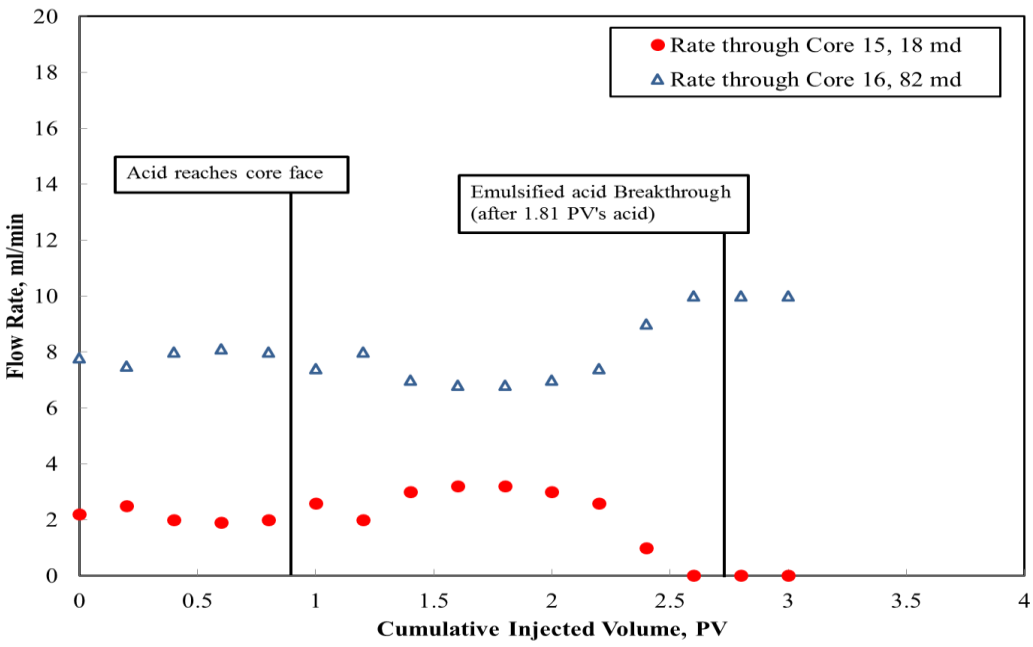

Fig. 7.9—Flow rate distribution in cores 15 and 16, emulsified acid treatment at rate of 10 cm^3/min, and temperature of 200°F.

Table 7.1—Summary of Experimental Results (Impact of Pore Structure Contrast)							
No.	Flow Rate (cm^3/min)	Core ID	PV (cm^3)	Initial K (md)	Final K (md)	Acid Volume (PV)	Diversion
1	1	1 2	15 21	14.3 12.2	acid breakthrough 22	0.83	Not Achieved
2	2	3 4	28 17	13.5 15.1	acid breakthrough 18	0.72	Not Achieved
3	5	5 6	20 24	17 18	acid breakthrough 18	0.51	Not Achieved
4	10	7 8	16 22	32.8 30	acid breakthrough 30	0.34	Not Achieved

Table 7.2—Summary of Experimental Results (Impact of Permeability Contrast)							
No.	Injection Rate (cm^3/min)	Core ID	PV (cm^3)	Initial K (md)	Final K (md)	Acid Volume (PV)	Diversion
5	1	9 10	17.4 21	11.3 47.2	acid breakthrough 86	1.67	Achieved
6	2	11 12	22 24.5	7.5 30	acid breakthrough 50.5	1.41	Achieved
7	5	13 14	13 24	17 71	26 acid breakthrough	1.1	Not Achieved
8	10	15 16	13.5 17.6	18 82	22 acid breakthrough	1.81	Not Achieved

7.4 SUMMARY OF COREFLOOD EXPERIMENTS

Table 7.3 compares the effect of pore structure contrast to the permeability contrast on the diversion ability of the emulsified acid. The percent of permeability increase in low permeability core is computed as:

$$Permeability\ Increase(\%) = (\frac{K_f}{K_i} - 1)\ x\ 100 \quad \text{..... (7.1)}$$

As shown in Table 7.3**,** the effect of the presence of carbonates of different pore structure along the treated formation on the acid fluid flow distribution is more severe than the permeability contrast. The emulsified acid was not able to divert into the homogenous cores at any injection rate. Therefore, a diverting agent should be tested against such cases.

Table 7.3—Coreflood Experiments Results Summary

No.	Injection Rate (cm^3/min)	Pore Structure Contrast	Permeability Contrast	
			Diversion	Percent of Permeability Increase in Low Permeability Core (%)
1	1	Diversion Not Achieved	Diversion Achieved	
2	2	Diversion Not Achieved	Diversion Achieved	
3	5	Diversion Not Achieved	Diversion Not Achieved	82.2
4	10	Diversion Not Achieved	Diversion Not Achieved	68.3

CHAPTER VIII

CONCLUSIONS AND RECOMMENDATIONS

8.1 CONCLUSIONS

This study presents an integrated theoretical and experimental work on the effect of carbonate pore structure on acid treatments. The most important technical contribution of this study is development of a new understanding of the effect of heterogeneity of carbonate rocks at pore scale on the acid fluid flow through porous media. Our approach combines coreflood experiments with a characterization study that includes thin section analysis, electrical measurements, nuclear magnetic resonance and mercury injection capillary pressure measurements, and tracer tests.

The flow of regular acid (15 wt% HCl) in calcite carbonate rock types of different pore structures was studied. Based on the results obtained, the following conclusions were drawn:

- The heterogeneity of carbonate rocks at pore scale has a significant effect on the acid stimulation treatment.
- The heterogeneity of carbonate rocks at pore scale is quantified using one parameter-flowing fraction. This parameter is defined as cumulative pore volume injected of the tracer fluid corresponding to the normalized tracer concentration at $C/C_0 = 0.5$.
- The number of acid pore volumes to breakthrough and the wormhole dissolution pattern were correlated to the heterogeneity of carbonate rocks at

pore scale. Carbonate rocks of high flowing fraction consumed more acid volume and had highly branched wormhole network than the rocks of lower flowing fraction.

- A new methodology to predict the performance of acid stimulation treatment based on non-destructive tracer tests was developed.
- The presence of carbonates of different rock types or different pore structures in the formation has a strong influence on the acid flow distribution and thus the outcome of the treatment.

The flow of the emulsified acid formulated at 1 vol% emulsifier and 0.7 acid volume fraction in calcite carbonate rock types of different pore structures was studied. Based on the results obtained, the following conclusions were drawn:

- The heterogeneity of carbonate rocks at pore scale exerts stronger influence on the emulsified acid stimulation treatment than the regular HCl acid.
- A new formulation for the tracer fluid was developed so that the performance of the emulsified acid stimulation treatments was predicted using non-destructive tracer test.

The flow of the emulsified acid formulated at 1 vol% emulsifier and 0.7 acid volume fraction in vuggy dolomitic rocks was studied. Based on the results obtained, the following conclusions were drawn:

- The efficiency of the acid treatment increases in the presence of vugs. The acid volume needed to propagate a wormhole in vuggy porosity

dominated rocks, at different flow rates, was less than that in homogenous rocks by a factor of 15 to 20 times.

- The efficiency of the wormholing process increases in vuggy carbonates when compared to homogenous ones. In vuggy carbonates, a single dominant wormhole will be created with less volume of acid. Examination of wormhole structure in homogeneous carbonates showed that a narrow branched wormhole network is present. Thus, in vuggy carbonates, a better outcome for the acid treatment is expected as characterized by a lower skin factor.
- Thin section observations for vuggy carbonates show that the vugs are distributed in a manner that creates a preferential flow path for the acid to propagate through until breakthrough. In field, the wide pore size distribution and preferential flow path will lead to deeper acid penetration and better permeability enhancement than expected.
- Vuggy carbonates show better cleanup characteristics than that in homogenous carbonates. In terms of acidizing practices, no need to flow back the wells in the case of vuggy carbonates. This could reduce the rig time and the cost of the stimulation job.
- In acidizing simulations, heterogeneities such as vugs should be included with the large scale heterogeneities such as laminations and fractures, for better design, monitoring, and evaluation of field acid treatments.

The effect of presence of carbonates of different pore structure along the treated formation, on the emulsified acid fluid flow distribution was studied and compared to the effect of permeability contrast of 1:4. Based on the results, the following conclusions were drawn:

- The effect of pore structure contrast on the acid fluid flow distribution is more severe than the effect of permeability contrast.
- At an injection rate of 1 cm^3/min, an acid breakthrough was observed in the vuggy core and a permeability improvement from 12.2 to 22 md in the homogenous core was achieved. In contrast, an acid breakthrough was observed in the low permeability core while the permeability was increased from 47.2 to 86 md in the high permeability core.
- At an injection rate of 2 cm^3/min, an acid breakthrough was also observed in the vuggy core and a permeability improvement of 19% in the homogenous core was achieved compared to 80% at the injection rate of 1 cm^3/min. In contrast, an acid breakthrough was observed in the low permeability core while the permeability was increased from improvement from 30 to 50.5 md in the high permeability core.
- At higher injection rates, an acid breakthrough in the vuggy carbonate was remained the main feature while no permeability improvement was observed in the homogenous core. On the other side, an acid breakthrough was achieved in the high permeability cores and a permeability improvement was observed in the low permeability cores.

8.2 RECOMMENDATIONS FOR FOLLOW-UP WORK

Information about average pore radius, pore size distribution, pores connectivity, interfacial area, and structure-property relation parameters is needed to initialize the acidization models. The PV_{bt} curves and the petrophysical data in this study obtained by various methods such as thin section analysis, NMR, and mercury injection capillary pressure test, can be used to calibrate the acidization models. These models can be then used for rigorous simulation of acid treatment at well scale.

For design of matrix treatments in carbonates rocks, it is desirable to have the PV_{bt} at radial flow geometry at reservoir conditions. In this study, the tracer experiments were conducted on linear cores to obtain the flowing fraction for different carbonate rock types. Radial tracer experiments are recommended to be conducted so that the radial acid PV_{bt} can be predicted.

The results reported here are for regular acid treatment (15 wt% HCl) or for shear thinning fluids such as the emulsified acid. Many treatment fluids are viscoelastic in their nature. For these fluids, the pore structure are expected to have stronger influence than the ones observed in this study.

REFERENCES

Al-Anazi, H.A., Nasr-El-Din, H.A., Mohamed, S.K. 1998. Stimulation of Tight Carbonate Reservoirs Using Acid-In-Diesel Emulsions: Field Application. Paper SPE 39418 presented at the SPE Formation Damage Control Conference, Lafayette, Louisiana, USA, 18–19 February.

Al-Mutairi, S.H., Hill, A.D., Nasr-El-Din, H.A. 2008. Effect of Droplet Size, Emulsifier Concentration, and Acid-Volume Fraction on the Rheological Properties and Stability of Emulsified Acids. *SPE Prod & Oper* **23** (4): 484–497.

Archie, G.E. 1952. Classification of Carbonate Reservoir Rocks and Petrophysical Considerations. *AAPG Bulletin* **36** (2): 278–298.

Arbogast, T., Brunson, D.S., Bryant, S.L., Jennings, J.W. 2004. A Preliminary Computational Investigation of a Macro Model for Vuggy Porous Media. *Developments in Water Science* **55** (1): 267‑278.

Batycky, J.P., Maini, B.B., Fisher, D.B. 1982. Simulation of Miscible Displacement in Full Diameter Carbonate Cores. *SPE J.* **22** (5): 647–657.

Bretz, R.E., Specter, R.M., Orr, Jr. 1988. Effect of Pore Structure on Miscible Displacement in Laboratory Cores. *SPERE* **3** (3): 857–866.

Buijse, M.A. and Van Domelen, M.S. 2000. Novel Application of Emulsified Acids to Matrix Stimulation of Heterogeneous Formations. *SPEPF* **15** (3): 208–213.

Choquette, P.W., Pray, L.C. 1970. Geologic Nomenclature and Classification of Porosity in Sedimentary Carbonates. *AAPG Bulletin* **54** (2): 207–250.

Coats, K.H. and Smith, B.D. 1964. Dead-End Pore Volume and Dispersion in Porous Media. *SPE J.* **4** (1): 73–84.

Daccord, G. and Lenormand, R. 1987. Fractal Patterns from Chemical Dissolution. *Nature* **325**: 41–43.

Dauba, C., Hamon, G., Quintard, M., Cherblanc, F. 1999. Identification of Parallel Heterogeneities with Miscible Displacement. SCA Paper 99-33, Colorado, USA.

Dunham, R.J. 1962. Classification of Carbonate Rocks According to Depositional Texture. *AAPG Memoir* **1** (0): 108–121.

Dong, C., Hill, A.D., Zhu, D. 1999. Acid Etching Pattern in Naturally-Fractured Formations. Paper SPE 56531 presented at the SPE Annual Technical Conference and Exhibition, Houston, Texas, USA, 4–6 October.

Dong, C., Hill, A.D., Zhu, D. 2000. Modeling of Acidizing Process in Naturally-Fractured Formations. Paper SPE 63183 presented at the SPE Annual Technical Conference and Exhibition, Dallas, Texas, USA, 2–4 October.

deRozieres, J., Chang, F.F., Sullivan, R.B. 1994. Measuring Diffusion Coefficients in Acid Fracturing Fluids and Their Application to Gelled and Emulsified Acids. Paper SPE 28552 presented at the SPE Annual Technical Conference and Exhibition, New Orleans, Louisiana, USA, 25–28 September.

Dick, M.A., Heinz, T.J., Svoboda, C.F., Aston, M. 2000. Optimizing the Selection of Bridging Particles for Reservoir Drilling Fluids. Paper SPE 59793 presented at the SPE International Symposium on Formation Damage, Lafayette, Louisiana, USA, 23–24 February.

Fredd, C.N. and Fogler, H.S. 1999. Optimum Conditions for Wormhole Formation: Influence of Transport and Reaction. *SPE J.* **4** (3): 196–205.

Freeman, J.J., Appel, M., Perkins, R.B. 1999. Restricted Diffusion and Internal Field Gradients. Paper SPWLA-1999-FF presented at SPWLA 40th Annual Logging Symposium, Oslo, Norway, 30 May–3 June.

Grunewald, E. and Knight, R. 2011. The Effect of Pore Size and Magnetic Susceptibility on the Surface NMR Relaxation Parameters T2. *Near Surf. Geophys.* **9** (2): 169–178.

Hidajat, I., Mohanty, K.K., Flaum, M., Hirasaki, G. 2004. Study of Vuggy Carbonates Using NMR and X-Ray CT Scanning. *SPEREE* **7** (5): 365–377.

Hoefner, M.L. and Fogler, H.S. 1987. Role of Acid Diffusion in Matrix Acidizing of Carbonates. *JPT* **39** (2): 203–208.

Hoefner, M.L. and Fogler, H.S. 1988. Pore Evolution and Channel Formation during Flow and Reaction in Porous Media. *AICHEJ.* **34** (1): 45–54.

Hoefner, M.L. and Fogler, H.S. 1989. Fluid-Velocity and Reaction-Rate Effects During Carbonate Acidizing: Application of Network Model. *SPE Prod & Oper* **4** (1): 56–62.

Huang, T., Hill, A.D., Schecter, R.S. 2000. Reaction Rate and Fluid Loss: The Keys to Wormhole Initiation and Propagation in Carbonate Acidizing. *SPE J.* **5** (3): 287–292.

Izgec, O., Zhu, D., Hill, A.D. 2010. Numerical and Experimental Investigation of Acid Wormholing during Acidization of Vuggy Carbonate Rocks. *J. Petrol. Sci. Eng.* **74** (2): 51–66.

Kalia, N. and Balakotaiah, V. 2007. Modeling and Analysis of Wormhole Formation in Reactive Dissolution of Carbonate Rocks. *Chem. Eng. Sci.* **62** (4): 919–928.

Kalia, N. and Balakotaiah, V. 2009. Effect of Medium Heterogeneities on Reactive Dissolution of Carbonate Rocks. *Chem. Eng. Sci.* **64** (2): 376–390.

Kenyon, W.E. 1992. Nuclear Magnetic Resonance as a Petrophysical Measurement. *Nuclear Geophysics* **6** (2): 153–171.

Kleinberg, R.L., Kenyon, W.E., and Mitra, P.P. 1994. Mechanism of NMR Relaxation of Fluids in Rock. *J. of Magn. Reson. Ser.A* **108** (2): 206–214.

Korringa, J., Seevers, D.O., and Torrey, H.C. 1962. Theory of Spin Pumping and Relaxation in Systems with a Low Concentration of Electron Spin Resonance Centers. *Phys. Rev.* **127** (4): 1143–1150.

Li, C., Xie, T., Pournik, M., Zhu, D., Hill, A.D. 2005. Fine-scale Simulation of Sandstone Acidizing, *Journal of Energy Resources Technology* **127** (3): 225-233.

Loucks, R.G., Reed, R.M., Ruppel, S.C., Hammes, U. 2012. Spectrum of pore types and networks in mud rocks and a descriptive classification for matrix-related mud rock pores. *AAPG Bulletin* **96** (6): 1071–1098.

Lucia, F.J. 1983. Petrophysical Parameters Estimated from Visual Description of Carbonate Rocks: A Field Classification of Carbonate Pore Space. *JPT* **35** (3): 626–637.

Lynn, J.D. and Nasr-El-Din, H.A. 2001. A Core Based Comparison of the Reaction Characteristics of Emulsified and In-situ Gelled Acids in Low Permeability, High Temperature, Gas Bearing Carbonates. Paper SPE 65386 presented at the SPE International Symposium on Oilfield Chemistry held in Houston, Texas, USA, 13–16 February.

Moctezuma-Berthier, A. and Fleury, M. 2000. Permeability Mapping on Vuggy Core Samples Using Tracer Experiments and Streamline Simulations. Paper SPE 58992 presented at the SPE Annual Technical Conference, Villahermosam, Mexico, 1–3 February.

Myers, M.T. 1991. Pore Combination Modeling: A Technique for Modeling the Permeability and Resistivity Properties of Complex Pore Systems. Paper SPE 22662 presented at the SPE Annual Technical Conference and Exhibition, Dallas, USA, 6-9 October.

Navarrete, R.C., Holms, B.A., McConnell, S.B., Linton, D.E. 1998. Emulsified Acid Enhances Well Production in High-Temperature Carbonate Formations. Paper SPE 50612 presented at the European Petroleum Conference, The Hague, The Netherlands, 20–22 October.

Neeraj, R. and Hirasaki, G. 2011. Pore Structure of Vuggy Carbonates and Rate Dependent Displacement in Carbonate Rocks. SCA Paper 2011-21, Austin, Texas, USA, 18-21 September.

Nierode, D.E., and Williams, B.B. 1971. Characteristics of Acid Reactions in Limestone Formations. *SPE J.* **11** (4): 406–418.

Panga, M., Ziauddin, M., Balakotaiah, V. 2005. Two Scale Continuum Model for Simulation of Wormholes in Carbonate Acidizing. *AIChE J.* **51** (12): 3231–3248.

Ramakrishnan, T.S., Schwartz, L.M., Fordhan, E.J., Kenyon, E.J., Wilkinson, D.J. 1998. Forward Models for Nuclear Magnetic Resonance in Carbonate Rocks. Paper SPWLA-1998-SS presented at SPWLA 39th Annual Logging Symposium, Keystone, Colorado, USA, 26–28 May.

Ratnakar, R.R., Kalia, N., Balakotaiah, V. 2007. Modeling, Analysis and Simulation of Wormhole Formation in Carbonate Rocks with In Situ Cross-linked Acids. *Chem. Eng. Sci.* **90** (0): 179–199.

Rojas, M.R., Müller, A.J., and Sáez, A.E. 2008. Shear Rheology and Porous Media Flow of Wormlike Micelle Solutions Formed By Mixtures of Surfactants of Opposite Charge. *J. Colloid and Interface Science* **326** (1): 221–226.

Sayed, M.A., Nasr-El-Din, H.A., Zhou, J., Zhang, L., Holt, S. 2012. A New Emulsified Acid to Stimulate Deep Wells in Carbonate Reservoirs: Coreflood and Acid Reaction Studies. Paper SPE 151062 presented at the North Africa Technical Conference and Exhibition, Cairo, Egypt, 20–22 February.

Sayed, M.A. and Nasr El-Din, H.A. 2012. Reaction Rate of Emulsified Acids and Dolomite. Paper SPE 151815 presented at the SPE International Symposium on Formation Damage, Lafayette, Louisiana, USA, 15-17 February.

Shook, G.M. 2003. A Simple, Fast Method of Estimating Fractured Reservoir Geometry from Tracer Tests. *Transactions of the Geothermal Resources Council* **27** (0): 407–411.

Skauge, A., Vik, B., Pourmohammadi, S., Spildo, K. 2006. Dispersion Measurements Used in Special Core Analysis of Carbonates. SCA Paper 2006-14, Trondheim, Norway, 12-16 September.

Straley, C., Rossini, D., Vinegar, H. 1997. Core Analysis by Low-Field NMR. *The Log Analyst* **38** (2): 84–95.

Sørland, G.H., Djurhuus, K., Widerøe, H.C. 2007. Absolute Pore Size Distributions from NMR. *Diffusion Fundamentals* **5** (2): 4.1–5.15.

Strum, P.W. and Johnson, W.E. 1950. Field Experiments with Chemical Tracers in Flood Waters. *Producers Monthlv* **15** (2): 11–18.

Swanson, B.F. 1981. A Simple Correlation between Permeabilities and Mercury Capillary Pressure. *JPT* **33** (12): 2498-2504.

Toumelin, E., Torres-Verdin, C., Chen, S. 2002. Analysis of NMR Diffusion Coupling Effects in Two-Phase Carbonate Rocks: Comparison of Measurements with Monte Carlo Simulations. Paper SPWLA-2002-JJJ presented at SPWLA 43rd Annual Logging Symposium, Oiso, Japan, 2–5 June.

Toumelin, E., Torres-Verdin, C., Chen, S. 2003. Reconciling NMR Measurements and Numerical Simulations: Assessment of Temperature and Diffusive Coupling Effects on Two-Phase Carbonate Samples. *Petrophysics* **44** (2): 91–107.

Wang, Y., Hill, A.D. and Schechter, R.S. 1993. The Optimum Injection Rate for Matrix Acidizing of Carbonate Formations. Paper SPE 26578 presented at the SPE Annual Technical Conference and Exhibition, Houston, Texas, USA, 3–6 October.

Xu, B., Kamath, J., Lee, S.H., Yortsos, Y.C., 1998. Use of Pore Network Models to Interpret Laboratory Experiments on Vugular Rocks. *J. Petrol. Sci. Eng.* **4** (3): 179–186.

Zakaria, A.S., Hafez, M.M., Ochi, J., Zaki, K.S., Loloi, M., Abou-Sayed, A. 2011. Application of Genetic Algorithm to the Optimization of Pressure Transient Analysis of Water Injectors using Type Curves. Paper SPE 143386 presented at the SPE European Formation Damage Conference, Noordwijk, The Netherlands, 7–10 June.

Zhang, L., Bryant, S.L., Jennings, J.W., Arbogast, T.J., Paruchuri, R. 2004. Multi-scale Flow and Transport in Highly Heterogeneous Carbonates. Paper SPE 90336 presented at the SPE Annual Technical Conference, Houston, Texas, USA, 26–29 September.

Zhang, L., Nair, N., Jennings, J.W., Bryant, S.L. 2005. Models and Methods for Determining Transport Properties of Touching-vug Carbonates. Paper SPE 96027 presented at the SPE Annual Technical Conference, Dallas, Texas, USA, 9–12 October.

Ziauddin, M. and Bize, E. 2007. The Effect of Pore-Scale Heterogeneities on Carbonate Stimulation Treatments. Paper SPE 104627 presented at the SPE Middle East Oil & Gas Show and Conference, Bahrain, Kingdom of Bahrain, 11-14 March.